ABSTRACT

Modeling and Control of Advanced Pumped Storage Hydropower for Power System Resiliency Enhancement

Soumyadeep Nag, Ph.D.

Mentor: Kwang Y. Lee, Ph.D.

With the gradual increase in renewable penetration, system operators are searching for flexible resource that can help mitigate problems of future low-inertia power systems. To analyze the benefit of advanced pumped storage hydro (PSH) configurations as flexible resources, the mathematical models and controls for each configuration are required but are not available with academic or commercial software platforms. Thus, effort is dedicated to the development of these models and displaying that they can be integrated with test systems for power system studies in MATLAB/Simulink.

First, a governor model is constructed for pump and generator modes separately for the adjustable speed PSH (ASPSH). Second, a governor model is constructed for ternary PSH (TPSH). Finally, a governor model for Quaternary PSH (QPSH) was constructed. For ASPSH and TPSH configurations, governor models and inverter controls were formulated and a single-machine-infinite-bus (SMIB) integration and a 9-bus system integration tests were performed.

The ASPSH model was able to regulate the speed of the turbine successfully and hence maintain the high efficiency, while tracking real power references in both generation and pump modes. Also, through the integration tests in the 9-bus test system it has been demonstrated that, the governor structure can provide primary frequency regulation in both pump and generation modes. Further, an adaptive droop (AD) system was designed for the ASPSH system which showed that the AD algorithm in-hand with the converter control could provide enhanced primary regulation for the system.

For the TPSH configuration, the SMIB integration results demonstrate that the governor model can track power references accurately in the pump mode and that, the model can demonstrate the mode change pump to generator and vice-versa without the loss of synchronism. Simultaneously, the 9-bus test system integration displayed that the pump mode reference tracking could be of great benefit for the network, but the mode change capability is an important emergency response tool for the system operators.

The QPSH system with the converter-based pump model was constructed and integration studies in the western interconnection system for different renewable penetrations showed that QPSH could support greater penetrations of renewable energy in the same network.

Finally, the revenue earning potential of the PSH configurations was evaluated, which concluded that TPSH could earn higher revenue even while considering wind penetration and seasonal variation of load and wind profiles.

Modeling and Control of Advanced Pumped Storage Hydropower for Power System Resiliency Enhancement

by

Soumyadeep Nag, B.Tech., M.Tech.

A Dissertation

Approved by the Department of Electrical and Computer Engineering

_____

Kwang Y. Lee, Ph.D., Chairperson

Submitted to the Graduate Faculty of
Baylor University in Partial Fulfillment of the
Requirements for the Degree
of

Doctor of Philosophy

Approved by the Dissertation Committee

_____

Kwang Y. Lee, Ph.D., Chairperson

_____

Annette Von Jouanne, Ph.D.

_____

Mack Grady, Ph.D.

_____

Scott Koziol, Ph.D.

_____

Kenneth Van Treuren, Ph.D.

Accepted by the Graduate School

December 2020

_____

J. Larry Lyon, Ph.D., Dean

Page bearing signatures is kept on file in the Graduate School.

TABLE OF CONTENTS

LIST OF FIGURES vii

LIST OF TABLES xi

LIST OF ABREVIATIONS xiii

ACKNOWLEDGMENTS xv

DEDICATION xvii

ATTRIBUTIONS xviii

CHAPTER ONE 1
Introduction 1
1.1 Growth of Renewable Energy *1*
1.2 Resiliency *2*
1.3 Power System Inertia *4*
1.4 Energy Market *5*
1.5 Grid Support Functions from the Energy Storage System (ESS) *7*
1.6 The Evolution of Pumped-Storage Hydropower *8*
1.7 Other Forms of PSH to Overcome Geographic Limitations *12*
1.8 Scope and Contributions of this Dissertation *12*

CHAPTER TWO 14
Literature Review 14
2.1 Grid-Scale Energy Storage Technologies *14*
2.2 Pumped Storage Hydropower *18*
2.3. Policy and Economics *25*
2.4 Dynamic Modeling and System Integration Studies and Controls *30*

CHAPTER THREE 32
Modeling and Control of Adjustable Speed Pumped-Storage Hydropower Units 32
3.1 Introduction *32*
3.2 Generator Mode Model *35*
3.3 Pump Mode Model *37*
3.4 DC-Link Modeling and Control *39*
3.5 Modeling of DFIM *46*
3.6 SMIB System and Reference Tracking Results *53*
3.7 The 9-bus Testbed and ASPSH Integration *56*
3.8 Dynamic Performance Comparison with CPSH *60*
3.9 Adaptive Droop-Based Primary Control *61*
3.10 Conclusion *64*

CHAPTER FOUR 65
Modeling and Control of Ternary Pumped Storage Hydropower 65
4.1 Introduction *65*
4.2 Technology Description *65*
4.3 Dynamic Modeling *67*
4.5 Results and Discussion *70*
4.6 Conclusion *75*
CHAPTER FIVE 76
Network and Reserve Constrained Economic Analysis of Pumped-Storage Hydropower 76
5.1 Introduction *76*
5.2 Modeling PSH Configurations *78*
5.3 Problem Formulation *78*
5.4 Optimization Algorithms *83*
5.5 System Data *87*
5.6 Results and Observations *89*
5.7 Discussion *94*
5.8 Conclusion *95*
CHAPTER SIX 97
Impacts of Quaternary Pumped Storage Hydropower 97
6.1 Introduction *97*
6.2 GE's PSLF and EPCL for User-Defined Component Modeling *99*
6.3 Structure of QPSH *101*
6.4 Modelling and Control of QPSH *102*
6.4 Simulation Results and Discussion *104*
6.5 Results and Discussion *106*
6.6 Conclusion *110*
CHAPTER SEVEN 111
Conclusions 111
7.1 Research Summary *111*
7.2 Future Work *113*
APPENDIX A 115
ASPSH and TPSH Mask Parameters and Internal Construction 115
BIBLIOGRAPHY 123

LIST OF FIGURES

Figure 1.1. A rough comparison of a traditional and resilient power systems 3

Figure 1.2. Effect of renewables on frequency stability 5

Figure 1.3. (a) CPSH, (b) synchronous machine based fully-fed ASPSH, (c) Doubly-fed induction machine based ASPSH, and (d) TPSH 9

Figure 1.6. Quaternary PSH 10

Figure 2.1. Redox flow battery energy storage system showing physical components 15

Figure 2.2. Schematic diagram of flywheel energy storage……17

Figure 3.1. Configurations of ASPSH: a) fully fed synchronous machine based system and b) DFIM-based system 33

Figure 3.2. Generator mode governor diagram 36

Figure 3.3. Pump mode governor diagram 38

Figure 3.4. a) DC-link capacitor, b) inductive filter model in d*q*-axis, and c) simulation model of the filter showing inputs and outputs 39

Figure 3.5. Transformation from normal conditions to grid voltage orientation: a) before, and b) after the transformation 41

Figure 3.6. Schematic layout for actual implementation of Grid voltage-oriented control of DC bus voltage 43

Figure 3.7. DC bus voltage regulation schematic assuming proper compensation used for tuning the PI controllers 45

Figure 3.8. The *q*- and *d*-axis equivalent circuits of DFIM 47

Figure 3.9. Simulation blocks of the DFIM (a) rotor, (b) stator, and (c) mutual flux model 48

Figure 3.10. Stator flux orientation 50

Figure 3.11. Control loops for RSC 52

Figure 3.12. A SMIB system with ASPSH, where P/T is the reversible pump turbine, *G* = gate, *vd* and *vq* are *d*- and *q*-axis reference voltages and *Pm* is the mechanical power 53

Figure 3.13. Generation mode: (a) Electrical Power, (b) Mechanical Power, (c) Electrical power zoomed in, and (d) Speed tracking 54

Figure 3.14. Pump mode power and speed reference tracking 55

Figure 3.15. The 9-bus test system showing G2 with AC source commented for dynamic simulation 57

Figure 3.16. Masks for the turbine, pump, and the DFIM with converter control 58

Figure 3.17. Components inside the new G2 59

Figure 3.18. Fast Frequency Test Performance comparison of CPSH and ASPSH for Fixed Droop coefficient in (a) Generating mode and (b) Pumping mode 60

Figure 3.19. Four scenarios of the frequency profile 61

Figure 3.20. The DFIM Droop gain adaptation logic 62

Figure 3.21. Adaptive droop based supplementary control 62

Figure 3.22. Adaptive droop response: (a, b) frequency, (c, d) electric power output, and (e, f) droop for (generator, pump) modes, respectively 63

Figure 4.1. Functional diagram of TPSH 66

Figure 4.2. Block diagram for dynamic model of TPSH 69

Figure 4.3. A 9-bus IEEE test system 70

Figure 4.4. (a) Pump mode power reference tracking with hydraulic short circuit, (b) Water flow distribution 71

Figure 4.5. Baseline analysis of the test system in pump mode of CPSH 72

Figure 4.6. Comparison of (a) power output with (b) system frequency of CPSH and TPSH during a load trip event 73

Figure. 4.7. Comparison of (a) power output with (b) system frequency of CPSH and TPSH during a load addition event 73

Figure 5.1. Operating ranges of PSH configurations 77

Figure 5.2. Illustration of proposed GA with selective evaluation. WI1, WI2 and WI3 are the worst individuals originated from the first, second and third iterations 86

Figure 5.3. Objective functions of GA, PSO, DE and GA with selective evaluation 87

Figure 5.4. The modified 24-bus RTS system 88

Figure 5.5. Weekly (a) Load and (b) Wind Profile for summer and winter 89

Figure 5.6. Weekly revenue collected from the energy and regulation markets combined with the storage technologies from the 24-bus system for summer and winter weeks 90

Figure 5.7. Weekly revenue collected from the energy and regulation markets earned by the PSH technologies from the 24-bus system with and without 30% wind 92

Figure 6.1. IEEE Type-1 speed governor model 99

Figure 6.2. Functional diagram of QPSH 102

Figure 6.3. Governor turbine model for the QPSH with HYGOV based turbine control and inertia and low frequency oscillation damping controller through the converter 103

Figure 6.4. Control system for QPSH where, C=converter, M=motor, P=pump, G=generator and T=turbine and governor 104

Figure 6.5. WECC System response to a plant trip event under 20%, 40%, 60% and 80% renewable penetration 107

Figure 6.6. Analysis of WECC system: (a) frequency and (b) net response with QPSH vs. with CPSH under 20% RE penetration 108

Figure 6.7. Analysis of WECC system: (a) frequency and (b) net response with QPSH vs. with CPSH under 80% RE penetration 108

Figure 6.8. Electrical power from the (a) pump, (b) turbine and (c) combination 109

Figure 6.9. Summary chart for system frequency nadir and settling frequency indicating CPSH frequency nadir with 80% RE penetration to be below 59.5Hz during pump mode operation 110

Figure A.1. Pump mode hydraulic dynamics and primary regulation with ..... gate completely open 115

Figure A.2. ASPSH pump mode mask for parameter value entry 116

Figure A.3. Turbine mode governor and hydraulic dynamics for ASPSH 117

Figure A.4. ASPSH turbine mode mask for parameter value entry 118

Figure A.5. DFIM machine and control mask, generator parameter entry 119

Figure A.6. DFIM machine and control mask, converter parameter entry 120

Figure A.7. DFIM machine and control mask, controller parameter entry 121

Figure A.8. TPSH (a) governor mask and (b) parameter entry interface 122

LIST OF TABLES

Table 1.1. Worldwide installed PV (GW) 1

Table 1.2. Worldwide installed wind energy (GW) 2

Table 1.3. Worldwide change in renewable resources 4

Table 1.4. Worldwide change in equivalent inertia 4

Table 1.5. Comparison of ASPSH and TPSH 11

Table 3.1 Parameters of the SMIB system 53

Table 5.1. PSH data for CPSH, ASPSH and TPSH 81

Table 5.2. Forecast error data. Wind was normalized by the installed capacity and load was normalized by the average load 83

Table 5.3. Additional system data 87

Table 5.4. Time spent [%] in each mode of operation over the week; positive being generation and negative being pumping; S = summer and W = winter 91

Table 5.5. Time spent [%] in each mode of operation over the week with positive being generation and negative being pumping; S = summer and W = winter 93

Table 5.6. Curtailment in MWhrs 94

Table 6.1 Comparison of CPSH and QPSH 98

Table 6.2. Governor and generator models for the WECC system 105

Table 6.3. Wind and PV penetration for different developed cases 106

Table A.1. Parameters and definitions of the ASPSH pump mode mask 116

Table A.2. Parameters and definitions of the ASPSH mask 119

Table A.3. Parameters and definitions of the DFIM machine and control mask for generator parameter entry 120

LIST OF ABREVIATIONS

AD	Adaptive Droop
AGC	Automatic Generation Control
ASPSH	Adjustable speed Pump storage hydro power
BESS	Battery Energy Storage System
CAES	Compressed Air Energy Storage
CPSH	Conventional Pump storage hydro power
CSP	Concentrated Solar Power
DE	Differential Evolution
DFIM	Doubly Fed Induction Machine
ERCOT	Electricity Reliability Council of Texas
FERC	Federal Energy Regulatory Commission
FESS	Flywheel Energy Storage System
FN	Frequency Nadir
FPA	Flower Pollination Algorithm
GA	Genetic Algorithm
GPC	Generalized Predictive Control
GSC	Grid side converter
HSC	Hydraulic short-circuit
ISO	Independent System Operator
LMP	Locational Marginal Pricing

MISO	Midcontinent Independent System Operator
OPF	Optimal Power Flow
PCM	Phase Change Materials
PID	Proportional integral derivative
PJM	Pennsylvania-New Jersey-Maryland
PSH	Pumped-storage hydro
PSO	Particle Swarm Optimization
QPSH	Quaternary Pump storage hydro power
RES	Renewable energy system
ESS	Energy storage system
RFB	Redox flow batteries
ROCOF	Rate of change of frequency
RSC	Rotor side converter
RTO	Regional Transmission Operator
RTS	Reliability Test System
SEGA	Genetic algorithm with Selective evaluation
SMIB	Single machine infinite bus
STENSEA	Stored energy in the sea
TES	Thermal energy storage
TPSH	Ternary Pump storage hydro power
VSG	Virtual synchronous generator
WECC	Western Electricity Coordinating Council

ACKNOWLEDGMENTS

It gives me immense pleasure to express my deep sense of gratitude and thanks to my supervisor Dr. Kwang Y. Lee, for recruiting me into his Power and Energy Systems Lab and for his invaluable guidance, support, and suggestions. It was a privilege to be a part of this great group. Without his support I would not be able to develop my research aptitude and materialize my thoughts. Through the tenure of my doctoral studies, he has helped me broaden my research perspective and encouraged me to look at future possibilities and overcome the difficulties encountered in my research. Also, through Dr. Lee, I came to know and learn more about Jesus Christ.

I would also like to thank my committee members: Dr. Annette von Jouanne, Dr. Scott Koziol, Dr. Mack Grady and Dr. Van Treuren, for their time and suggestions toward my dissertation and defense.

I am also thankful to Dr. Randal Jean for recruiting me for this doctoral candidate position in the department of Electrical and Computer Science Engineering at Baylor University and for all the opportunities that have come along with it. I am also thankful to the department administrators for they not only funded all my travel but also provided me with the opportunity to be able to support myself during my doctoral studies and gain valuable teaching experience.

I would like to take this opportunity to thank Dr. Jin Tan from the National Renewable Energy Lab (NREL). She recruited me into the dynamic modeling group at

NREL for a summer internship to work on a DOE sponsored project. This opportunity helped me significantly to shape my efforts in my dissertation.

I would also like to thank my mentor, Dr. D. Suchitra, from SRM University, Chennai, India as she played a key role in shaping my research perspective towards power systems, renewable energy and energy storage. She supervised my Master's Thesis. She has also reviewed a few papers from the tenure of my doctoral studies. She has always been a guiding force for my future goals.

Finally, I would like to thank my wife, Sushmita Nag, for all the patience, faith and strength. Without her, I would not be able to complete this endeavor. Also, my parents, late Mrs. Mousumi Nag and Dr. Subrata Nag. Time and time again, their suggestions have guided and inspired me through many situations.

Last but not the least, I am truly thankful for all the blessing from the Lord Jesus Christ who has been with me through every moment of my journey.

To my dear Wife Sushmita Nag (Bini),

To my Dad Dr. Subrata Nag,

And in Lieu of Flowers to my Mom Mousumi Nag.

ATTRIBUTIONS

Chapter 4 - Modeling and Control of Ternary Pumped Storage Hydropower

S. Nag – Investigation and documentation

K. Y. Lee – Problem formulation and review

D. Suchitra – Problem formulation and review

Chapter 5 - Network and Reserve Constrained Economic Analysis of Pumped-Storage Hydropower

S. Nag – Investigation and documentation

K. Y. Lee – Problem formulation and review

CHAPTER ONE

Introduction

1.1 Growth of Renewable Energy

In recent years, a significant growth in renewable energy penetration has been observed as can be seen in Tables 1.1 and 1.2. In [1], Kavlak, McNerney and Trancik attempt to understand the cause for the rapid drop in price of solar photovoltaic (PV) systems and reveal that, R&D and large-scale of installations are primary causes for the drop in PV cost. More specifically, increase in module efficiency, decrease in non-silicon material costs and the decrease in price of silicon itself are prime contributor to the reduced PV prices from the R&D perspectives. Significant amount of research is dedicated to the efficiency enhancement of solar PV modules and materials. National Renewable Energy Laboratory (NREL) has achieved 47.1% cell efficiency with their multi-junction concentrator-based technology. While the commonly used single junction crystalline silicon cells have reached 26.7% cell efficiencies. Two latest innovations in this area are the Dye sensitized cells which can be used to replace windows, as they are

Table 1.1. Worldwide installed PV (GW)

Year	2015	2016	2017	2018	2019
China	43.53	78.07	131	175.018	204.7
European Union	94.57	101.433	107.15	115.234	131.7
United States	25.62	40.3	51	62.2	75.9
Japan	34.41	42.75	49	55.5	63
Germany	39.7	41.22	42	45.93	49.2
India	5.05	9.01	18.3	26.869	42.8

Table 1.2. Worldwide installed wind energy (GW)

Year	2015	2016	2017	2018	2019
China	145	169	188	211	236
European Union	142	154	169	179	192
United States	74	82	89	97	105
Germany	45	50	56	59	61
India	27	29	33	35	38
Spain	23	23	23	23	26
United Kingdom	14	15	19	21	24

transparent, and Perovskite cells that can be printed with a normal 3D printer. With such developments, exponential growth of solar PV installations is projected.

The worldwide increase in installed capacity can also be seen in the case of wind energy. The main boosting factor in case of wind energy is the increase in capacity factor. As the cut-in speeds of the turbines decrease due to increase in blade size and hub heights, their availability increases and so does their capacity factor. Also, the scale of projects and growth of in-house industrial production has been a significant factor in the price drop of wind energy.

1.2 Resiliency

With the growth of renewable energy source (RES) penetration, and with the growing frequency of high impact natural disasters such as storms, hurricanes, earthquakes [2] forest fires, and man-made cyberattacks, the level of uncertainty in the power system has increased. Also, the increased RES penetration displaces conventional fossil fuel-based generation resources and the ancillary services that they provided. Thus, the resilience of such a power system is compromised to a great extent.

Power system resiliency and reliability are subtly different. Reliability reflects an idea that the light must be on in a consistent manner. This is a binary view of system performance where the system is either functional or failed. Reliability is generally measured by interruption indices such as load not served. On the contrary, resiliency is the ability of the system to recover itself after a disruptive event. A more resilient system will experience disruptive events of lesser magnitude and/or duration. Resilience can thus be thought of an idea of the system existing in the state between functional and failed. Resiliency enhancement builds upon the fact that, disruptive events cannot be predicted with complete certainty but when they do occur, the system should adapt and recover [3]. Resiliency indices are currently under development.

Figure 1.1 describes the difference between the resilient system and a traditional system. Here, if $F(t)$ is a time-varying state-variable during a disturbance, the resilient system shows higher ability to resist and absorb, reduced time to respond and recover as compared to the traditional system. Much research is ongoing to design metrics for resilience in power systems. A very naive way to quantify system resilience would be to consider the resiliency metric R, where,

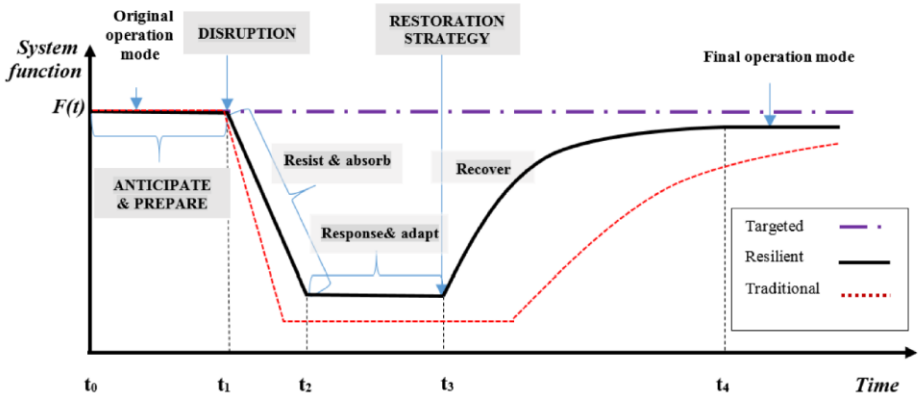

Figure 1.1. A rough comparison of a traditional and resilient power systems [4].

$$R=\int_{t_1}^{t_4}\left(F_o\left(t\right)-F\left(t\right)\right)dt \tag{1.1}$$

where, t_1 and t_4, indicate the beginning of an event till the end of the recovery phase. As such, for most of this work, the frequency of the system is considered as the main state-variable. In this work, effort is dedicated to the enhancement of the frequency profile upon the occurrence of an event, with the help of an Adjustable-speed, Ternary and quaternary Pumped-storage Hydropower.

1.3 Power System Inertia

All rotating equipment have inertia which is a critical parameter for the health and stability of the power system. However, as shown in Tables 1.3 and 1.4, the gradual increase in worldwide renewable penetration has led to the drop in equivalent inertia of continents [5]. This is mainly because, the renewable energy sources do not contribute to network equivalent inertia as they are interfaced by converters to the grid. Also, they displace the synchronous generator-based fossil fuel plants which further reduces network synchronous inertia.

Table 1.3. Worldwide change in renewable resources

Year	1996	2016
Conventional resources	80%	76%
Renewables	20%	24%
Wind	1.5%	16%
Solar	1.5%	5%
Hydro	92%	68%
Others	5%	9%

Table 1.4. Worldwide change in equivalent inertia

Year	1996	2016
North America	4	3.9
South America	3.5	3.4
Europe	4	3.3
Asia	4	3.9
Africa	4	4.2

Figure 1.2 shows the frequency profile due to a plant failure event under different penetration of renewable energy. It is evident that with the decrease in inertia we have lower frequency nadirs, meaning higher amount of load shedding, faster drop in frequency meaning reduced time to react for relays and lower settling frequency due to the lack of controllable resources. Thus, the work done in this dissertation looks at pumped hydro as a controllable resource and examines the extent to which the advanced pumped hydro sources can enhance frequency profile.

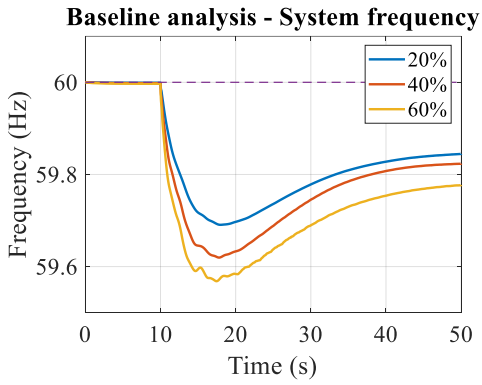

Figure 1.2. Effect of renewables on frequency stability.

1.4 Energy Market

Usually, low energy price periods occur at night, however, as RES penetration increases, the number of low energy price periods tend to increase and occur at random. Thus, operating inflexible resources during these hours is not economical. However, this provides a chance for grid-scale energy storage systems to improve system economy and simultaneously provide flexibility to the network. In fact, depending upon the type of RES with the highest penetration, the entire price and load profile changes, or shifts.

With the increase in RES penetration, the average price of energy decreases but the value of ancillary services and capacity increases by a factor of 2 to 8. Also, with the retirement of fossil fuel-based generators, the energy scarcity hours with high energy prices will increase, which will result in investment in grid-scale energy storage.

Another RES induced change in the energy markets is the price volatility. High solar cases have resulted in the highest amounts of price volatility as compared to wind, although solar has an explainable profile. High wind cases have induced irregularity in the price patterns. Stronger price variability and irregularity will favor flexible resources that can start and stop frequently and on short notice, including storage. These changing conditions with the increase in renewable energy penetration, calls for adaptation of energy markets [6].

As mentioned before, that the increase of RES penetration has introduced a higher level of uncertainty in power systems. To cope with the higher uncertainty levels, controllable resources must participate. To remunerate the participating resources, the energy market offers revenue streams. There are two main revenue streams that are considered in this work: a) arbitrage and b) regulation. Arbitrage involves the purchase of energy when its price is low and selling the stored amount of energy during times of high energy cost. Regulation is the ability of a resource to dither its operating point whenever commanded.

With the increasing awareness of resilience among system operators, not only are they remunerating the storage systems capability to respond, but also rewarding the quality of response (speed and accuracy) from the storage device. This dissertation work dedicates effort to investigate the ability of advanced pumped hydro systems to

participate in these markets and earn higher revenue as compared to the conventional PSH.

1.5 Grid Support Functions from the Energy Storage System (ESS)

If ESS are controlled in a proper manner, the following functionalities [7] can be achieved through them that greatly benefit the grid.

1. Peak shaving and load leveling: Peak shaving responds to reducing the peak demands while load leveling responds to leveling the entire load profile. These functions have several benefits as they can reduce emissions and cost by reducing the use of fossil fuel based peaking plants, they can relieve system congestion, reduce system losses, improve voltage profile, etc.
2. Integration of renewables: Renewables, as discussed above, present the network with unpredictable power generation, and hence significant error between forecast and actual power generation exists in the network. Also, RESs are not always available when it is needed. Hence ESS can be used to bridge the gap between demand and RES based generation and to accommodate the forecast error. Solar PV can fluctuate to a large extent in a small timescale, and to cope with the high ramping nature of RES, ESS can be used to provide ancillary services.
3. Voltage and frequency regulation: The ESS can absorb real power when the frequency is above nominal and inject real power into the grid when the frequency is below nominal. Similarly, ESS can absorb or inject reactive power when the voltage is above or below acceptable limits, respectively.
4. Harmonic compensation: Due to the increase of electronics loads, harmonic components have increased. Passive filters can be used to suppress these harmonics,

however, with additional capital cost. On the other hand, the ESS can be used to perform harmonic compensation.

5. Reserve: For instant response during a contingency, spinning and non-spinning reserves are essential. These reserves can be supplied by ESS. Without these reserves, power system instability can rise, which will result in involuntary load-shedding. As mentioned before quick responses from the grid is required to cope with RES ramping, and ESS can respond to such contingencies within a few cycles.
6. Black start: The ESS like pumped hydro have the capability to start-up without any external support and provide the grid with required power to start the entire grid.

1.6 The Evolution of Pumped-Storage Hydropower

The evolution of PSH configurations is targeted toward meeting the flexibility and ancillary service requirements of future power systems. These configurations have been comprehensively listed below but have been described in detail in each chapter separately.

- Conventional Pumped-Storage Hydropower (CPSH), as in Figure 1.3(a) consists of a reversible pump-turbine with a synchronous machine on the same shaft. The reversible pump-turbine acts as a turbine in one direction and a pump in the other. During the pump mode the system is a fixed load and can only be controlled by turning the unit on or off. In the turbine mode, the unit has a governor to regulate the speed and track the required power setpoint.
- Adjustable-speed Pumped-Storage Hydropower (ASPSH), as in Figures 1.3(b) and 1.3(c) consists of the same reversible pump-turbine as before. However, the electrical

machine can be either a synchronous machine interfaced to the grid with a fully-fed converter or a doubly-fed induction machine (DFIM) with a partially rated converter. Unlike CPSH, the ASPSH can be controlled in the pump mode with the help of the back-to-back converters.

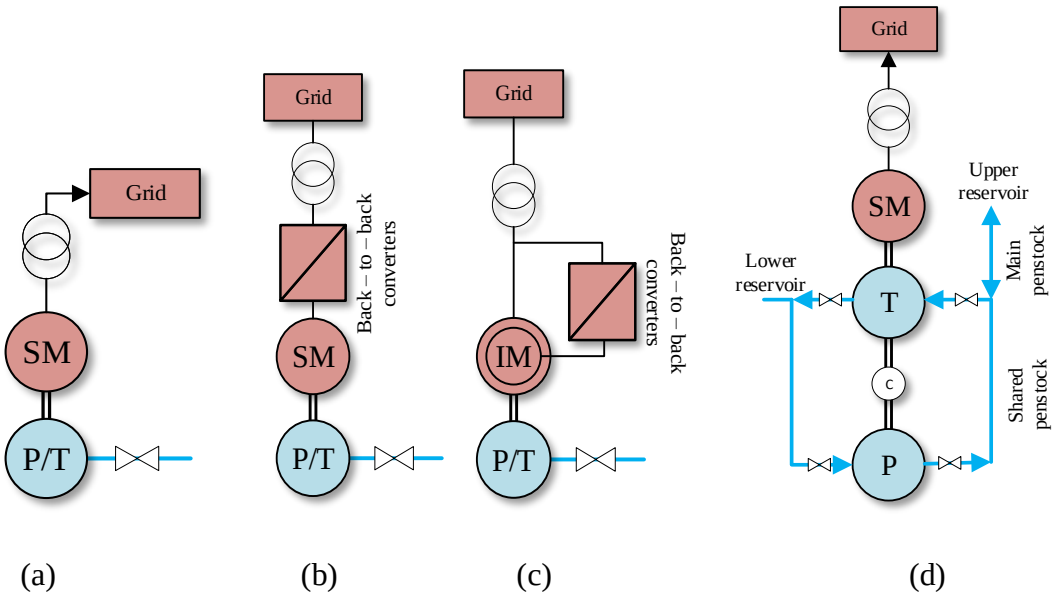

Figure 1.3. (a) CPSH, (b) synchronous machine based fully-fed ASPSH, (c) Doubly-fed induction machine based ASPSH, and (d) TPSH.

- Ternary Pumped-Storage Hydropower (TPSH), as shown in Figure 1.3(d) consists of a synchronous machine, a turbine, and a pump that are separated by a clutch in between. The configuration uses a hydraulic short circuit (HSC) or a shared penstock between the pump and the turbine to drive the turbine during the pump mode. Using this configuration, pump mode power consumption can be controlled, and a rapid mode change can be performed. Table 1.5 compares ASPSH and TPSH.
- Quaternary Pumped-Storage Hydropower (QPSH), as shown in Figure 1.4, consists of a fixed speed turbine and a variable speed pump on two separate shafts with two

separate electrical machines. The configuration implements the features of TPSH and ASPSH, namely, the hydraulic short-circuit and the back-to-back converters. The QPSH is a conceptual design and is still in the design phase. There are three main advantages of this configuration,

- The simultaneous response of the pump and turbine to any disturbance provides greater support to the network compared to a single, TPSH or ASPSH unit;
- The construction required for the elongated shaft of the TPSH can be avoided;
- The unit is more redundant as the pump and turbine maintenance can be performed separately.

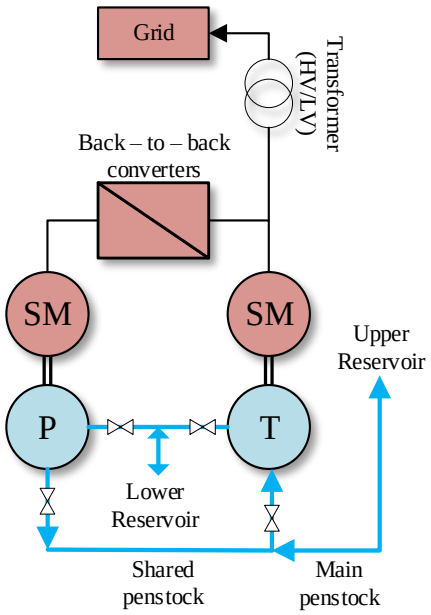

Figure 1.4. Quaternary PSH.

Table 1.5. Comparison of ASPSH and TPSH

Attribute	ASPSH	TPSH
Converter requirement	Type 1 requires converters rated 10% of the machine, Type 2 requires fully rated converters	Does not require converters for grid interfacing.
Efficiency	Peak efficiency will be reduced compared to the CPSH. Part-load efficiencies can be improved with speed variation.	Peak efficiency same as that of CPSH. Part-load efficiencies are better than CPSH as TPSH uses a pure turbine instead of pump-turbine.
Mode-change time	Time required to change from the pumping to generating mode is in the order of a few minutes.	Time required to change from the pumping to generating mode is significantly reduced. Seamless mode change can be performed as shaft rotated in a single direction.
Shaft inertia	Same as CPSH.	The shaft consists of the electrical machine and the separate pump and a separate turbine. Thus, in the hydraulic short circuit mode the shaft has comparatively more inertia.
Design optimization	The pump-turbine is optimized as a pump and then as a turbine. Thus, during off-design operating conditions as a turbine, the efficiency decreases drastically.	The pump and the turbine can be separately optimized. This leads to higher cycle efficiency.
Frequency regulation	Possible but only with auxiliary control.	Fully capable.
Natural inertia and synchronous frequency response	The converter's natural tendency is to act against grid frequency. The direction of change of speed and change of torque (and hence the current) are opposite.	Its natural tendency is to support the grid frequency, which allows the machine to slow down and release energy into the network.
Range of flexibility	Limited range of flexibility is available. Range is limited by cavitation limits and converter size.	Higher range of flexibility due to the use of a separately optimized turbine and pump.
Smooth start capability for pumping mode	Possible but only with auxiliary control.	Fully capable as the pump can be started with the turbine.
Possibility of failure	Increases as the number of components increases.	Low because the number of components is comparatively lower.

1.7 Other Forms of PSH to Overcome Geographic Limitations

Although, PSH plants are a solution to the ever-fluctuating renewable energy resources, many regions in the world do not have the geographic condition required to build a PSH. To overcome this problem, the following solutions have been devised:

1. *STENSEA* (Stored Energy in the Sea) where a tank, equipped with a pump-turbine-generator system, is placed at the bottom of the ocean bed. This structure generates electricity when filled and uses electricity to pump out water out of the system [8].
2. *Wind turbines with water storage* are a recent invention and are the only source where the two forms of energy are physically integrated. Here wind turbines pump water up their tower and into tall tanks beside them and utilize the stored energy when required [8].
3. *Gravity power modules* implement the principle of a hydraulic jack and gravity to generate electricity. A very heavy mass slides down a hole in the ground pushing water below the mass into the pump-turbine (through a narrow hole) to generate electricity. The same pump-turbine is used to pump the mass up to its initial level to store energy [10].

1.8 Scope and Contributions of this Dissertation

1. *Development of dynamic model and governor structures for ASPSH, TPSH and QPSH.* For the ASPSH system, separate governor systems for pump and generator mode operation has been constructed. A positive sequence *dq*-axis dynamic model for the DFIM is also developed. The governor models for the above mentioned PSH systems are not available in commercial or academic analytical software packages and hence need to be constructed. Mask development in Simulink for CPSH, ASPSH

and TPSH systems have been performed and is a key procedure while modeling a new device as it helps in proper parameter entry and initialization of the device model.

2. *Resilience benefit comparison and realization* through integration study of designed ASPSH and TPSH models to a single-machine-infinite-bus to observe reference tracking and 9-bus test system to perform frequency stability assessment has been performed.
3. *Development of a framework for revenue optimization* and comparison from arbitrage and regulation for energy storage systems, where the pay-for-performance scheme was used for regulation market remuneration. This framework is then used to compare the revenue earning potential of CPSH, ASPSH and TPSH considering the considering network and reserve limitations.

CHAPTER TWO

Literature Review

2.1 Grid-Scale Energy Storage Technologies

Significant effort has been dedicated to the development of modern grid-scale energy storage systems worldwide that can help realize the benefits as mentioned in Section 1.5. The following section describes a few of these devices (apart from pumped storage hydro) and their important features along with relevant literature. To limit the scope of the literature, only the following devices have been considered in the category of modern grid-scale energy storage: a) Redox flow batteries, b) Compressed air, c) Thermal energy storage, and d) Flywheels.

2.1.1 Redox Flow Batteries

A redox flow battery (RFB) stores the ionic solution outside the cell in large tanks as shown in Figure 2.1. The ionic solutions exist in two separate tanks as the anolyte and the catholyte. To generate or store electricity the electrolyte is passed through the cell stack. This stack generally consists of a membrane through which ions are exchanged, while the electrons move through an externally completed circuit. Due to this action, redox flow batteries are often referred to as a form of regenerative fuel cells. During discharge, the anolyte gives off an electron that travels through the external circuit and is collected by the catholyte. During charge, the anolyte is given back its lost electron from the external circuit and the catholyte loses its electron to the external circuit. Thus, the anolyte and catholyte undergo oxidation and reduction during their discharge, and vice

versa during charge. In [11-13], a model for simulation studies and several control system design for the RFB are presented. One key feature of the RFB is that the amount of energy stored is a direct function of the volume of electrolyte that the plant can store which can be easily scaled up by increasing the number of storage tanks, while the power capacity is a function of the size of the stack. Also, the separation of power and energy is evident in the RFB. The amount of energy that the cell can discharge only depends upon the amount of electrolyte in the stack at any moment, which is extremely small compared to the total volume of stored electrolyte. Thus, under a fault condition, only a limited amount of energy will be dissipated to the grid unlike integrated cells where the entire amount of energy is always fully connected to the network.

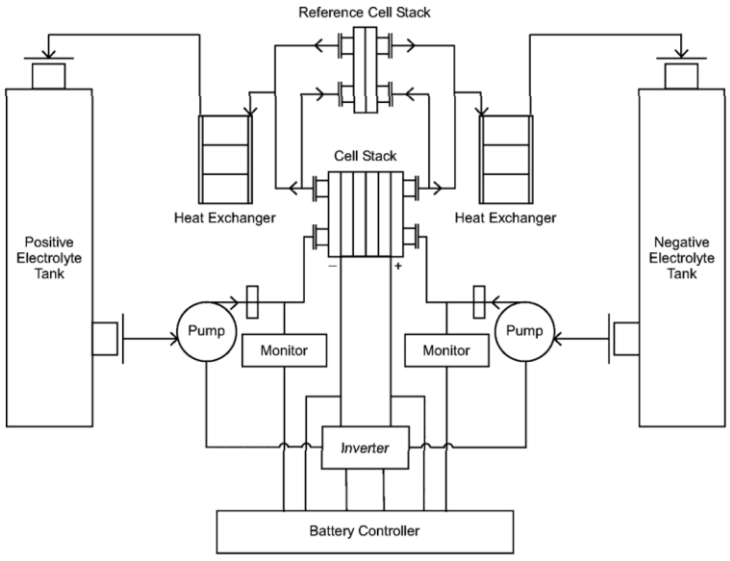

Figure 2.1. Redox flow battery energy storage system showing physical components.

2.1.2 Compressed Air Storage

A compressed air energy storage system (CAES) stores energy by compressing air at ambient pressure into high pressures tanks, underground caverns, or other

geological cavities. It discharges energy by allowing this compressed air to flow through an expander that in turn rotates the generator rotor. The expander usually burns a very small amount of natural gas to heat and expand the cold compressed air. The maximum achieved efficiency by this basic process is 42%. If the waste heat from the expander is used to heat the compressed air, the efficiency of the process can rise to 55%. By using an adiabatic process, where the heat of compression is stored to heat the cold air before the expander, results in efficiencies as high as 70%. Adiabatic CAES normally employs oil for storing the thermal energy produced during compression. Another more advanced form of this technology is the isothermal CAES with efficiencies around 80%. In isothermal energy storage, the gas is cooled as it is being compressed instead of being cooled in stages. Thus, the gas is made to follow a designed pressure-volume curve more accurately, which has been accomplished by injecting fine water droplets during compression of the gas using the reciprocating machine. In [14], a detailed model of the CAES system is presented.

2.1.3 Thermal Energy Storage with Concentrated Solar Power

By concentrating sunlight with the help of mirrors, concentrated solar power (CSP) plants produce heat which is used to produce steam which is then used to run a turbine connected to a generator. One key advantage of using CSP technology is that the heat collected during the day can be stored for several hours and hence can be used to generate power during the night. This gives rise to thermal energy storage (TES) systems. TES employs fluids that can be stored in tanks and hence can be easily scaled up by adding tanks. One of the most widely deployed fluids for heat transfer is molten salts. The amount of heat stored can be increased by using phase change materials (PCMs).

The PCMs have a high latent heat which is given off or absorbed when the PCM undergoes a phase change. Another advantage of CSP and TES are that they can be coupled with conventional fossil fuel burners to add to the amount of heat produced to generate more power [15]. Siemens Gamesa [16] is investing in thermal energy storage with packed bed technology for TES without CSP. Here energy is taken from the grid to heat up air and this heat is stored in a packed rock bed. When energy is required cold air is blown through the pack rock bed to absorb heat and generate steam. The TES technology can also be used to collect waste heat from industrial processes.

2.1.4 Flywheel Energy Storage System (FESS)

The FESS stores energy in the form of kinetic energy in a rotating mass, where the amount of energy stored depends upon the moment of inertia and the square of the speed of the rotating mass inside a protective shield as shown in Figure 2.2. The moment of inertia of the rotating mass is a function of its shape and material of construction. In most cases an induction motor, or a variable reluctance motor, or a permanent magnet motor connected to a back-to-back AC-DC-AC converter is implemented for the FESS.

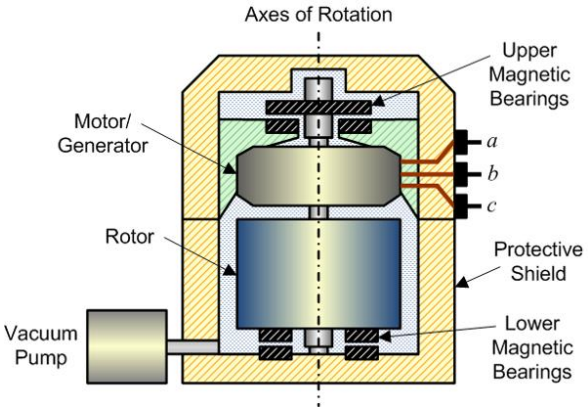

Figure 2.2. Schematic diagram of flywheel energy storage.

To realize the efficacy of FESS, bearing design has been given much importance. As such, low friction magnetic bearings have evolved to active magnetic bearings and even, superconducting magnetic bearings. To reduce drag losses, the entire motor-generator and flywheel assembly is encapsulated in a vacuum chamber. The FESS is mostly suited for pulsed power applications as they are fast acting regulators and used as spinning reserve by network operators. The dynamic modeling and control of flywheel systems has been presented in [17].

2.2 Pumped Storage Hydropower

The PSH technologies have long provided a form of valuable energy storage for electric power systems around the world. A PSH unit typically pumps water to an upper reservoir when loads and electricity prices are low, and subsequently releases the water back to a lower reservoir through a turbine when loads are high, and electricity is more expensive. The PSH is a flexible resource and its main role is to balance supply and demand in the power grid and helps integrate variable RES like wind and solar. The following sub-sections detail relevant work on CPSH, ASPSH and TPSH that have played a crucial role in shaping this dissertation.

2.2.1 CPSH

In [18], Zhang et al. investigate the optimal sizing of pumped storage hydro plant assuming investment cost in RMB/kW and later performs a sensitivity analysis of the variation of this investment cost and reservoir size. The reserve required is determined based upon the root mean square of the reserve requirement of load and wind. A penalty for curtailment is imposed and the sensitivity to this penalty is studied. The PSH operated

to cycle on a weekly basis. Operated when it is more economical than closed-cycle gas turbine or to provide the up and down reserves. The study concludes that with the increase of PSH capacity, the curtailment decreases rapidly. Increases in PSH capacity also reduces operating cost

In [19], Gioso et al. present the ability to rapidly load a Francis turbine from tail water depression mode to turbine mode to provide primary frequency regulation. In tail water depressed mode, the system behaves as a synchronous condenser. They study and verify the same using simulations and a hardware model and propose a three-stage transition mechanism to safely travel form the tail water depressed mode to the turbine mode.

Although PID controllers are popular in hydro governor applications Generalized Predictive Control (GPC) has been applied to control a multi-unit hydro power station model based on Dinowrig hydroelectric pumped hydro [20-22]. Comparison with PI control shows that that GPC offers significantly better performance across the plant's operating range. The studies consider the linearized transfer matrix of the multi-unit hydro plant indicating the cross-coupling between the units through off-diagonal and the self-terms using diagonal elements. In comparison to PI controllers, and unconstrained GPC, the constrained GPC showed superior performance compared to the unconstrained GPC and PI controllers.

In [23], Sankaramurthy et al. addressed the problem of congestion management technique using flower pollination optimization algorithm (FPA) to perform optimal rescheduling of resources. Results indicated reduction in operating cost due to the use of FPA but further reductions due to the use of PSH.

In [24], Harpman, Platt and Coberly focused on the application of evolutionary algorithms on dynamic dispatch problem for hydropower considering several system constraints. Three promising algorithms were identified, real-coded genetic algorithm, differential evolution, and particle swarm optimization. In comparison with calculus-based approaches, these approaches are slower although they usually tend to identify the region containing the global optimum very fast.

In [25], Harpman, Gaston and Steves study the application of the afore described algorithms and artificial bee colony optimization algorithm to the single unit optimization maximizing the real power, given the head which is in turn optimizing the efficiency. Secondly, they optimize a multi-unit hydro power plant where water requirement is minimized, and energy and reserve requirements are satisfied. Thirdly, they consider the hydrological impact of one plant on other plants in the same basin. Finally, types 4 and 5 describe optimal operation across a geographical region and optimal coordination of several different resources within this region, respectively.

In [26], Diniz presents test cases for hydro-thermal scheduling in both regulated and deregulated markets. Here the reservoir head is modeled as a fourth-degree polynomial of volume and discharge and the start-up cost as an exponential function of the time the unit has been off. Further he presents how the hydro-thermal scheduling problem can be formulated and what types of constraints to consider. He also specifies the location of the hydro units and thermal units, initial data of thermal and hydro units, and a load curve for the entire system for a period of 24 hours and other data for 24-bus, 57-bus, 118-bus and 300-bus systems.

In [27], Arroyo and Conejo present a mathematical method of representing the start-up and shut-down trajectories as constraints for optimization problem. They highlight the increase in computational time required to evaluate the constraint and increase in variables, but also highlight the effect on scheduling results.

In [28], Chazarra, Perez-Diaz and Garcia-Gonzalez present a mixed integer linear programming model for the hourly arbitrage and regulation reserve scheduling of the ASPSH system in the Iberian electric power system. The work considers the effect of the back-to-back converters with synchronous machines and asynchronous machines and with and without the back-to-back converters in the generating mode. Results indicate that ASPSH can increase the revenue of the plant significantly and that the regulation market is the main source of income for the ASPSH. Also, it was concluded that the DFIM-based ASPSH can earn more revenue compared to the synchronous machine based ASPSH. Moreover, if the converter is bypassed, higher day-ahead revenue from arbitrage is expected.

2.2.2 DFIM-based ASPSH

The power output of the plant depends upon the time required to adjust the wicket gates. The doubly-fed induction machine (DFIM) converts hydropower to electricity where a major fraction of the power is delivered from the stator. The rotor recovers or supplies the slip power. A slip of $\pm$30% is sufficient for the PSH application [29, 30]. A DFIM-based hydro generating plant is stable as simulations have shown that in the event of a three-line to ground (3LG) or a single-line to ground (SLG) fault the machine recovers to its steady-state power after the fault is cleared.

Starting up large motors and generators is often a critical task and may affect the network or plant. Constant voltage/frequency (V/f) based smooth-starting strategy is implemented for starting large DFIM-based pumps in [31] from the rotor-side converter (RSC). The stator windings are shorted and the grid side converter (GSC) controls the DC-link voltage. The RSC under post starting condition transitions from constant V/f control to stator-flux oriented control with the stator connected to the grid to ensure decoupled control of speed and reactive power. Starting DFIM from the low voltage side of the machine reduces the converter voltage rating. The constant V/f smooth-starting algorithm for smooth starting of a large DFIM-based pump-turbines in pumping mode has also been studied in [32]. Here it was mentioned that when the rotor reaches synchronous speed or >90% of the synchronous speed, the machine is synchronized and connected to the grid. Also, at this speed the control mode changes from V/f to vector control after the machine is synchronized.

In [33] along with the constant V/f algorithm a regenerative braking algorithm has also been devised. It was stated that the reversible pump-turbine can be reversed from maximum pumping load to maximum generation within 750s. Also, a point to note would be that the injection of power begins even before stopping due to the regenerative braking.

Dida and Benattous in [34] present a detailed model of the DFIG including a system of differential equations. The proportional-integral (PI) control system design is elaborated with the linear block diagrams. Later better control of the DFIG-based wind turbine (WT) was achieved by augmenting the inner-loop PI controllers with Fuzzy proportional-derivative (PD) controllers. Also, they have completely replaced linear PI controllers of the speed control loop and replaced them with fuzzy PD controller.

In [35], Schlunegger and Thoni elaborate their experience of a multi-unit TPSH plant operation and realize the difficulty in providing regulation with generation mode during winter with low inflow. To provide regulation during off-peak hours, the ability to operate during peak-load hours is reduced. As a solution one synchronous machine was modified to be interfaced with the grid through a fully fed converter. However, they do not consider the generation mode with converter as they remark that the converter losses would be large, which is agreeable as the size of the converter is equal to the machine rating. However, they do not consider hydraulic short-circuit either due to hydraulic transients.

In [36], Koritarov et al. provide the schematic for the control of ASPSH in the pump and generation mode. The generator mode with turbine governor-based speed control and converter based active power control is presented. Here the gate is used as a pump-mode control variable but can produce significant throttling losses.

In [37], Mishra et al. aim to improve the small signal stability of DFIM-based WT and provides a detailed model of the DFIM. Here the controllers are tuned by implementing bacterial foraging for all controller tuning to increase damping. The controller design also implements an angle control scheme used to provide damping to the system low-frequency oscillations.

In [38], Wu et al. aim to improve the small signal stability of DFIM-based WT and provides a detailed model of the DFIM. Here the PSO was implemented for all controller tuning with the objective of minimizing all eigenvalues to increase stability. The tuned controllers were used in a single-machine infinite-bus (SMIB) system analysis

and Kundur's 2-area system. Results show that the optimized controllers are better than the original controllers in terms of oscillation damping, tracking and regulation.

In [39], Harbort, Lein, and Goede presented the theoretical evaluation of variable speed operation and efficiency improvement for different hydraulic turbines. The results showed that a maximum of 20% improvement in efficiency is possible for Francis turbines in generation mode. However, very limited pump mode speed variability range is observed and hence, gain in efficiency in pump mode is also limited. Instead of efficiency enhancement in pump mode the benefit of using the ASPSH is the ability to provide pump mode regulation. This work also provides a governor structure for adjustable speed operation in turbine mode but does not provide much details about pump mode operation.

2.2.3. TPSH

A preliminary model for the TPSH is provided by Koritarov et al. [40], where the turbine model consisted of a PID governor and employed droop based on either speed or gate position. The gate dynamics included servo dynamics with non-linearities in a look-up table. This report also presents a model pump and suggests the variation of the model where the static head is replaced by the pump head which can be a function of flow and speed deviation. The gate is fixed at a certain position for pumping. However, the response of the system to disturbances was not shown and mode interchange was not shown either.

In [41], Nicolet et al. present a detailed modeling of wind, thermal and TPSH along with control systems. However, the TPSH model was not detailed enough for simulation purposes. The TPSH is used to compensate for the fluctuations in wind energy in the network by adjusting turbine inlet in pump mode through the hydraulic short-

circuit. For a large frequency transient, the mode change of the TPSH is presented but in a vague manner. It was concluded that with hydraulic short-circuit capacity, the TPSH compensates for wind fluctuations and with mode change capability the system is greatly benefited during a sudden wind farm shutdown.

2.3. Policy and Economics

Fair remuneration mechanism for energy storage systems is of great importance. To remunerate these grid-scale energy storage devices in a fair manner, the U.S. Federal Energy Regulatory Commission (FERC) has ordered independent system operators (ISOs) to make necessary changes to their markets. In 2007, FERC issued order 890 to ensure the fair and equitable participation of non-generation resources in the markets [42]. The FERC issued order 755 in 2011 and order 784 in 2013, which required independent system operators/regional transmission operators (ISO/RTO) to compensate resources for their frequency regulation services [43, 44]. In 2018, FERC issued order 841, which requires ISO/RTO to establish market rules and tariffs that, recognizing the physical capabilities and limitations of the energy storage sources, allows the participation of storage in the RTO/ISO markets [45]. To comply with these orders, most ISOs have introduced two main revenue streams, arbitrage and Regulation for energy storage systems.

Arbitrage exploits the advantage of the difference in cost of energy during different parts of the scheduling period. Periods of low demand, such as the weekends, produce low price energy and hence an opportunity to buy energy. Periods of peak demand during the weekdays provide the best opportunity to sell energy. The regulation market generally offers payments in two components, the capacity payment and mileage

payment. Capacity payments remunerate the unit for the capacity reserved for regulation, while the mileage payments remunerate the unit for regulation provided or reserve used. The “pay-for-performance” scheme also evaluates quality with which the mileage (or movement) was provided (speed and accuracy).

Recently FERC enacted order 755 according to which all ISOs are recommended to provide performance-based credits that will award fast acting plants. The new scheme of payment is called the pay for performance scheme wherein, the accuracy and with which a plant responds to the automatic generation control (AGC) signal is credited by a governing equation. Pay for performance accounts for the regulation capacity (also rewarded for previously), regulation millage (also rewarded for before) and the performance factor. This new scheme introduces a performance factor which (ranging from 0 to 1) that is multiplied with the net payment. The AGC regulation (Reg) signals in many ISOs are now divided into two categories, RegA (the fast component of the AGC signal) and RegD (the remaining slow component of the AGC signal). Energy storage systems like the current flywheel and battery systems can respond to RegA [46].

In [47], Nguyen et al. optimize the revenue that the energy storage can earn from Midcontinent Independent System Operator (MISO) considering its performance-based compensation and elaborate a generalized framework for performance evaluation of energy storage. This work considers historical nodal prices but does not consider the effect of storage on the nodal prices. Problem is formulated as an LP optimization problem, providing 2 models for optimization: a) arbitrage only, and b) arbitrage + regulation. However, this work describes how performance of different technologies can be classified. A ratio of output to input over several signals is considered and used for

proportional remuneration. Most importantly the revenue is much higher when participating in regulation market for flywheel type energy storage devices.

Similar to [47], Byrne, Concepcion, and Silva-Monroy [48] optimize the revenue that the energy storage can earn from Pennsylvania-New Jersey-Maryland (PJM) ISO considering its performance-based compensation. Similar conclusions are supported by Byrne and Silva-Monroy [49], where a performance-based scoring mechanism is not used. Instead, the fraction of activated to reserved capacity in upward and downward directions are calculated using historical regulation signal data. It was concluded that even without the use of performance measures, regulation market adds significant revenue to the storage system and the system is found to be participating in the regulation market most of the time.

In [50], Fong, Moreira and Strbac perform a similar analysis but for the Great Britain's (GB's) energy market. The revenue and pay-back periods for battery energy systems were analyzed considering arbitrage, frequency regulation, reserve and other network services as revenue streams in the GB market individually and together. While considering a price taker model, they conclude that participation in multiple services increases revenue of the storage system while frequency regulation service brings in the most revenue. While a combination of services can provide payback in 10 years, frequency regulation and arbitrage can do so in 12 years and frequency regulation alone in 18 years. With batteries there is always a risk of recovering the CAPEX and OPEX within the lifespan of the batteries but participating in multiple network services reduces such risks. From a PSH perspective, this risk can be naturally averted to a great extent if PSH is considered.

Zakeri and Syri [51] clarify that, arbitrage is a small fraction of the other services that energy storage systems can offer. Consequently, arbitrage earns a very small fraction of the revenue that could be generated by participating in ancillary services market.

In [52], Ahmed et al. consider a production costing simulation with and without a PSH. This indicated a benefit/cost ratio ranging 1.27~1.33 with a payback period of 18-21 years. When monetary value of ancillary services included, the benefit/cost ratio increase to be around 1.4~1.6 and the payback periods is reduced to about 10 years.

In [53, 54], Filipe et al. have analyzed the profit from arbitrage and regulation from a variable speed PSH in the Iberian Peninsula power market and more specifically in the Portugal region. They implement a short-term optimization for a period of one week to determine the optimal revenue for frequency regulation and arbitrage. The quality of performance is not considered but the ratio of activated to allocated reserve capacity is considered for remuneration. In pay-for performance terms, the performance is not remunerated but the mileage is. Like previous studies in [47-51], they conclude that the participation in regulation market more than doubles the amount of revenue earned; however, it does not affect the reservoir levels significantly as the regulation signals have zero mean.

In [55], Aburub, Basnet and Jewell used ASPSH to reduce emissions in the Western Electricity Coordinating Council (WECC). The study resulted in reduced emissions of CO2 by reducing the operational hours of gas turbines in the presence of wind energy for the purpose of load following. Also, the placement algorithm suggested a location closer to the renewable generation location.

In [56], Hozouri et al. discuss energy cost minimization, revenue maximization, renewable curtailment minimization, transmission expansion cost minimization, and optimal placement of the PSH units. They consider the IEEE RTS-24 network, MATPOWER for OPF and non-dominated sorting-based genetic algorithm (NSGA II) to arrive at multiple solutions that might be partially optimal. A fuzzy decision-making framework is implemented to arrive at a single solution thereby converting multi-objective optimization to a singular result. The work shows the application MATPOWER for the problem and the use of locational marginal price (LMP) for revenue calculation and that fuzzy inference systems could be used to reduce problem objectives.

Salevid [57] examines the profitability of PHES form arbitrage market and use historical data to find two price limits, one above which the plant generates and the other below which the plant acts as a pump. These prices are determined by an iterative method on a two-week basis based on an LMP forecasting model.

Combining RES with ESS is a great option, which however, requires significant initial investment. The combination of the two can have two main motives, minimize variations around predicted or bid hourly average output and maximize profit from day-ahead and hour ahead markets. Results from the comparison of PSH and BESS based combination with wind farms [58] suggest that optimized PSH schemes show better economic performance as BESS are limited to short discharge cycles. Conventional PSH plants respond slower than BESS and have lower roundtrip efficiency. This work, however, does not consider the AS version of PSH.

2.4 Dynamic Modeling and System Integration Studies and Controls

The virtual synchronous generator (VSG) mimics the frequency and voltage response of a synchronous generator through the controls of an inverter connected to the grid. Generally, P-f and Q-V droop characteristics are used to emulate the primary frequency and voltage response of a synchronous generator. The key idea is to generate real and reactive power references for the inverter which interfaces the RES or the ESS to the grid. These references are the output of the droop characteristics that represent a proportional relation to the deviation of frequency. Often a derivative of the frequency deviation is also added with a suitable gain alongside the proportional term [58] which replicates the inertia of the synchronous generator.

In [60], You et al. examine the benefits of two control strategies (P-f droop and rate of change of frequency (ROCOF)-based step response) deployed with two different types of devices (high energy devices like supercapacitors and flywheels and high power devices like PSH) in the electricity reliability council of Texas (ERCOT) system under different levels of renewable penetration. A dynamic simulation of the ERCOT system and other dynamic models was performed in PSS\E (Power System Simulation for Electromagnetic transient analysis by Siemens). It was concluded that the devices are most efficient in frequency support. The battery-based devices will die out within a short period of time and produce a second frequency dip, whereas the PSH systems have the ability to provide sustained support until secondary control re-adjusts generator set-points.

In [61], Hwang et al. focus on developing a ROCOF based adaptive droop scheme. To determine the appropriate amount of droop based on wind conditions is a

difficult task. Thus, they have proposed to use a droop which is a function of the ROCOF. As a result, the initial release of kinetic energy is large due to the large initial ROCOF but decreases as the ROCOF decreases.

In [62], Zhu et al. reveals that during the initial disturbance, the ROCOF loop is dominant, whereas around the frequency nadir the droop loop is dominant. Therefore, the combination of the two loops is effective in supporting the frequency, because both loops can mutually compensate the drawback of each loop. This dynamic droop-based inertial control scheme aims to (1) improve the frequency nadir (FN) without negatively impacting a power grid after the frequency rebound, and (2) ensures stable operation of a DFIG. The results of the two cases indicate that the proposed scheme can raise the FN more than the fixed scheme with the different wind conditions. the proposed scheme dynamically changes the droop to release a large amount of kinetic energy (KE) during the initial stage of a disturbance.

CHAPTER THREE

Modeling and Control of Adjustable Speed Pumped-Storage Hydropower Units

3.1 Introduction

With increase in renewable penetration, a more flexible power system is in demand. Due to the volatility of renewable energy resources and growing sizes [63] of solar farms, rapid ramping of conventional thermal plants is required which is not feasible due to thermal stress and physical limitation of materials. Energy storage is one solution to this problem and pumped-storage hydropower (PSH) is the most matured form of grid connected energy storage. The PSH plants provide great ramping capabilities without cycle limitations. However, conventional fixed speed PSH plants suffer from major drawbacks, such as (i) inability to generate power over a full range, (ii) reduced efficiency at partial load, (iii) lack of regulatory control during pumping [64], and (iv) slow response during generation mode. Also, almost all PSH units around the world are mainly fixed speed and employ a synchronous machine.

The above stated drawbacks of fixed speed operation can be overcome by transforming the fixed speed plant to a variable speed plant and given the fact that most plants are significantly above their half-life, variable speed machines would be a great option to consider. This chapter focuses on the generating and pumping mode of the PSH. A PSH while pumping is a significant load on the power system. If the PSH facility is DFIM-based plant, the converters can be used to control its power or speed and respond

to the changes in frequency and provide significant contribution unlike synchronous machines that are fixed loads.

Frequency disturbances result from the imbalance between generated and consumed power. System operators maintain balance by supplying generation reference commands for generating plants in intervals of 5 to 30 minutes. This interval varies from one system operator to another throughout the world. However, within this interval the generating plants will have to control the frequency locally. System inertia is the first to respond to change in frequency and hence larger system inertia aids to reduction of the rate of change of frequency (ROCOF). Conventionally, this is then followed by the action of the droop controller (primary frequency control) that arrests the decrease or increase in frequency. The plant's secondary or supplemental control then restores the speed or frequency to nominal speed. With the decommissioning of synchronous generators (SGs) in conventional power plants, system inertia is reduced which will in turn lead to higher

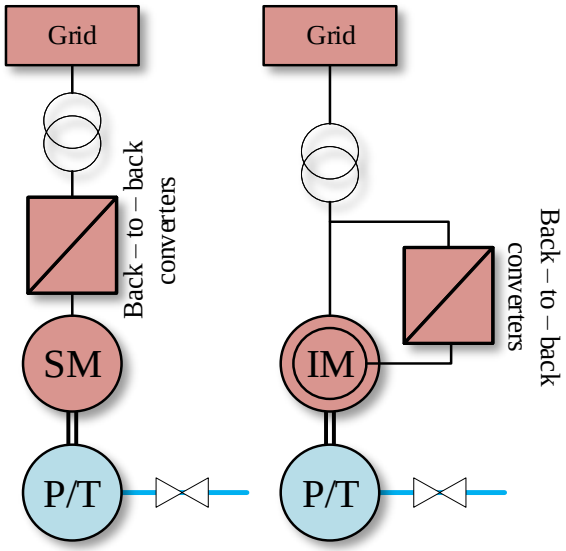

Figure 3.1. Configurations of ASPSH: a) fully fed synchronous machine-based system and b) DFIM-based system.

ROCOFs and lower nadirs [65]. Simultaneously, the decommissioning of SGs will lead to removal of their primary and secondary control schemes, which will further worsen the scenario.

Two possible configurations of the adjustable-speed PSH (ASPSH) exist. Configuration (a) in Figure 3.1 is where the synchronous machines are driven by full capacity rated back-to-back converters. Here, the size of the back-to-back converter is equal to that of the machine and is therefore a financial limitation for large multi-unit plants. Thus, configuration (b) in Figure 3.1 is the variable-speed pumped hydro deploying DFIM with rotor side converter with rating of 10%-30% of rated power of the machine as a feasible solution [64]. Additionally, the use of ASPSH facilitates rapid set-point tracking, which is not possible with conventional PSH systems as ASPSH governors and back-to-back converter decouple the mechanical and electrical systems to a certain extent.

This chapter displays the modeling, controller development and network integration aspects of ASPSH. Sections 2 and 3 show the governor models and hydraulic dynamics models of ASPSH and Sections 4 and 5 show the modeling and controller development of DC link and the DFIM. Section 6 displays the results of integration of aforementioned systems into an SMIB system. Section 7 explains the integration of ASPSH into the 9-bus test system and Section 8 displays an adaptive droop-based control of the ASPSH system.

3.2 Generator Mode Model

3.2.1 Turbine Hydraulic Dynamics

The penstock is modelled assuming an incompressible fluid and a rigid conduit of length L and cross-section A [66]. From the laws of momentum, the rate of change of flow in the conduit is given by

$$dQ / dt = \left[1 - h - h_l\right] / T_w \tag{3.1}$$

where, h_l is the head loss due to friction, *h* is head at turbine admission, in per unit (pu). The head at the inlet (or static head) of the penstock is 1pu. Usually, the static head of the plant remains fixed or varies very slowly and hence is not the subject of dynamic studies of power systems. However, if required, the model can simulate the effect of operating at a different static head. These quantities have been normalized by the maximum head, h_{base} . For pump mode operation, (3.1) is augmented with a negative sign. The water time constant, T_w, is defined as

$$T_w = LQ_{base} / \left(Ah_{base} g\right) \text{ s} \tag{3.2}$$

where Q_{base} is chosen with the turbine gates fully open (*G*=1), and *Q* is usually defined as a function of head, *h*, and gate *G* opening as

$$Q = G\sqrt{h} \tag{3.3}$$

Finally, the mechanical power developed by the turbine is given through

$$P_m = A_t h\ (q - q_{nl})\ - DG\Delta\omega \tag{3.4}$$

where A_t is the turbine power coefficient, q_{nl} is the no-load discharge, *D* is the damping coefficient, *G* is the gate opening, and $\Delta\omega$ is the deviation in speed. Note that the second

part of (3.4) is responsible for the reverse response characteristics and is a non-linearity that depends on the operating point, i.e., the gate opening.

3.2.2 Generator Mode Governor Modeling

The governor of the ASPSH system performs the function of a) speed tracking, b) power tracking, and c) primary frequency support. As shown in Figure 3.2 the optimum speed for the required power output and the operating head is given by the manufacturer and can be retrieved from a look-up-table at any instant. This optimum speed is tracked by the governor's proportional-derivative-integral (PID) controller by increasing or decreasing the gate opening G^* to the turbine and hence controlling the mechanical power produced. The primary frequency regulation is produced by the droop controller.

$$\Delta P = -\left(f_{nom} - f \right) / R_p \tag{3.5}$$

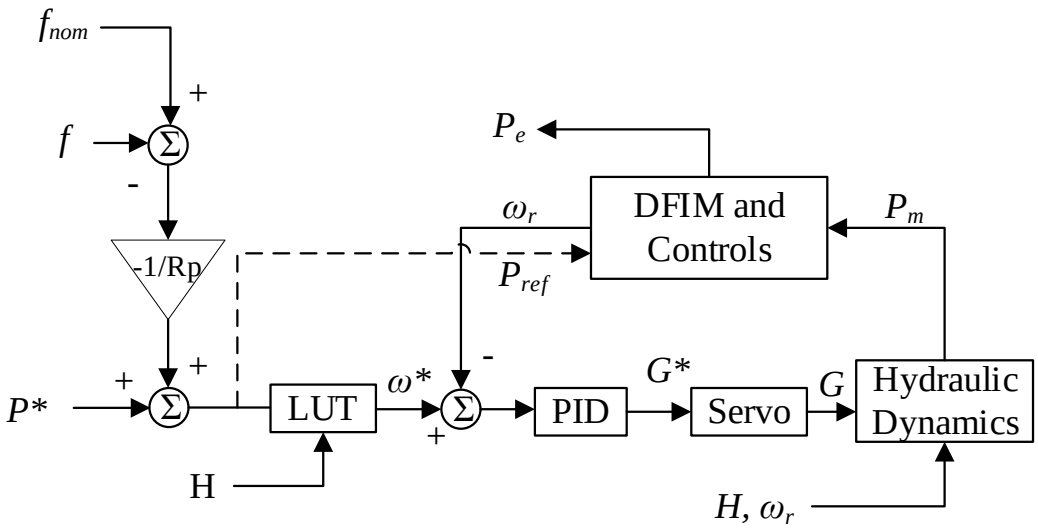

Figure 3.2. Generator mode governor diagram.

where, ΔP is the primary frequency regulation signal that is added to the reference power, R_p is the permanent droop which is usually set to 5% and, f_{nom} and f are the nominal and present system frequency, respectively.

3.3 Pump Mode Model

3.3.1 Pump Mode Hydraulic Dynamics

In pump mode the discharge produced by the pump-turbine is a function of the speed and head. Thus, (3.3) in the governor model of the turbine needs to be reframed as discharge needs to be a function of head and speed. By fitting the manufacturer-given characteristics, the relation between head and discharge of the pump is given by [67]:

$$H = A - BQ^{1.75} \tag{3.6}$$

where, H is the head, Q is the discharge of the pump, and A and B are the coefficients of fitting. Usually the mathematical equation relating head, discharge and efficiency are not exclusively given by the manufacturer but can be deduced from the characteristics and affinity principles. We know that,

$$\frac{Q}{Q_o} = \frac{n}{n_o} \tag{3.7}$$

and,

$$\frac{H}{H_o} = \left(\frac{n}{n_o}\right)^2 \tag{3.8}$$

Here, Q_o, H_o, and n_o are nominal discharge, rated head and synchronous speed at rated power. Thus, (3.6) can be transformed to

$$H = A\left(\frac{n}{n_o}\right)^2 - B\left(\frac{n}{n_o}\right)^{0.25} Q^{1.75} \tag{3.9}$$

$$P_m = A_t H \ (q - q_{nl}) \ - DG\Delta\omega \tag{3.10}$$

which now relates the discharge to the head and speed. Equation (3.9) is used by the model to calculate the head instead of (3.3) in the generator mode operation because (3.3) is not a function of speed. Equations (3.1) is negated and used to model the rate of discharge and (3.10) power consumed in the pump mode. Here, the governor does not have a gate controller as the gate is considered to be fully open to prevent any loss of energy.

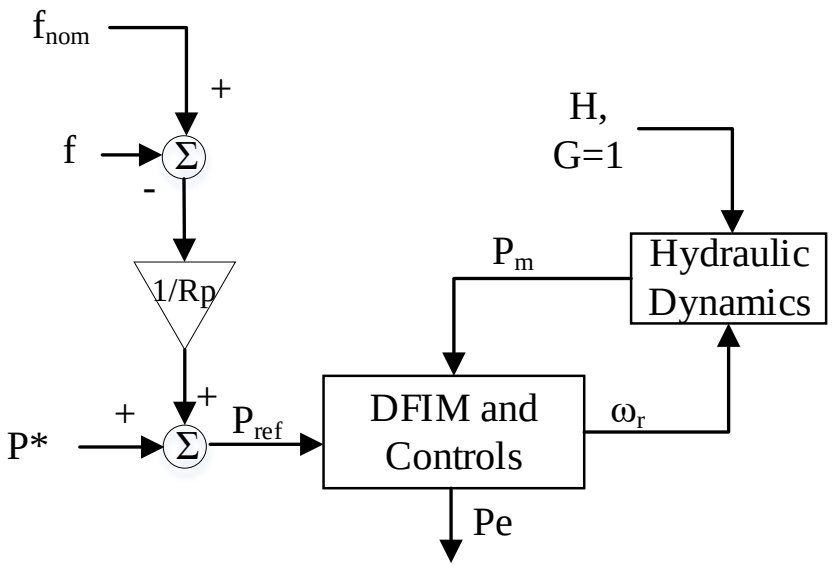

Figure 3.3. Pump mode governor diagram.

3.3.2 Pump Mode Governor Modeling

Note, the main function is pump mode regulation instead of efficiency tracking. The reference power is tracked by the PI controllers of the RSC of the DFIM. The hydraulic dynamics reflect the mechanical power and speed that would be required to

operate under the present head conditions. This governor structure assumes a completely open gate or $G = 1$, as shown in Figure 3.3.

3.4 DC-Link Modeling and Control

3.4.1 DC-Link Modelling

The mathematical model of DC-link capacitor in Figure 3.4(a) is commonly modeled as an integrator and is given by

$$V_{dc}(t) = \frac{\left(P_{ac\_grid\_conv} - P_{ac\_rotor\_conv}\right)/V_{dc}(t-1)}{sC} \tag{3.11}$$

where,

$$P_{ac\_grid\_conv} = V_{dg} i_{dg} + V_{qg} i_{qg} \tag{3.12}$$

$$P_{ac\_rotor\_conv} = V_{dr} i_{dr} + V_{qr} i_{qr} \tag{3.13}$$

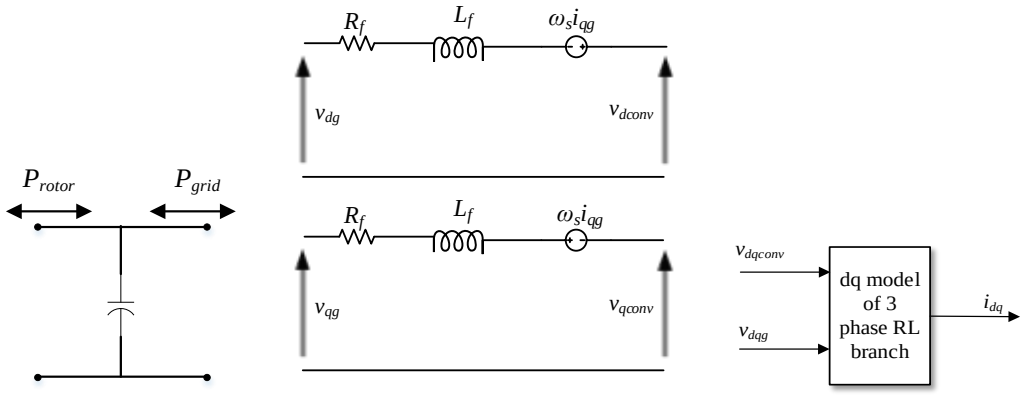

(a) (b) (c)

Figure 3.4. a) DC-link capacitor, b) inductive filter model in *dq*-axis, and c) simulation model of the filter showing inputs and outputs.

Here, V_{dc} is the DC-link voltage. $P_{ac\_grid\_conv}$, V_{dg}, i_{dg}, V_{qg}, and i_{qg} are the power exchanged grid-side converter, the grid-side *d*-axis voltage, *d*-axis current, *q*-axis voltage, *q*-axis current, respectively; $P_{ac\_rotor\_conv}$ is the power exchanged by the rotor side converter; and V_{dr}, I_{dr}, V_{qr} and I_{qr} are the grid-side *d*-axis voltage, *d*-axis current, *q*-axis voltage, *q*-axis currents, respectively.

To maintain a constant DC-link voltage, the power exchanged with the grid and that with the rotor converter must be equal. This task is achieved with the help of the grid-side-converter (GSC). The GSC exchanges power with the grid through the inductive filter.

3.4.2 Inductive Filter Modelling

Considering the *dq*-axis model of the inductive filter from Figure 3.4 (b), we have

$$v_{dg} - v_{dconv} = R_f i_{dg} + L_f \frac{di_{dg}}{dt} - \omega_s L_f i_{qg} \tag{3.14}$$

$$v_{qg} - v_{qconv} = R_f i_{qg} + L_f \frac{di_{qg}}{dt} + \omega_s L_f i_{dg} \tag{3.15}$$

Here, v_{dconv}, R_f and L_f, are converter side d-axis voltage before the filter, filter resistance and inductance, respectively. The simulation of the filter is performed with the inputs as v_{dqg} and v_{dqconv}. The differential equations are then solved to determine the resulting *dq*-axis currents as in Figure 3.4(c).

3.4.3 Grid Voltage Oriented Vector Control of DC-Bus Voltage

To decouple the control of real and reactive power via converter, the grid voltage is assumed to be oriented or aligned with the *d*-axis at all times as shown in Figure 3.5.

To achieve this, the angular distance between the *d*-axis and the positive sequence grid voltage vector is determined and set to zero. The positive sequence voltage is given by

$$V_1 = \frac{1}{3}\left(V_a + aV_b + a^2V_c\right) = |V_1| \angle \theta_{V1} \tag{3.16}$$

where V_a, V_b, and V_c, are instantaneous phase voltages and $a = 1\angle 120^o$. Orienting the grid voltage vector to the *d*-axis yields

$$|V_1| \angle \theta_{V1} \underset{grid\ voltage\ orientation}{\Leftrightarrow} |V_1| \angle 0$$

$$|I_1| \angle \theta_{I1} \underset{grid\ voltage\ orientation}{\Leftrightarrow} |I_1| \angle \left(\theta_{I1} - \theta_{V1}\right)$$

With this assumption, the *d*-axis component of the voltage equals the positive sequence magnitude $|V_1|$ and v_{qg} equals 0. With this orientation, both real and reactive power can be calculated as:

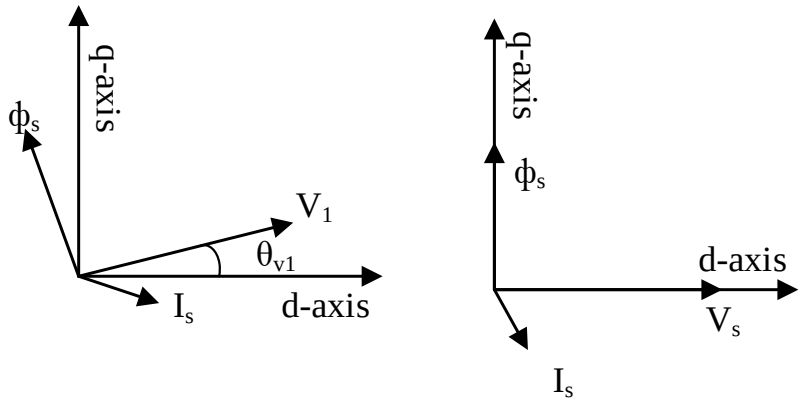

(a) (b)

Figure 3.5. Transformation from normal conditions to grid voltage orientation: a) before, and b) after the transformation.

$$P_g = \frac{3}{2} Re\left\{ v_g i_g^* \right\} = \frac{3}{2}\left[v_{dg} i_{dg} + v_{qg} i_{qg} \right] = \frac{3}{2}\left[v_{dg} i_{dg} \right] \tag{3.17}$$

$$Q_g = \frac{3}{2} Im\left\{ v_g i_g^* \right\} = \frac{3}{2}\left[v_{qg} i_{dg} - v_{dg} i_{qg} \right] = \frac{3}{2}\left[-v_{dg} i_{qg} \right] \tag{3.18}$$

Thus, due to the orientation, the decoupled control of P_g and Q_g possible by controlling i_{dg} and i_{qg} separately.

However, the filter characteristics also need to be compensated for, as the filter will cause additional losses and delay. This gives rise to cascaded control of a power converter shown in Figure 3.6.

The external proportional-integral (PI) controller regulates the DC bus voltage by controlling the power exchanged from the grid, while the internal loop compensates for the filter characteristics and ensures that this amount of power is taken from or given to the grid. The PI controllers are then tuned for required conditions assuming proper compensation. In order to tune the PI controllers first, the process transfer function is obtained from (3.14) and (3.15) as

$$\frac{i_{dg}}{\left(v_{dg} + \omega_s L_f i_{qg} \right) - v_{dconv}} = \frac{1}{sL_f + R_f} \tag{3.19}$$

$$\frac{i_{qg}}{\left(v_{qg} - \omega_s L_f i_{dg} \right) - v_{qconv}} = \frac{1}{sL_f + R_f} \tag{3.20}$$

With proper compensations the transfer functions can be further simplified to,

$$\frac{i_{dg}}{v_{dconv}^*} = \frac{1}{sL_f + R_f} \tag{3.21}$$

$$\frac{i_{qg}}{v_{qconv}^*} = \frac{1}{sL_f + R_f} \tag{3.22}$$

The compensation is an essential part of the control schematic as (3.14) and (3.15) reveal the mutual coupling between the voltage and current of two axes. However, the compensation terms can be dealt with, in a feedforward manner as all of its components are known as shown in Figure 3.6, as

$$v_{dcomp} = |V_1| + i_{qg}\omega_s L_f \tag{3.23}$$

$$v_{qcomp} = -i_{dg}\omega_s L_f \tag{3.24}$$

The DC bus is interfaced with the grid through the converter and filter arrangement, while on the other hand it is also connected to the rotor side converter of the DFIM. To supply the rotor currents at the required rotor voltage, the DC bus voltage must be maintained within a margin of +15%.

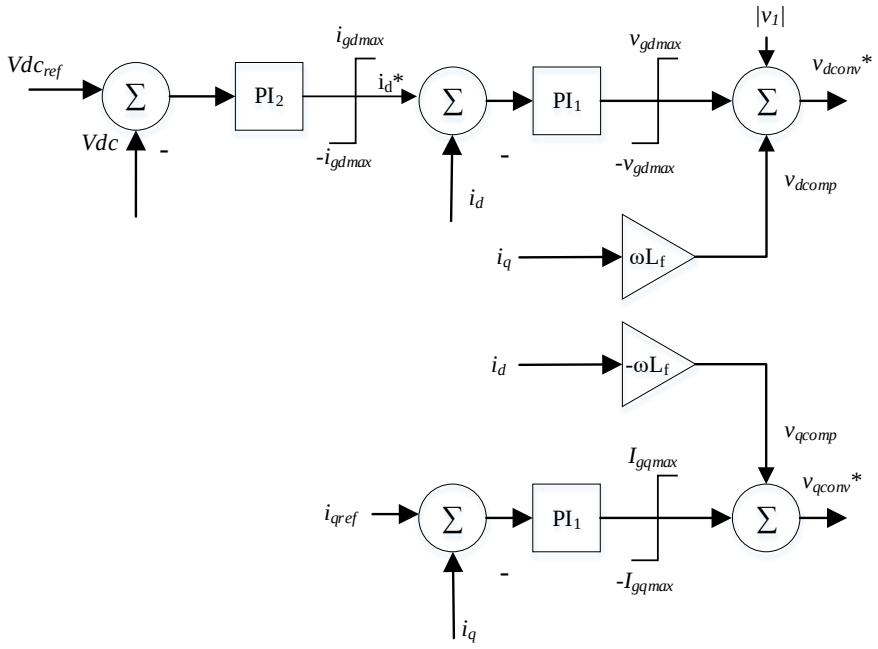

Figure 3.6. Schematic layout for actual implementation of Grid voltage-oriented control of DC bus voltage.

3.4.4 Tuning PI Controllers

If the compensation term or the cross-coupling between the *d* and the *q*-axis is ignored, the process diagram for the GSC can be reduced to Figure 3.7(a) where PI1 is the PI controller that performs current reference tracking and the second PI controller or PI2 tracks the DC reference voltage. The PI2 generates the reference current for PI1 and PI1 produces the voltage required to exchange power with the grid through the inductive filter.

The proportional and integral gains can be chosen in many ways. Here, pole zero cancelation has been used to design the PI controller. Consider, PI1 first, with proportional and integral gains as K_{p1} and K_{i1}, respectively. Identical gains are used for the d and q axis. The open loop process in Figure 3.7(b) can be given by,

$$\frac{i_{dg}}{v^{*}_{qconv}} = \left(K_{p1} + \frac{K_{i1}}{s} \right) \frac{1}{sL_f + R_f} \tag{3.25}$$

$$= \frac{K_{p1}\left(s + \frac{K_{i1}}{K_{p1}} \right)}{s} \frac{1/L_f}{s + R_f / L_f} \tag{3.26}$$

If, $\frac{K_{i1}}{K_{p1}} = R_f / L_f$, the pole and zero cancel out. Closing the loop with the remaining we have,

$$\frac{i_{dg}}{v^{*}_{qconv}} = \frac{1}{sL_f / K_{p1} + 1} \tag{3.27}$$

Next, we choose the close loop time constant as

$$\tau_i = \frac{L_f}{K_{p1}} \geq 3\tau_{conv} \tag{3.28}$$

With K_{p1} from the above equation and R_f and L_f as known parameters of the filter, K_{i1} is calculated. For the outer loop, only a proportional gain K_{p2} is calculated as the DC-link capacitor, C itself acts as an integrator. A very small integral gain is selected on a trial and error basis. From the Figure 3.7(c) we have,

$$\frac{V_{dc}}{i_{dg}^{*}} = \frac{K_{p2}}{sC} \tag{3.29}$$

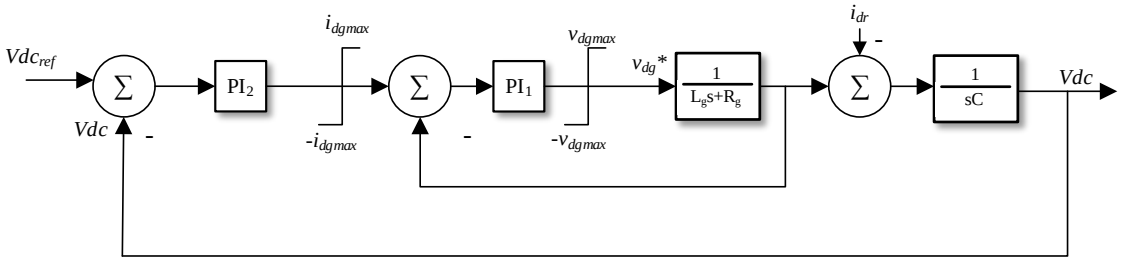

(a)

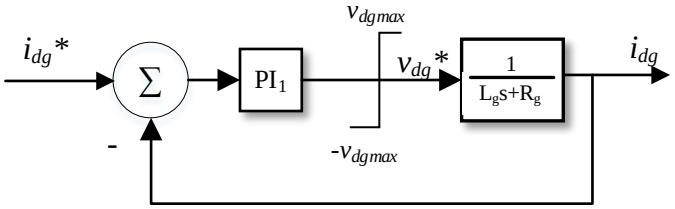

(b)

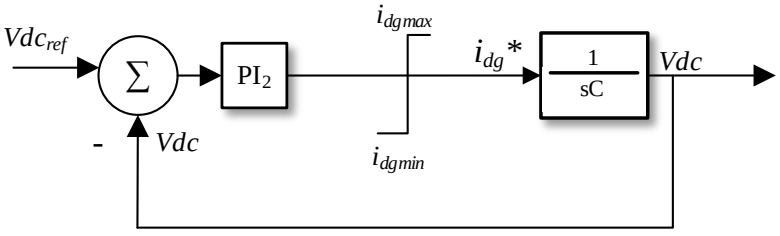

(c)

Figure 3.7. DC bus voltage regulation schematic assuming proper compensation used for tuning the PI controllers.

Closing the loop we have,

$$\frac{V_{dc}}{i_{dg}^{*}} = \frac{1}{1 + sC / K_{p2}} \tag{3.30}$$

Also, we assume that the inner loop or the current control loop is much faster than the outer loop. K_{p2} is chosen such that,

$$C / K_{p2} \geq 3\tau_i \tag{3.31}$$

where, τ_i is the previously chosen time constant of the inner loop.

3.5 Modeling of DFIM

A set of differential and algebraic equations have been used to describe the model of the DFIM. To describe the quantities used in these equations, subscripts *d* and *q* indicate the *d*- and *q*-axis quantities, respectively, while subscripts *r* and *s* represent the rotor and stator quantities, respectively, and *v*, *I*, *R*, and Φ represent the voltage, current, resistance and flux, respectively. All quantities are specified in per unit unless otherwise mentioned.

Represented by four states, i.e., the *d*- and *q*-axis flux of rotor and stator (Φ_{dr}, Φ_{ds}, Φ_{qr}, and Φ_{dr}), the model of the DFIM can be obtained from the respective equivalent circuits displayed in Figure 3.8 as:

$$v_{qr} = R_r i_{qr} + \omega_{sl}\Phi_{dr} + \frac{d\Phi_{qr}}{dt} \tag{3.32}$$

or,

$$\frac{d\Phi_{qr}}{dt} = v_{qr} - R_r i_{qr} - \omega_{sl}\Phi_{dr} \tag{3.33}$$

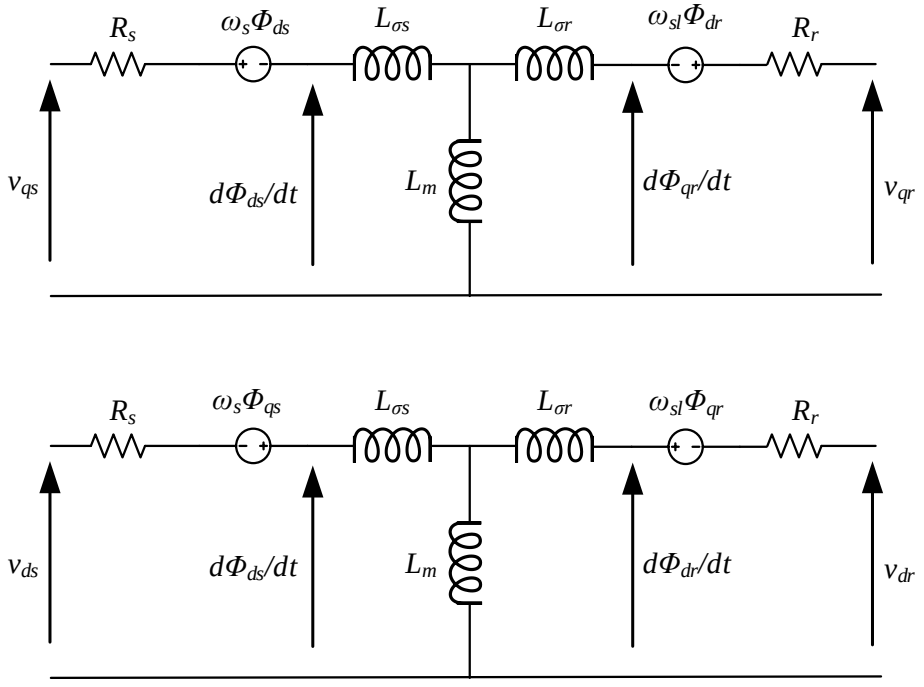

Figure 3.8. The *q*- and *d*-axis equivalent circuits of DFIM.

Similarly,

$$\frac{d\Phi_{dr}}{dt} = v_{dr} - R_r i_{dr} + \omega_{sl}\Phi_{qr} \tag{3.34}$$

$$\frac{d\Phi_{qs}}{dt} = v_{qs} - R_s i_{qs} - \omega_s\Phi_{ds} \tag{3.35}$$

$$\frac{d\Phi_{ds}}{dt} = v_{ds} - R_s i_{qs} + \omega_s\Phi_{qs} \tag{3.36}$$

Here, ω_{sl} is the slip speed or $\omega_{sl} = 1 - \omega_r$, where ω_r is the speed of the rotor and ω_s is the synchronous speed. To calculate the currents, the following algebraic equation is used,

$$\Phi_{qr} = \left(L_{lr} + L_m\right) i_{qr} + L_m i_{qs} \quad \text{and} \quad \Phi_{qs} = \left(L_{ls} + L_m\right) i_{qs} + L_m i_{qr} \tag{3.37}$$

where, L_{ls}, L_{lr} and L_m are the leakage inductance of stator and rotor, and mutual inductance between stator and rotor windings, respectively, and

$$L_r = L_{lr} + L_m \qquad \text{and} \qquad L_s = L_{ls} + L_m \tag{3.38}$$

where, L_r, is the total rotor inductance. Similarly,

$$\Phi_{qr} = L_r i_{qr} + L_m i_{qs} \tag{3.39}$$

$$\Phi_{dr} = L_r i_{dr} + L_m i_{ds} \tag{3.40}$$

$$\Phi_{qs} = L_s i_{qs} + L_m i_{qr} \tag{3.41}$$

$$\Phi_{ds} = L_s i_{ds} + L_m i_{dr} \tag{3.42}$$

The equations (3.32)-(3.42) are arranged in blocks to be solved in Simulink. The respective inputs and outputs of the blocks have been displayed in Figure 3.9.

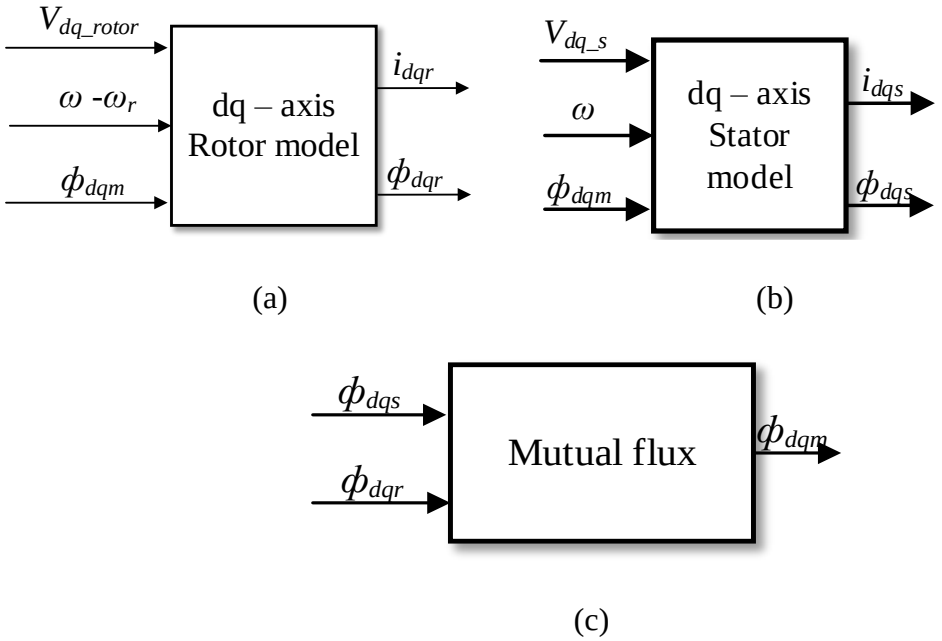

Figure 3.9. Simulation blocks of the DFIM (a) rotor, (b) stator, and (c) mutual flux model.

3.5.1 Stator Flux Orientation

To obtain the control of real and reactive power at the stator terminals through the rotor, the rotor current control needs to be used. Also, the real and reactive powers must be controlled independently. Thus, the stator flux orientation is used as shown in Figure 3.10.

$$|V_1|\angle\theta_{V1} \underset{grid\ voltage\ orientation}{\Leftrightarrow} |V_1|\angle\left(\theta_{V1}-\theta_{\phi s}\right)$$
$$|I_1|\angle\theta_{I1} \underset{grid\ voltage\ orientation}{\Leftrightarrow} |I_1|\angle\left(\theta_{I1}-\theta_{\phi s}\right)$$

As such,

$$v_{ds}=0 \qquad and \qquad v_{qs}=|V_1| \tag{3.43}$$

The stator real and reactive power equations are given as,

$$P_s=\frac{3}{2}\left(v_{qs}i_{qs}+\ v_{ds}i_{ds}\right) \tag{3.44}$$

and,

$$Q_s=\frac{3}{2}\left(v_{qs}i_{ds}-\ v_{ds}i_{qs}\right) \tag{3.45}$$

Using the flux current relations in (39-42) and (3.43), P_s and Q_s can be simply written as

$$P_s=\frac{3}{2}\left(V_{qs}i_{qs}\right)=-\frac{3}{2}\frac{L_m}{L_s}\left(v_{qs}i_{qr}\right) \tag{3.46}$$

and,

$$Q_s=\frac{3}{2}\left(v_{qs}i_{ds}-\ v_{ds}i_{qs}\right)=-\frac{3}{2}v_{qs}\left(\frac{\phi_s}{L_s}-\frac{L_m i_{dr}}{L_s}\right) \tag{3.47}$$

Thus, P_s can be controlled using i_{qr} and Q_s can be controlled using i_{dr}. Note the above algebraic manipulations help translate (3.44) and (3.45) in terms of controllable quantities, i.e., rotor currents.

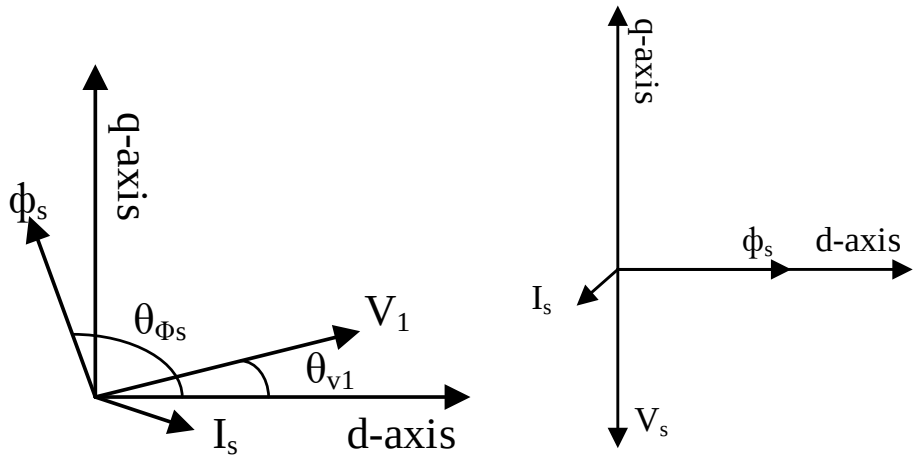

Figure 3.10. Stator flux orientation.

3.5.2 Real and Reactive Power Controllers

In order to tune the controllers shown in Figure 3.11, the model for the process is required which in this case is the DFIM. Equation (3.34) can be rewritten as,

$$v_{dr} = R_r i_{dr} - \omega_{sl}\Phi_{qr} + \frac{d\Phi_{dr}}{dt} \tag{3.48}$$

Substituting (3.39) and (3.40) in the above equation we have,

$$v_{dr} = R_r i_{dr} - \omega_{sl}\left(L_r i_{qr} + L_m i_{qs}\right) + \frac{d\left(L_r i_{dr} + L_m i_{ds}\right)}{dt} \tag{3.49}$$

$$v_{dr} = R_r i_{dr} - \omega_{sl}\left(L_r i_{qr} + L_m i_{qs}\right) + L_r \frac{d\left(i_{dr}\right)}{dt} + L_m \frac{di_{ds}}{dt} \tag{3.50}$$

To control the DFIM by controlling rotor currents, the process should be expressed in terms of rotor currents only. Substituting i_{ds} and i_{qs} from (3.41) and (3.42) in (3.50) we have,

$$v_{dr} = R_r i_{dr} - \omega_{sl} L_r i_{qr} - \omega_{sl}\frac{L_m^2}{L_s} i_{qr} + L_r \frac{d\left(i_{dr}\right)}{dt} - \frac{L_m^2}{L_s}\frac{di_{dr}}{dt} + \frac{L_s}{L_m}\frac{d\phi_{ds}}{dt} \tag{3.51}$$

As grid voltage remains constant, $\frac{d\phi_{ds}}{dt} = 0$, and if $\sigma = 1 - \frac{L_m^2}{L_s L_r}$ is defined as the leakage factor we have,

$$v_{dr} = R_r i_{dr} - \sigma\omega_{sl} L_r i_{qr} + \sigma L_r \frac{d\left(i_{dr}\right)}{dt} \tag{3.52}$$

Taking Laplace transform we obtain,

$$\frac{i_d}{v_{dconv} + \sigma\omega_{sl} L_r i_{qr}} = \frac{1}{s\sigma L_r + R_r} \tag{3.53}$$

$$\frac{i_q}{\left(v_{gq} - \omega L_r i_d\right) - V_{qconv}} = \frac{1}{s\sigma L_r + R_r} \tag{3.54}$$

With proper compensations the transfer functions can be further simplified to,

$$\frac{i_d}{v_{dconv}^*} = \frac{1}{s\sigma L_r + R_r} \tag{3.55}$$

$$\frac{i_q}{v_{qconv}^*} = \frac{1}{s\sigma L_r + R_r} \tag{3.56}$$

where the inputs are assumed to be pre-compensated with

$$v_{dcomp} = -\sigma\omega_{sl} L_r i_{qr} \tag{3.57}$$

$$v_{qcomp} = \left(v_{qg} - \omega_{sl} L_r i_{dr}\right) \tag{3.58}$$

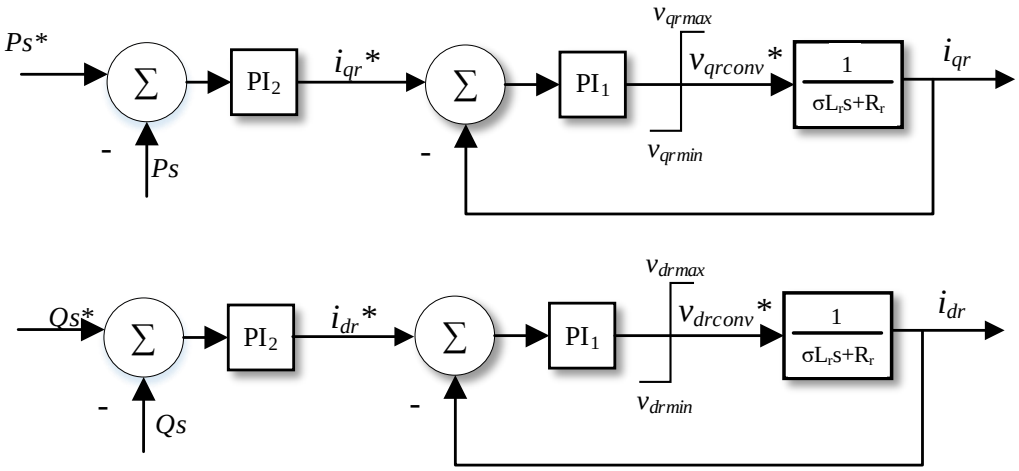

Figure 3.11. Control loops for RSC.

3.5.3 Controller Tuning for RSC

To tune the PI1 controller above, pole-zero cancellation along with the time constant thumb rule is applied to arrive at

$$\frac{K_{i1}}{K_{p1}} = \frac{R_r}{\sigma L_r} \qquad \textit{and} \qquad K_{p1} = \frac{\sigma L_r}{\tau_{cli}} \tag{3.59}$$

And we choose τ_{cli}, such that,

$$\tau_{cli} > 3\tau_{conv} \tag{3.60}$$

where, τ_{conv} is the switching frequency of the converter, and PI2 controller gains were tuned on a trial and error basis with K_{p2}, and K_{i2} tuned individually. The *dq* components of magnetizing flux are calculated by Figure 3.9(c) are obtained as

$$\Phi_{mq} = L_m \left(i_{qr} + i_{qs} \right) \tag{3.61}$$

$$\Phi_{md} = L_m \left(i_{dr} + i_{ds} \right) \tag{3.62}$$

Since the magnetizing flux does not contribute to controlled power, it is removed from the main flux before the equations (3.33)-(3.37) are solved.

3.6 SMIB System and Reference Tracking Results

The network for primary analysis was represented by a single machine infinite bus (SMIB) system as shown in Figure 3.12. The entire network to which a particular generator is connected can be reduced to the Thevenin's equivalent of the network external to the machine. The dynamics associated with the machine will cause virtually no change in the

Table 3.1 Parameters of the SMIB system

SMIB Parameters	Values
Phase-to-phase voltage rms	230 kV
Nominal frequency	60 Hz
X/R ratio	7
3 phase short – circuit level at base voltage	200 kVA

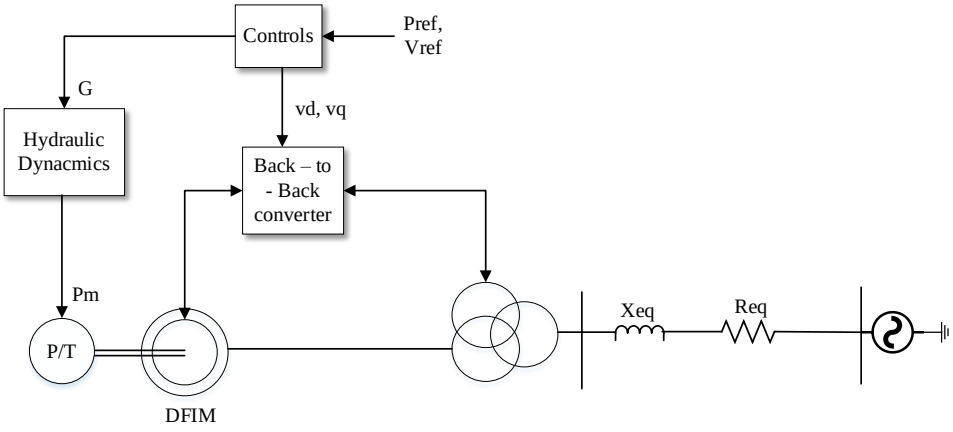

Figure 3.12. A SMIB system with ASPSH, where P/T is the reversible pump turbine, *G* = gate, *vd* and *vq* are *d*- and *q*-axis reference voltages and *Pm* is the mechanical power.

Thevenin's voltage and frequency of the external system. The electromechanical system consisting of the governor model, DFIM model, DC-Link model and controllers were integrated into the network to test its reference tracking capabilities. The SMIB and ASPSH system parameters are mentioned in Table 3.1 and Figures A.2, A.4, A.5, A.6 and A.7.

Figure 3.13 represents the generator mode results. As can be seen in Figure 3.13(a), the DFIM controls produce instantaneous tracking capability as the output overlaps the reference, which cannot be obtained with the CPSH. However, zooming in on the response in Figure 3.13(c), a 2.7% overshoot exists with a settling time of 0.1

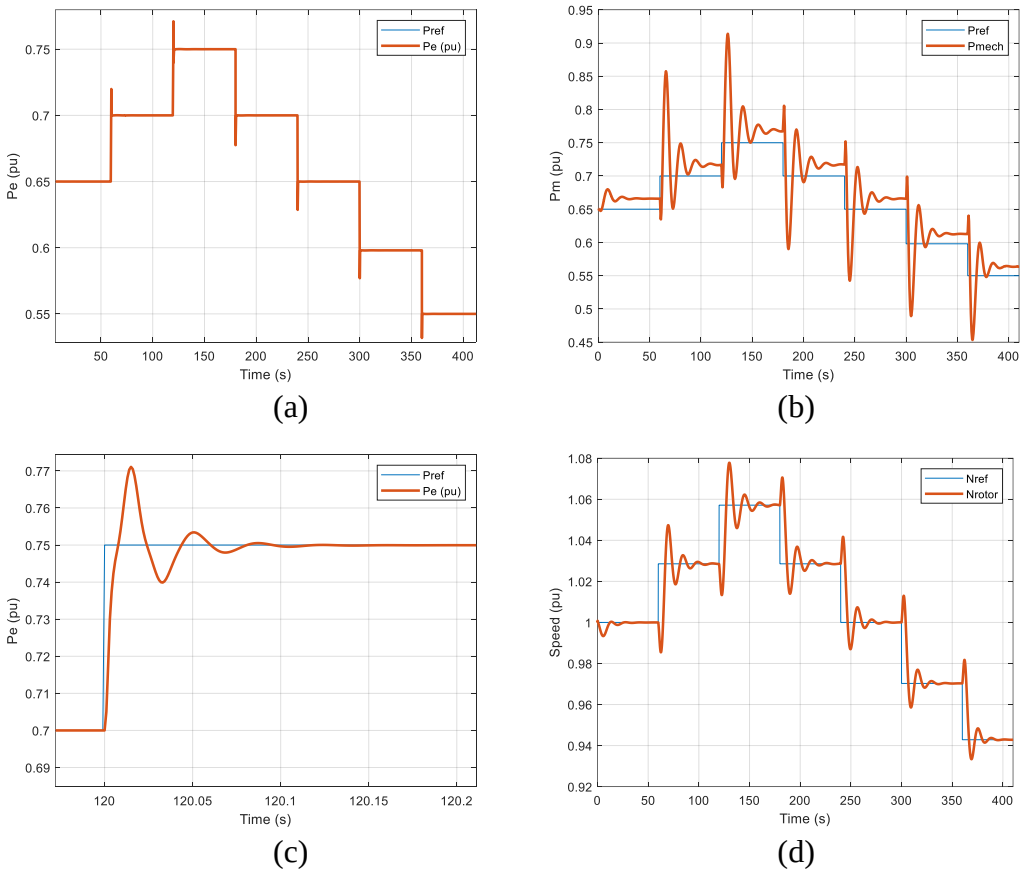

Figure 3.13. Generation mode: (a) Electrical Power, (b) Mechanical Power, (c) Electrical power zoomed in, and (d) Speed tracking.

seconds. Figure 3.13(b) displays the mechanical power output while Figure 3.13(d) displays the optimum speed tracking performance of the PID governor. At every set-point the optimal speed can be seen to be tracked by the PID governor, which in turn provides a balance between the electrical and mechanical power. The important point to note here is that the deviations in mechanical power do not affect the electrical power output as the inertia of the shaft compensates for the slow mechanical response. Also, the offset of the mechanical power shows the capability of the PID governor to meet the losses of the electrical and mechanical system.

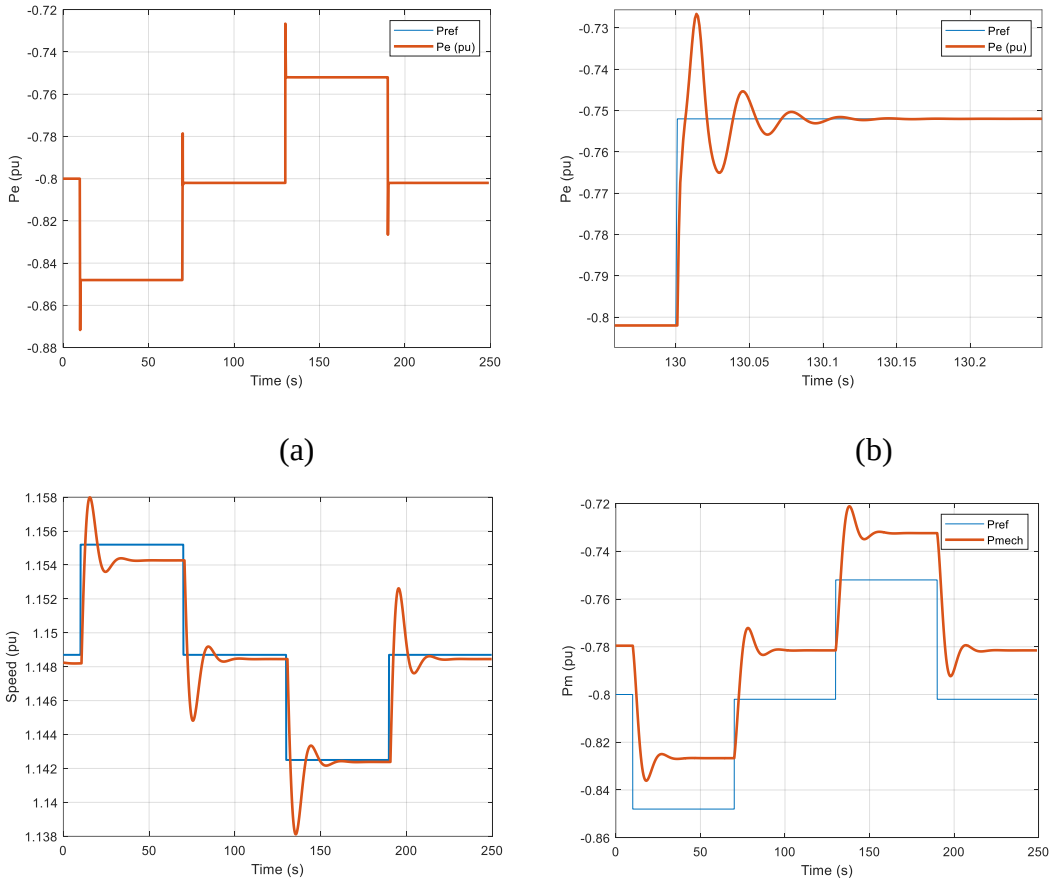

Figure 3.14. Pump mode power and speed reference tracking.

Similar results are obtained for the pump mode operation, as can be seen in Figure 3.14. In Figure 3.14(a) the power references are tracked by the DFIM in the pump mode. Figure 3.14(b) presents a zoomed-in presentation of the same. Figure 3.14(c) displays the change in speed with the change in set point. In Figure 3.14(d) the mechanical power is slightly higher than the reference power as the electrical and mechanical losses are subtracted from the total power input.

3.7 The 9-bus Testbed and ASPSH Integration

In order to study the dynamics and control of power systems, a testbed is of high importance. In [68], researchers at Hydro-Québec's Institut de recherche d'Hydro-Québec (IREQ), have presented their work on testbed development and simulation of the same in sim power systems (SPS) environment of MATLAB/Simulink. These testbeds are available online at MATLAB's central file exchange, where each simulation file is accompanied by the data file in *.m* format.

The 9-bus test system (Figure 3.15) is a widely used testbed for integration and stability issues. This testbed consists of 3 generators which are the major generator busses and 3 load centers. All generators are equipped with voltage regulators and power system stabilizers (PSSs). The SPS built-in library blocks of IEEE Type-1 excitation systems and IEEE Type-1 steam governing system are used with the SPS synchronous machine blocks. The masks or blocks for the ASPSH governor systems and the suitable DFIM for integration into the phasor model are not available in SPS and hence were constructed in Simulink.

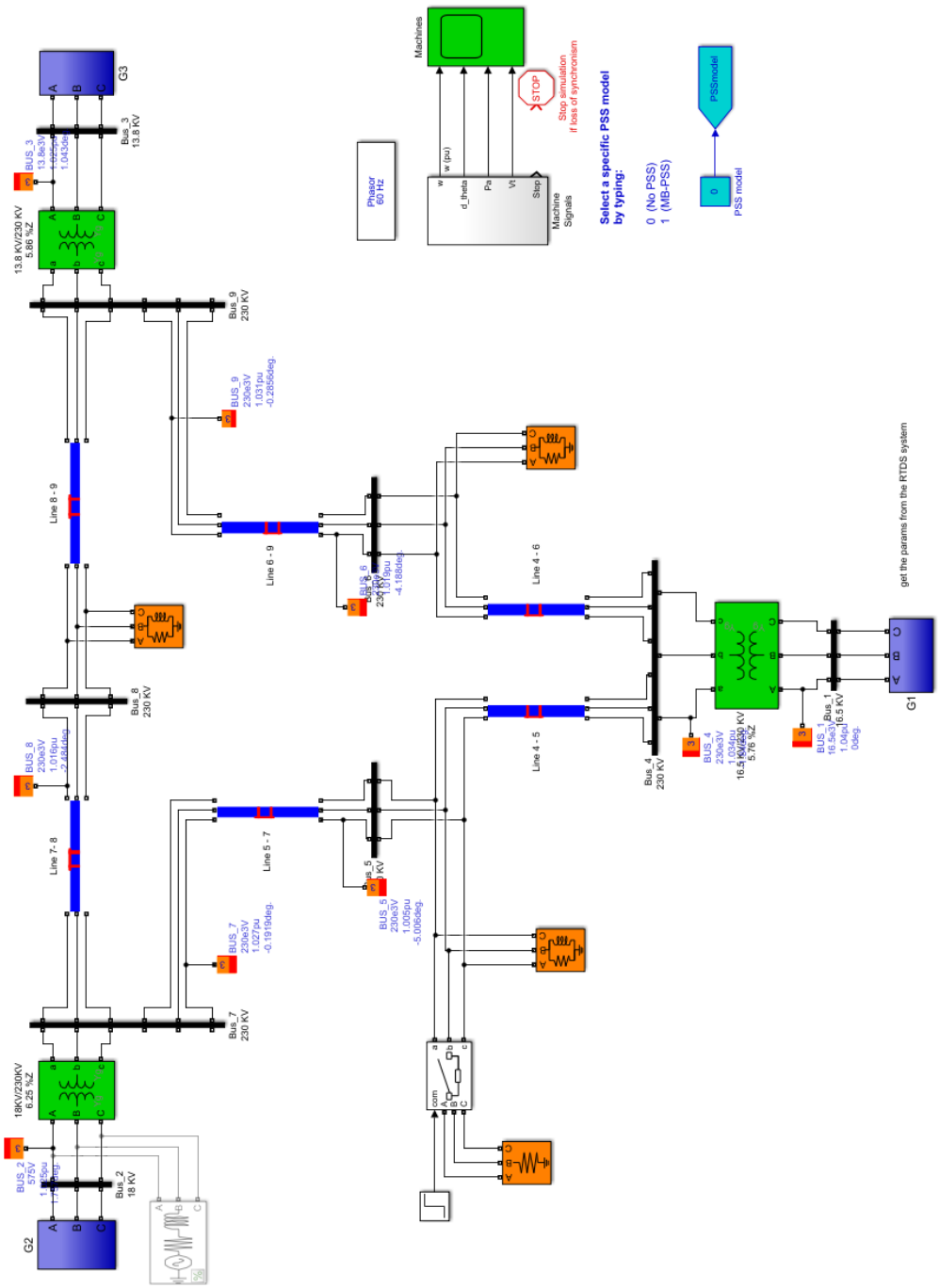

Figure 3.15. The 9-bus test system showing G2 with AC source commented for dynamic simulation.

For the purpose of integrating the ASPSH system, the generator at bus 2 is replaced with the DFIM-based ASPSH and its hydraulic governor. First, the load flow is performed, followed by system initialization so that the simulation begins from near steady-state.

Three separate masks are created, one for the ASPSH governor in generation mode, another for the same in pump mode and the other for the DFIM as displayed in Figure 3.16. In both the generation and the pump modes the inputs are rotor mechanical speed in per unit (*wr_pu*), desired reference real power (*Pref**), Head available (*H*) and the frequency of the system (*f*) in Hz. The outputs of the mask are the mechanical power output in *pu* and the reference power for the converter (*Pref*) in *pu*. The output *Pref* is a combination of the desired reference and primary frequency regulation.

The mask for the doubly-fed machine has the three terminals (A, B, and C) to connect to a three-phase system along with inputs, mechanical torque (*Tm*), trip (*trip*) and the reference power to be produced or consumed by the electrical system (*Pref*). The DFIM with control mask also produces signals to monitor such as the mechanical speed in per unit (*wr_pu*), real and reactive power *P*(*pu*) and *Q*(*pu*), terminal voltage (*Vabc*) among other important quantities.

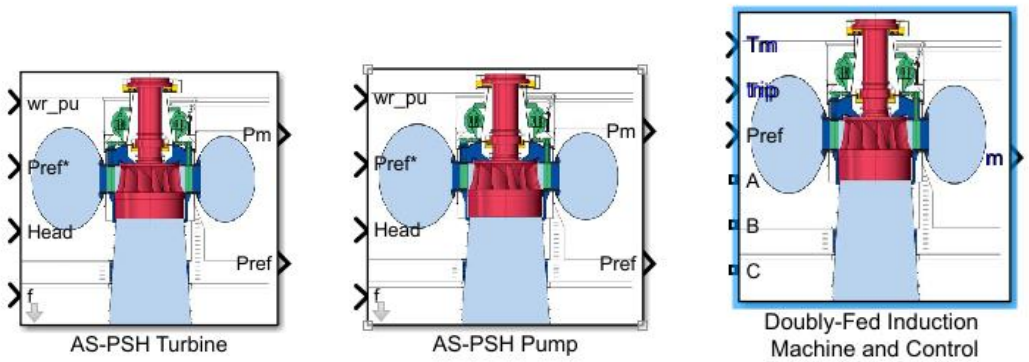

Figure 3.16. Masks for the turbine, pump, and the DFIM with converter control.

The details of mask parameters are given in Figures A.2, A.4, A.5, A.6 and A.7. To integrate the ASPSH system, the generator at G2 is removed and the mode respective governor and the DFIM and control blocks created above are added (Figure 3.17). Here, there was a challenge to overcome. The load flow system of Simulink does not recognize the user-defined masks or blocks. Thus, for the purpose of load flow, an AC source block was implemented with the G2 block commented. Later after the load flow data was extracted from the load flow results, the ASPSH system was initialized and uncommented. The AC source was commented once the load flow was complete.

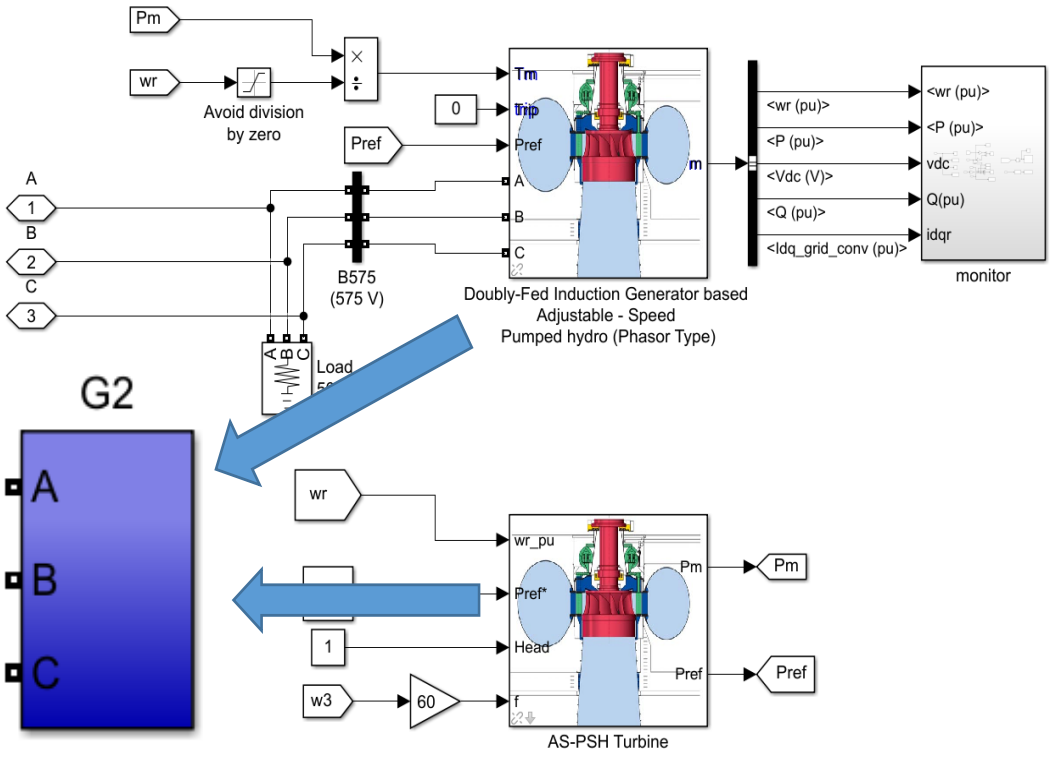

Figure 3.17. Components inside the new G2.

3.8 Dynamic Performance Comparison with CPSH

Using the test bed described above and the system models in the prior sections, a comparison of dynamic performance between the ASPSH and the CPSH was conducted. A fast frequency response test was performed when a 10% load change was applied at bus 5 during both the generating and pump modes. Note, that to simulate the pump mode, the system load had to be reduced, which resonates with practical conditions as pumping is usually performed at light load conditions.

Both CPSH and ASPSH utilized fixed *f-P* droop coefficients of 5%. Results in Figure 3.18 indicate the benefit of instantaneous response from ASPSH. Using ASPSH we have a higher frequency nadir than the with the CPSH in both the generating and pumping mode. In the generating mode the settling frequency is worse with the ASPSH which is due to the nature of primary control. Droop based primary control strategies are proportional control strategies where the response of all droop-controlled generators in the system are proportional to the extent of frequency deviation. Since, the extent of

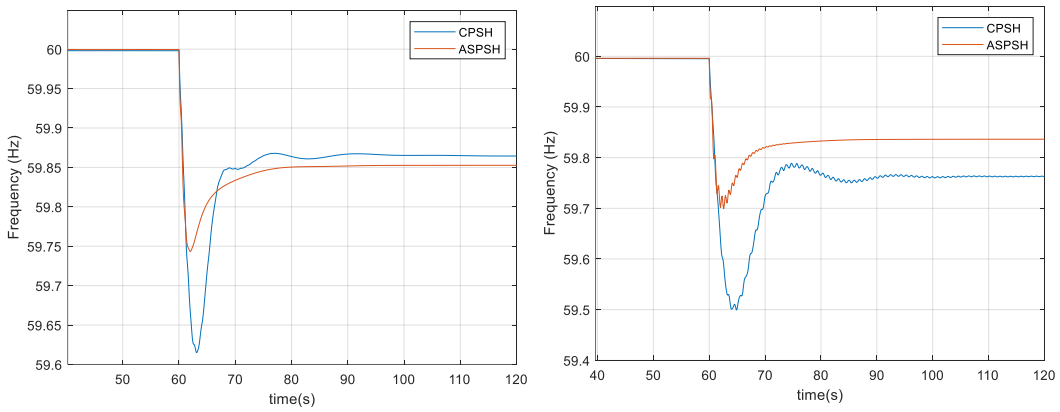

Figure 3.18. Fast Frequency Test Performance comparison of CPSH and ASPSH for Fixed Droop coefficient in (a) Generating mode and (b) Pumping mode.

frequency deviation is less in case of ASPSH the response from all other units is also lesser than in the case with CPSH, which in turn degrades the settling frequency. The frequency nadir in case of pump mode is extremely low in case of CPSH as the CPSH does not participate in primary control in pump mode. Having more participants in primary control explains the higher settling frequency for the pump mode with ASPSH. Another notable feature is that the ASPSH can damp-out small low frequency oscillations in pump mode.

3.9 Adaptive Droop-Based Primary Control

To enhance the contribution of the ASPSH even further, an adaptive droop scheme has been designed and implemented. Depending on the sign of frequency f and df/dt four different scenarios can be formed and identified, as shown in Figure 3.19, and depending on these logic scenarios the droop constant may be varied accordingly as can be seen in Figure 3.20 such that the droop coefficient is $1\% \leq y \leq 5\%$ and implemented after a time lag as in Figure 3.21. A time lag with gain $K_{f\omega s}$ is presented to the output of the logic circuit to ensure smooth variation of gain and hence the power output.

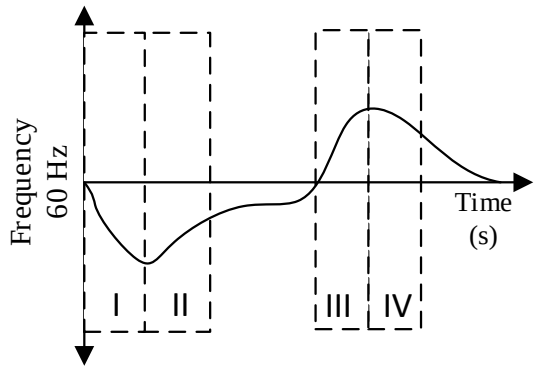

Figure 3.19. Four scenarios of the frequency profile.

The frequency degradation phase is given a higher amount of droop which will arrest the frequency nadir at a higher value. Also, the increased action from the ASPSH will reduce action of other mechanical governors in the system. The frequency recovery phase is given a standard value of droop which will allow all plants to return to pre-disturbance conditions to preserve system economy. To improve the settling frequency, the droop coefficient could be lowered further to allow other generators in the system to respond.

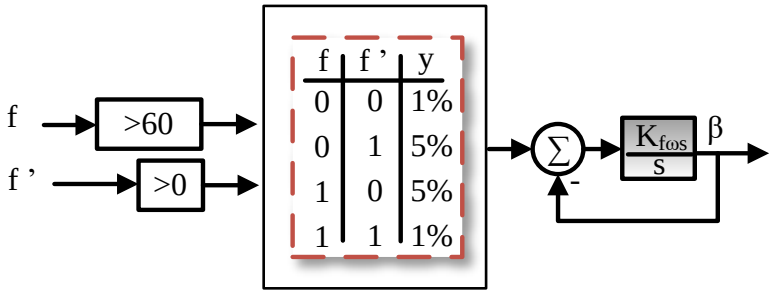

Figure 3.20. The DFIM Droop gain adaptation logic.

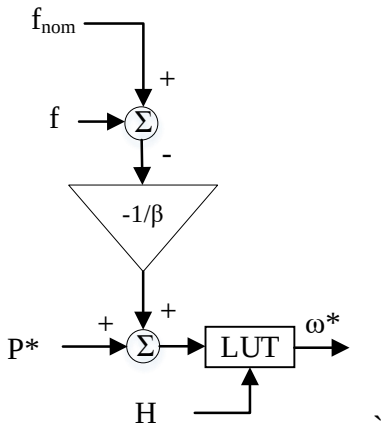

Figure 3.21. Adaptive droop based supplementary control.

The variation of droop parameter can produce noticeable benefits in system frequency profile. Figure 3.22 demonstrates the system frequency of the 9 bus-system when a load addition event is simulated. To bring out the effect of load addition, a 10%

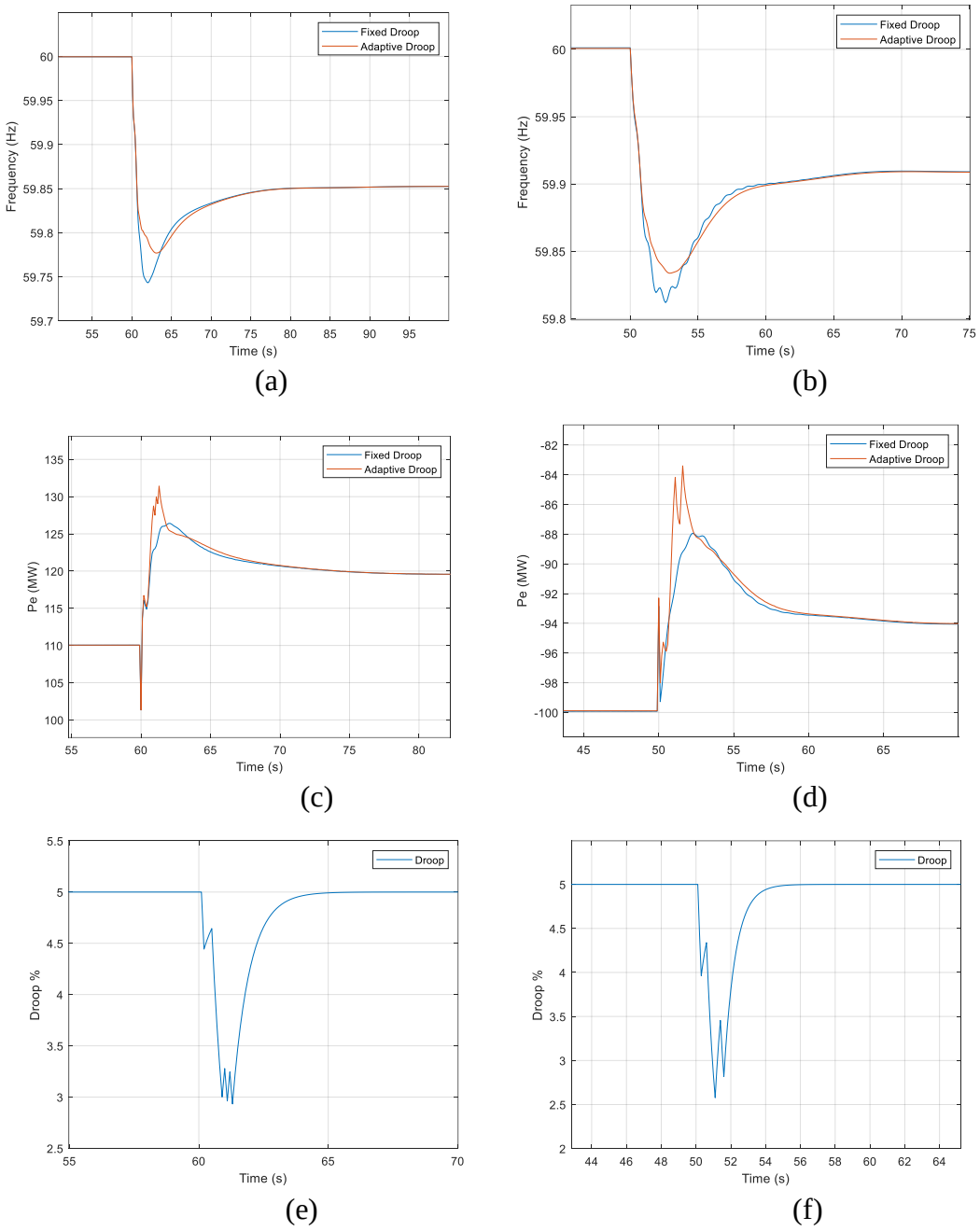

Figure 3.22. Adaptive droop response: (a, b) frequency, (c, d) electric power output, and (e, f) droop for (generator, pump) modes, respectively.

load addition was performed at bus 5. Through Figures 3.22(a) and (b) the adaptive droop scheme proves to be effective in arresting the frequency nadir at a higher point for both generator and pump modes. Figures 3.22(c) and (d) display the additional response of the ASPSH system due to the adaptive droop scheme. Finally, Figures 3.22(e) and 3.22(f) demonstrate the droop variation during the event. In the presented adaptive droop scheme, the droop reduces to below 3% which in turn adds to the primary response of the system.

3.10 Conclusion

This chapter presents the modeling and control of ASPSH followed by their ability to perform set-point tracking and improve power system frequency response. Modeling of generator-mode and pump-mode hydraulic and systems and the electrical machine has been performed along with the design of converter controls. Results show, that the ASPSH and its controls are able to track power references accurately. The comparison of dynamic performance with CPSH reveals that ASPSH could be highly beneficial for system resilience enhancement. To improve the response of the ASPSH further, an adaptive droop method for varying the droop gain has been proposed and has resulted in higher frequency nadirs, thereby increasing the resiliency of the system. The models and masks have been constructed in Simulink and simulated using phasor simulations.

CHAPTER FOUR

Modeling and Control of Ternary Pumped Storage Hydropower

This chapter is published as: S. Nag, K. Y. Lee, and D. Suchitra, "A Comparison of the Dynamic Performance of Conventional and Ternary Pumped Storage Hydro," *Energies*, vol. 12, no. 18, p. 3513, Sep. 2019.

4.1 Introduction

This chapter investigates, how Ternary Pumped Storage Hydropower (TPSH) can help enhance power system resiliency by contributing primary frequency regulation in both pumping and generating modes. As renewable penetration increases, power system inertia decreases. Simultaneously, the frequency of storms and earthquakes have increased. As such, power system resiliency is a key issue in low inertia power systems. To cater to this issue, this chapter investigates the ability of TPSH to provide primary frequency support in pumping and generating mode. The governor dynamics of the IEEE 9-bus system and TPSH have been modeled and integrated. When the system is subjected to a step increase or decrease in load, results display that not only can the TPSH provide pump mode regulation using the hydraulic short-circuit, but it can also transit smoothly between pumping and generating mode within a few seconds using the clutch. By changing its mode, the TPSH unit can provide a regulation capability equal to twice that of the unit rating.

4.2 Technology Description

The TPSH is a fixed speed system that uses a synchronous machine. The three main components of the TPSH are the synchronous machine, turbine and pump [40]. The

TPSH is unique in its construction as the turbine and pump share the same shaft as that of the synchronous machine. A clutch disconnects the pump and the rest of the shaft. Fig. 4.1 shows a schematic of the TPSH. Having both pump and turbine on the same shaft makes the direction of rotation of the pump and the turbine the same. Also, the turbine and the pump share the same penstock, which means that the unit can either be operating as a pump or a turbine at any instant. This is another unique structural feature of the TPSH, called the hydraulic short-circuit (HSC). With the HSC, a part of (or all) the water pumped by the pump is transferred to the turbine by opening the turbine inlet via the turbine governor. This in turn causes the turbine to produce torque that is supplied to the shaft. This mechanical torque from the turbine will reduce the current drawn from the grid while still rotating at the synchronous speed. After supplying the turbine through the turbine governor, remaining discharge of the pump travels to the upper reservoir.

The HSC takes advantage of the fact that the head generated by the pump is either equal or greater than that of the upper reservoir at any instant as long as the pump rotates

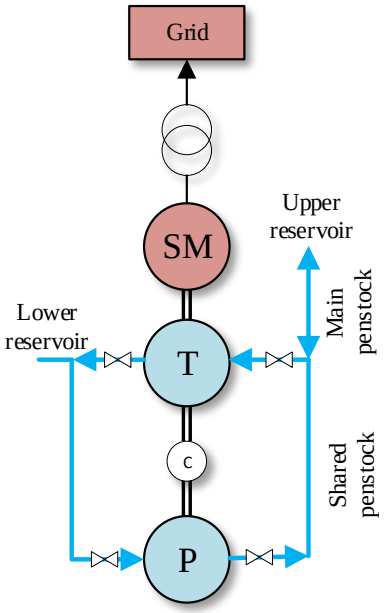

Figure 4.1. Functional diagram of TPSH. SM=synchronous machine, T=turbine and P=Pump.

at synchronous speed. The turbine being connected right next to the pump experiences the pump generated head, which is in fact the rated head of the turbine, which enables it to generate power.

4.3 Dynamic Modeling

The dynamic model of the TPSH is displayed as a block diagram in Figure 4.2 which has been constructed with subcomponents from [66]. A PID governor has been implemented to control the turbine and respond to system frequency deviations. The flow dynamics, assuming non-linear non-elastic water column, can be used to describe the relationship between head and discharge.

$$\frac{dq_t}{dt} = \frac{H_t - h - h_l}{T_w} \tag{4.1a}$$

$$\frac{dq_p}{dt} = \frac{-[H_p - h - h_l]}{T_w} \tag{4.1b}$$

where H_t, H_p, h and h_l define the available head for the turbine, generated head by the pump, and head at turbine entrance head loss due to friction as $h_l = f_p Q^2$, respectively, and T_w is the water starting time constants to accommodate the interaction between the turbine and pump, or vice versa. Since the turbine and pump are connected, it is required that we consider the interaction between the two. This can also be found in [66] as the paper described plants with multiple units. Collectively, the hydraulic dynamics for the pump and turbine and their mutual connection can be given by:

$$\begin{bmatrix} Tw_{tt} & Tw_{tp} \\ Tw_{pt} & Tw_{pp} \end{bmatrix} \begin{bmatrix} \frac{dq_t}{dt} \\ \frac{dq_p}{dt} \end{bmatrix} = \begin{bmatrix} \Delta h_t \\ \Delta h_p \end{bmatrix} \tag{4.2}$$

Here Tw_{tt}, Tw_{tp}, Tw_{pp}, Tw_{pt} are the water starting time constants to accommodate the interaction between the turbine and pump or vice versa. Where the discharge and the head for the turbine is given by

$$q_t = G\sqrt{h} \tag{4.3}$$

where G is the turbine gate and h is the head at turbine inlet. Similar representation for the pump can also be done.

The power output from the turbine or input to the pump is given by:

$$P_m = A_t h\ (q - q_{nl})\ - DG\Delta\omega \tag{4.4}$$

Finally, the power from the turbine and pump are summed up to give the net output power:

$$P_{shaft} = P_t + P_p \tag{4.5}$$

The head and discharge immediately at the pump outlet is given by:

$$H_p = [H_0 + H_1(q) + H_2(q)^2](1 + \Delta\omega)^2 \tag{4.6}$$

where H_0, H_1, and H_2 are coefficients for relating discharge and head.

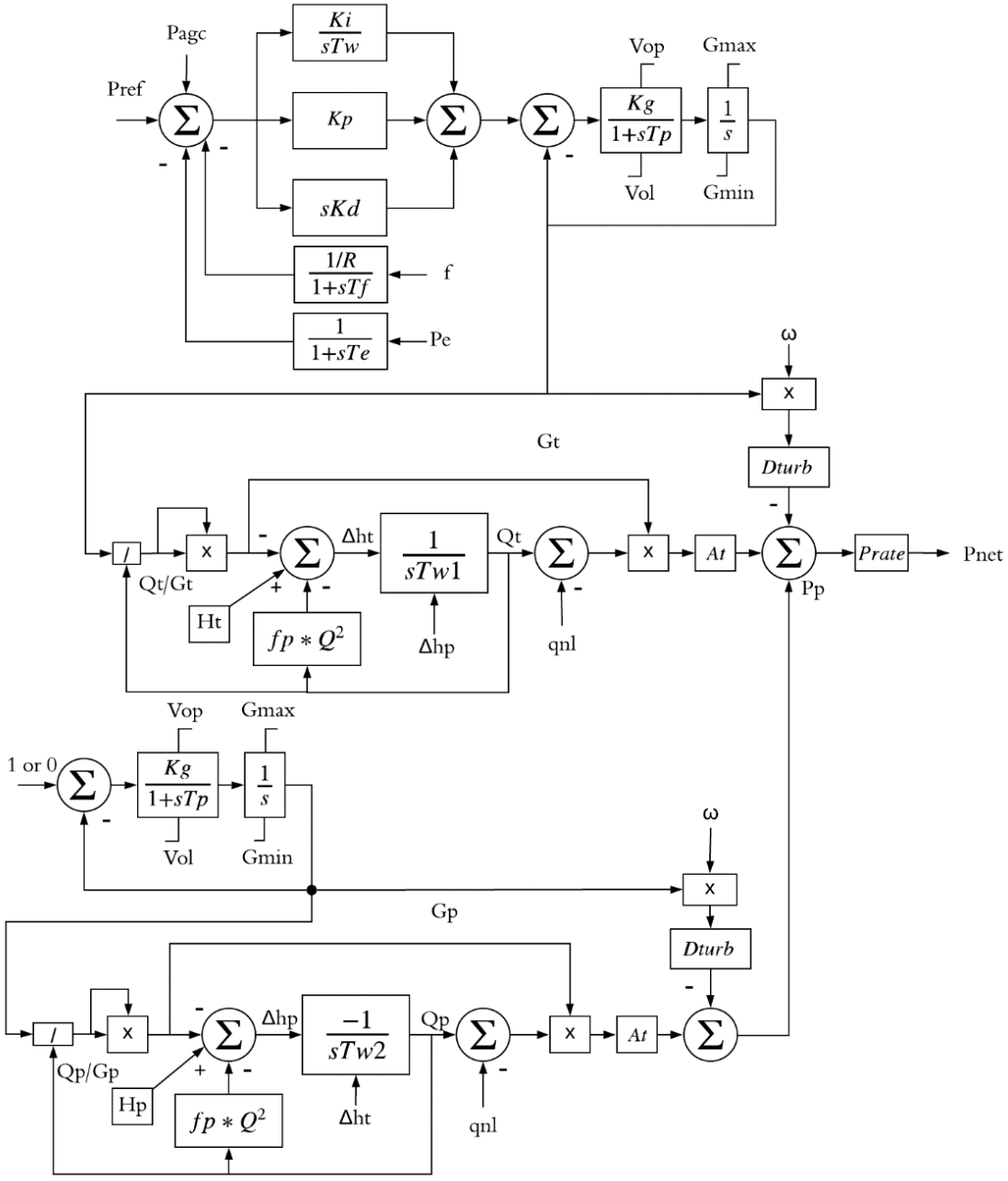

Figure 4.2. Block diagram for dynamic model of TPSH.

4.5 Results and Discussion

The governor turbine model described above in Figure 4.2 was integrated to the SMIB system described in section 3.6 (ASPSH) and the IEEE 9-bus system as shown in Figure 4.3. The thermal plants in the 9-bus test system were equipped with IEEET1 governors. To realize the effect of the loss of inertia, the thermal plant at bus 1 rated 500 MW was replaced by a PV plant of equal capacity and a CPSH plant of 500 MW was placed at bus 7 to form the baseline cases. Later, for the purpose of comparison, the CPSH was replaced by a TPSH of 500 MW.

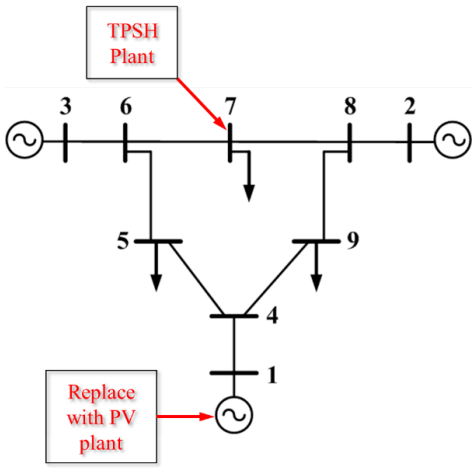

Figure 4.3. A 9-bus IEEE test system.

4.5.1 Reference Tracking in Hydraulic Short Circuit Mode in the SMIB System

To realize the benefits of the HSC that is facilitated by the structure of the TPSH, the governor described in Figure 4.2 is connected with the synchronous machine connected to an infinite bus (SMIB). Reference tracking results in Figure 4.4(a) display the capability of the model to replicate the pump-mode reference tracking of the system. The results clearly display the expected reverse response characteristics of the turbine

governor system. As discussed before, the discharge from the pump is divided into two parts when the HSC is in use. Figure 4.4(b) shows the same results. Since shaft rotates at a constant speed, the pump's discharge remains constant. However, the turbine inlet flow varies as the power reference to its governor is changed. This results in the variation in the net flow to the upper reservoir.

4.5.2 Baseline Analysis of Test System in Pump Mode of CPSH

This baseline analysis answers the question as to what happens when large capacity PV farms were added to the system in the presence of a CPSH operating as a pump. The addition of the PV farm caused the retirement of a similar capacity thermal plant or exclusion of the thermal plant from scheduling. However, this resulted in the loss of inertia and to make matters worse, the primary and secondary frequency response services that were provided by the thermal plant were also lost. This situation was simulated by removing the 500 MW thermal plant from the system and adding a 500 MW PV farm into the system whose dispatch was adjusted to match that of the thermal plant

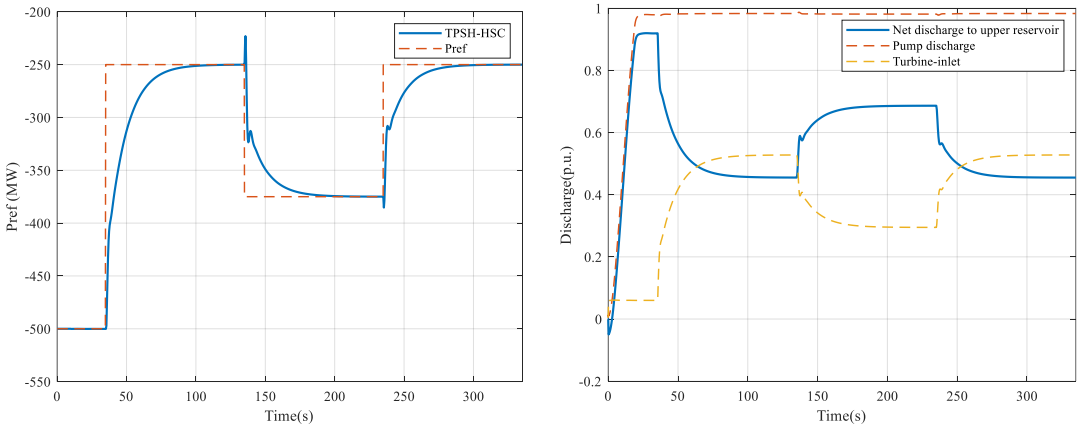

(a) (b)

Figure 4.4. (a) Pump mode power reference tracking with hydraulic short circuit, (b) Water flow distribution.

that it replaced. A load change from 33% to 66% was simulated to the system at 50 s, which caused the system frequency to drop significantly as to initiate governor action.

Before the addition of RES the frequency nadir was 59.72 Hz. Figure 4.5(a) reveals that when the system inertia was reduced and primary frequency services previously provided by the generator at bus 1were excluded, the frequency nadir decreased to 59.68 Hz. The usual frequency limit set by FERC was ±0.5 Hz, hence the system was not in critical condition as to trigger load shedding or the tripping of PV inverters but the possibility of such events was valid in the face of further reduction of inertia with further addition of RES. Figure 4.5(b) illustrates that under the given test conditions, the thermal plants experience increased governor action. This will result in higher wear and tear or thermal governor. Hence, there is an ardent need for flexibility of network resources, which helps increase network resiliency to cope with such events.

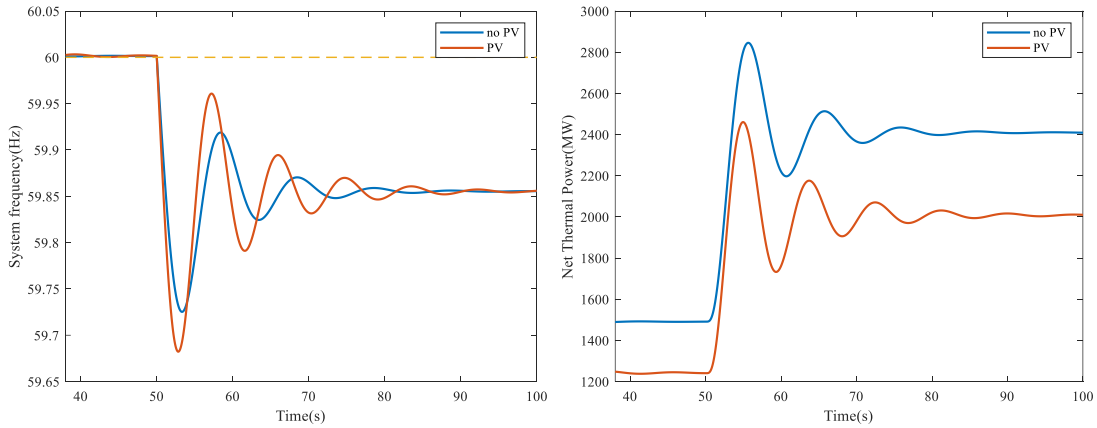

(a) (b)

Figure 4.5. Baseline analysis of the test system in pump mode of CPSH.

4.5.2 Mode Change Capability

To display the mode change capability of the model, a load trip event and a load addition event were simulated. For the load trip event, the TPSH plant was initially set to work as a generating unit with its pump as idle. Later, as the disturbance occurs the plant changes its mode from generating mode to pumping mode as displayed in Figure 4.6(a) within 45 seconds. As a result, the primary regulation provided to the system is twice that

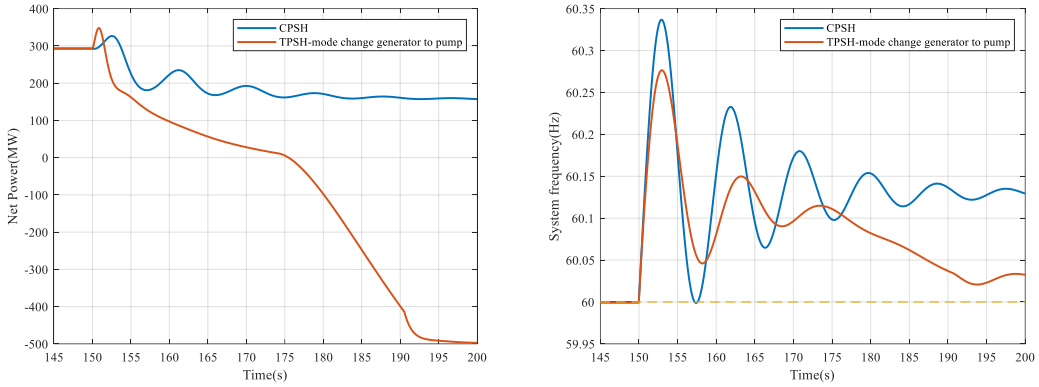

(a) (b)

Figure 4.6. Comparison of (a) power output with (b) system frequency of CPSH and TPSH during a load trip event.

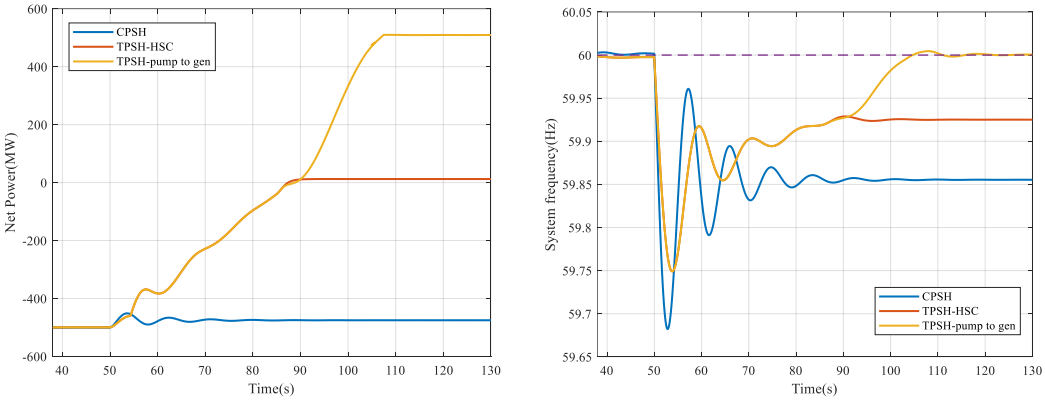

(a) (b)

Figure 4.7. Comparison of (a) power output with (b) system frequency of CPSH and TPSH during a load trip event.

of the units capacity (2×500MW) as compared to the droop-based response of the CPSH plant providing only 120MW of regulation for the same event. This results in a visibly better frequency profile with a reduced overshoot and significant proximity to the 60Hz standard.

For the load addition event, the TPSH plant was initially set to work as a pump. Later as the load was added to the system, the plant could either use its hydraulic short-circuit and remain in pumping mode or change from pumping mode to generating mode. Again, the mode change allows the plant to provide regulation capacity of twice that of the unit rating (2×500MW). This is a significant contribution of the TPSH technology as the primitive CPSH unit provides no support at all. Figure 4.6(a) and (b) display the frequency profile and the net power from the TPSH unit when the disturbance is simulated.

The process of mode change was realized by controlling the setpoints *Pref* for the turbine and 1 or 0 reference for the pump. The pump can only be turned on or off which is indicated by the input status switch. However, a certain sequence of operation was followed to prevent output power transients. For pump to generator, when the system is initially operating in pump mode, the turbine inlet gate is opened to make the net power zero. The pump outlet gate is slowly closed until it reached its lower limit and is then disconnected from the shaft using the clutch. For generator to pump mode, first the turbine gates are closed and simultaneously the clutch is engaged to engage the pump. When the turbine gate is completely closed, the pump outlet is opened. The turbine controller parameters are set to match the mode change timings as mentioned in the

report from [40] for a Francis turbine. Thus, pump to generator is completed within 60 seconds and generator to pump is completed in 45 seconds.

4.6 Conclusion

This chapter presents the modeling and control of a TPSH. Also, this chapter displays the effectiveness of TPSH in enhancing power system resiliency by contributing to primary frequency regulation. With the ability to change its mode from generating to pumping and vice versa, TPSH provides primary regulation capacity twice that of the unit's rating and hence significantly improves system resiliency. Also, with the help of the developed model, the hydraulic short-circuit has been simulated and shown that the TPSH is capable of pump-mode regulation.

CHAPTER FIVE

Network and Reserve Constrained Economic Analysis of Pumped-Storage Hydropower

This chapter is published as: S. Nag and K. Y. Lee, "Network and Reserve Constrained Economic Analysis of Conventional, Adjustable-Speed and Ternary Pumped-Storage Hydropower," *Energies*, vol. 13, no. 16, p. 4140, Aug. 2020.

5.1 Introduction

With increasing renewable penetration and projected increase in natural disasters, the reliability and resiliency of a power system become crucial issues. As network inertia drops with increasing penetration of renewables, operators search for flexible resources that can help cope with a disruptive event or manage renewable intermittency. Energy storage is a solution, but the type of storage solution needs to be profitable to exist in the current and upcoming power markets. Advanced pumped-storage hydropower (PSH) is one solution that can help cope with such requirements, which will in turn help to increase the renewable penetration in the system. This chapter qualitatively compares the revenue earning potential of PSH configurations, including, adjustable-speed PSH (ASPSH) and ternary PSH (TPSH) in comparison to conventional PSH (CPSH) from the arbitrage and regulation markets, with and without the presence of wind penetration. In addition, a framework for quantitative analysis of any energy storage system has been proposed. A 24-bus reliability test system (RTS) system is studied with summer and winter variations in load and in wind power. Through revenue and operational mode analysis, this chapter reveals that TPSH has the highest revenue earning potential, which is mainly due to its ability to operate with a hydraulic short circuit (HSC).

The primary control reserves and regulation services are crucial for enhancing the reliability and resiliency of power systems. Primary frequency regulation and load following reserves enable power systems not only to cope with any disruptive events, but also to absorb the intermittency of renewable energy and load. However, as the penetration of renewable energy increases, fossil-fuel powered thermal generators are removed from the schedule, which simultaneously removes the reserves and regulatory services provided previously by these generators. Thus, we look forward to grid-scale energy storage technologies such as pumped-storage hydropower (PSH). However, from an economic standpoint, it becomes important to understand which candidate of the PSH portfolio is most beneficial.

This chapter considers some of these practices and evaluates the revenue earning potentials of different PSH technologies as well as the benefits to the power network. This work assumes that the day-ahead nodal price and the real-time price are equal and considers the effect of wind penetration on the operation and revenue of the PSH

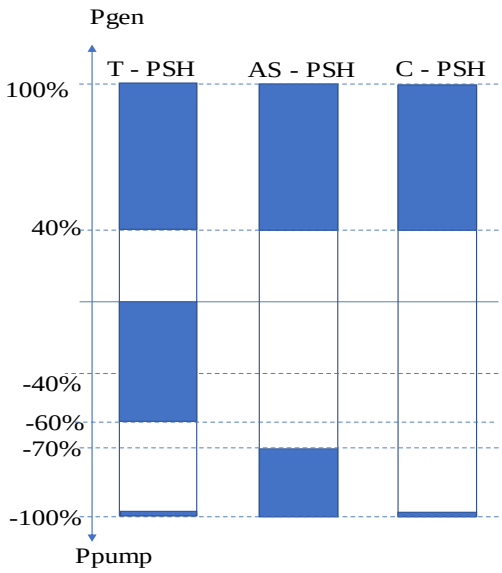

Figure 5.1. Operating ranges of PSH configurations.

configurations. Solar photovoltaic (PV) penetration has not been considered as the time of PV power production coincides, approximately, with the time of peak load requirement. Thus, the scope for arbitrage with the presence of PV becomes less obvious. However, future studies with PV and both wind and PV will be performed.

5.2 Modeling PSH Configurations

In order consider PSH configurations for the optimization problem, the feasible operating range of the configurations are required. The turbine considered for CPSH, ASPSH and TPSH have a range of 40% to 100%. The ASPSH considered is equipped with a converter of 20% rating, and the operating range for the ASPSH is within the nominal range of 100% to 40% in the generating mode. The synchronous speed is marked at 60% power output. In the pump mode, the power consumed ranges between to −70% to −100%, as shown in Figure 5.1.

The turbine mode operating range is the same as that of the CPSH. With the help of the hydraulic short circuit, the entire turbine range can be used to provide regulation during the pump mode. Hence, the pump can or operate at full load at −100%, or with the hydraulic short circuit in the range of 0% to −60%, since the entire working range of the turbine which is 40% to 100% is used. These details of CPSH, ASPSH, and TPSH are diagrammatically illustrated in Figure 5.1.

5.3 Problem Formulation

To understand the profitability of a grid-scale storage technology such as PSH, it is required to simulate a network over a significantly long duration. Also, it is important to consider network constraints for a more practical realization of the revenue earning

potential of the different PSH configurations. Therefore, a reserve and network constrained dynamic optimization problem is formulated to minimize:

$$J_1 = \sum_{t=1}^{T}\left(C_{g,t} + Loss_t + P_{cur,t} + Pen_{vol,t} - Rev_{st,t}\right) \tag{5.1}$$

where,

$$C_{g,t} = \sum_{i=1}^{N}\left(f(P_{gi}) + RC_{gi}\Delta P_{gi}\right) \tag{5.2}$$

$$Loss_t = \sqrt{\left(P_{loss}^2 + Q_{loss}^2\right)} \tag{5.3}$$

$$P_{cur,t} = \bar{P}_{w,t} - P_{w,t}^{*} \tag{5.4}$$

$$Pen_{vol,t} = K_p(vol_{ref} - vol_t) + K_i\sum_{j=1}^{t}(vol_{ref} - vol_j) \tag{5.5}$$

$$Rev_{st,t} = Rev_{en,t} + Rev_{reg,t} \tag{5.6}$$

$$Rev_{reg,t} = \lambda_{reg}RA_{st,t} + \eta RM_{st,t}\lambda_{bus} \tag{5.7}$$

$$Rev_{en,t} = \lambda_{bus}P_{gst,t} - \lambda_{bus}\gamma P_{pst,t} \tag{5.8}$$

$$eff_{gst} = p_1P_{gst}^3 + p_2P_{gst}^2 + p_3P_{gst} + p_4 \tag{5.9}$$

Equation (5.1) consists of four different terms and considers the objectives of both the ISO and the storage facility as it accounts for revenue maximization and reservoir volume as well as system reserves, operating cost and losses. The *first term* in (5.1) is the cost of generation $C_{g,t}$, which is further detailed in (5.2) and comprises of the value of the objective function at each hour from the OPF, $f(P_{gi})$, and the ramping costs of thermal generators, $RC_{gi}\Delta P_{gi}$. The *second term* in (5.1), $Loss_t$, is the apparent power loss as detailed in (5.3). The *third term* in (5.1) is the curtailment of wind energy $P_{cur,t}$ as

detailed in (5.4) as the difference between the maximum available wind energy $\bar{P}_{w,t}$ and the amount that was actually dispatched, $P^{*}_{w,t}$. The effect of solar energy has not been considered. The *fourth term* in (5.1) is the penalty $Pen_{vol,t}$ that enforces the constraint that the final volume at the end of the week must be equal to the initial volume. The penalty is applied as in (5.5), where vol_{ref} is the target energy level at the end of the scheduling period and, K_p and K_i are penalty constants.

The *fifth term* in (5.1), $Rev_{st,t}$ calculates the revenue earned by the storage facility from the energy market, $Rev_{en,t}$, and the regulation market, $Rev_{reg,t}$, as in (5.6). Here, the revenue from the regulation market, $Rev_{reg,t}$, is divided into two parts as shown in (5.7) and (5.8); in (5.7) the first term simply states the revenue for reserve allocation $RA_{st,t}$ and the second term states the revenue collected proportional to the regulation mileage $RM_{st,t}$ or actually activating the reserve. Equation (5.7) assumes a performance-based payment scheme where the performance factor, η, describes the speed and accuracy of response of the PSH plant. The allocated reserve earns a revenue proportional to the regulation capacity price of the PSH plant, λ_{reg}, while the activated reserve is sold at the LMP λ_{bus} as in (5.8), where the revenue from the energy market $Rev_{en,t}$, is the difference between the revenue earned from generation of P_{gst} and the amount paid for pumping P_{pst}. Here, the price for pumping is discounted by the factor γ. The efficiency of the plant in generating mode (or pumping mode with P_{pst}) are separately accounted for by (5.9)

assuming constant head with p_1, p_2, p_3 and p_4 being required coefficients (see Table 5.1) and P_{gst} being the generation mode power output from the PSH.

At every time step (1 hour) the power network was internally optimized so as to maintain system security and generate the nodal energy prices used for the revenue calculation. The MATPOWER [70] was used to perform the optimal power flow for the system which solved:

$$\min J_2 = \sum_{i=1}^{Ng} \left(f(P_{gi}) + \pi_{i,t} r_{i,t} \right) \tag{5.10}$$

Table 5.1. PSH data for CPSH, ASPSH and TPSH

Parameter	Value
Power rating	300 MVA
Energy rating	7230 MWhrs
Performance factor η	CPSH and TPSH η = .85 ASPSH η = .9
Discount factor γ	.5

Efficiency - CPSH and TPSH	Pump mode efficiency = 89%
	Generator mode efficiency coefficients
	p1 = -0.2778; p2 = 0.2738;
	p3 = 0.4016; p4 = 0.521;

Efficiency - ASPSH	Pump mode efficiency coefficients
	p1 = -2.222; p2 = 4.238;
	p3 = -2.206; p4 = 1.08;
	Generator mode efficiency coefficients
	p1 = 0.2778; p2 = -0.8452;
	p3 = 0.9984; p4 = 0.5005;

CPSH operating range	Generator mode [.4 to 1pu] Pump mode -1pu
ASPSH operating range	Generator mode [.4 to 1pu] Pump mode [-.7 to -1pu]
TPSH operating range	Generator mode [.4 to 1pu]; Pump mode -1pu; Pump mode with hydraulic short circuit [0 to -.6pu]

$$P_f(\theta,V) + P_{di} + P_{gi} = 0 \tag{5.11}$$

$$Q_f(\theta,V) + Q_{di} + Q_{gi} = 0 \tag{5.12}$$

$$F(\theta,V) < F_{max} \tag{5.13}$$

$$\theta_{i,min} < \theta_i < \theta_{i,max} \tag{5.14}$$

$$V_{i,min} < V_i < V_{i,max} \tag{5.15}$$

$$P_{gi,min} < P_{gi} < P_{gi,max} \tag{5.16}$$

$$Q_{gi,min} < Q_{gi} < Q_{gi,max} \tag{5.17}$$

$$\sum_{i=1}^{N} r_{i,t} \geq \max\left(\sum_{j=d,w} \mu_j + 3\sigma_j, \max(P_{gi}) \right) \tag{5.18}$$

In (5.10) the cost for energy and reserves are minimized while respecting the constraints described by (5.11) through (5.18). Equations (5.11) and (5.12) describe the nodal balance constraints while (5.13) describes the power flow $F(\theta,V)$ limits. Equations (5.14), (5.15), (5.16) and (5.17) limit the voltage angle and magnitude and respective generator productions within specified limits. Equation (5.18) specifies the amount of reserve for the hour $r_{i,t}$. This is to select the reserve level according to the stricter of the two criteria: (*i*) the *N*-1 requirement or the maximum generation for the hour, $\max(P_{gi})$; and (*ii*) mean error $\mu_{d,w}$ plus three times the standard deviation $\sigma_{d,w}$ of the combined load and wind prediction errors, indicated by subscripts *d* and *w*, respectively [71, 72]. Load and wind forecasting error distributions can be found in Table 5.2.

The *N*-1 criterion ensures that enough reserve is scheduled to balance demand and generation after the outage of any single generation unit or tie-line. An underlying assumption is that other network disturbances such as a sudden load increase or load

Table 5.2. Forecast error data. Wind was normalized by the installed capacity and load was normalized by the average load

Parameter	Value
Mean load forecast error, μ_d	-0.002
Standard deviation of load forecast error, σ_d	0.026
Mean wind forecast error, μ_w	-0.004
Standard deviation of wind forecast error, σ_w	0.13

prediction errors are less severe and are thus covered under the umbrella of the *N*-1 criterion. With the advent of high levels of wind power, the *N*-1 criterion may not be sufficient and need to be revised to reflect the possibility of wind power prediction errors being greater than the power imbalance resulting from the loss of any single piece of apparatus. To avoid such a situation, we consider (5.18).

5.4 Optimization Algorithms

When considering long optimization routines, nonlinear objectives and constraints and the necessity to obtain a global optimum in stipulated amount of time, and the selection of the optimization algorithm become very important. Due to significant discontinuity of search space of the PSH candidates, classical optimization algorithms have not been preferred. Moreover, MATPOWER's MOST tool released in 2019 [73] performs scheduling using quadratic programming but only for continuous search spaces. In order to handle large-scale complex nonlinear optimization problems, modern heuristic optimization techniques have been introduced in recent years with applications to power systems [74]. In this chapter, three most popular modern heuristic optimization algorithms were chosen: a) Differential evolution, b) Genetic algorithm and c) Particle

swarm optimization. The test problem selected for the choice of algorithms was the optimization of 24-hour operation of TPSH in the 24-bus network.

5.3.1. Differential Evolution

Differential Evolution (DE) was formulated by Storn and Price [75] and consists of 4 main steps: a) initialization, b) mutation, c) crossover, and d) selection. The mutation operator is a unique property of DE in that the a randomly chosen individual evolves according to the weighted difference between two or more randomly chosen individuals. The crossover operation combines randomly chosen dimensions from the mutant and the parent according to a pre-designed law. Finally, the selection operation formulates the new population by evaluating and selecting the new individuals with improved fitness.

5.3.2. Genetic Algorithm

Genetic Algorithm (GA) was formulated by Goldberg [76]. Similar to DE, GA also performs a) initialization, b) crossover, c) mutation, and d) selection. The main differences between the two is that; a) the mutation operation occurs after the crossover operation, and b) the mutation operation in case of GA is not related to the difference between any individuals. In GA, the crossover operation is performed when two selected individuals or parents exchange parts of their genetic material to form two new individuals. The mutation operator then randomly selects a few individuals from the newly formed population and mutates. The mutated individuals are also added to the new children population. The selection mechanism is the same as that in DE.

5.3.3. Particle Swarm Optimization

Particle Swarm Optimization (PSO) was formulated by Kennedy and Eberhart [77]. Similar to DE, the population evolves according to the two differences: a) between the position of the global best individual and that of the chosen individual, and b) between its personal best and present position of the chosen individual.

5.3.4. Genetic Algorithm with Selective Evaluation

The proposed variant of GA has the same steps of crossover, mutation, and selection. This is generally followed by the evaluation of the objective function. However, since the evaluation of the objective function is a significantly long task in certain situations, the evaluation of a large population might be of significant burden. Therefore, a GA with selective evaluation (SEGA) is proposed in this chapter, where not all children need to be evaluated.

The algorithm, after every generation, stores the chromosomes of the worst individual and makes use of this database to evaluate the children for the generations to come. In case the new child to be evaluated is within a radius of *r* of any previously stored worst solution, the child is directly assigned the cost of that worst individual. Hence, before the objective function is evaluated, the distance from the stored worst individuals are calculated for every child.

As shown in Figure 5.2, not all of the new children (C1, C2, …, C8) are evaluated; C6 is directly assigned the cost of worst individual-1 (WI1) as its distance from WI1 is less than that from WI2 and C7 is directly assigned the cost of WI3, where WI1, WI2 and WI3 originated from the first, second and third iterations, respectively.

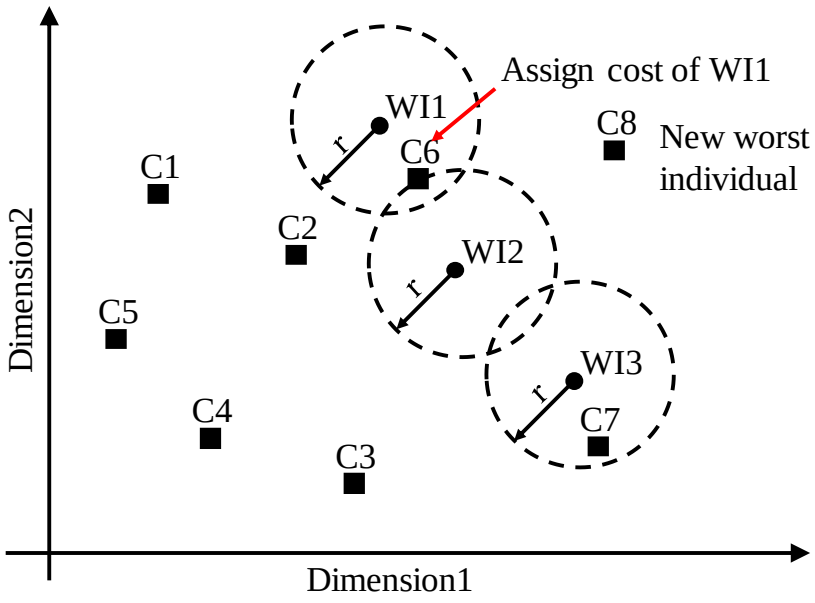

Figure 5.2. Illustration of proposed GA with selective evaluation. WI1, WI2 and WI3 are the worst individuals originated from the first, second and third iterations, respectively.

On average, *SEGA takes 66.46 seconds per iteration and conventional GA takes 72 seconds per iteration,* while they converge to approximately the same value of the objective function as can be seen in Figure 5.3. The proposed variant is therefore a memory-based optimization algorithm that exploits the data collected from previous iterations.

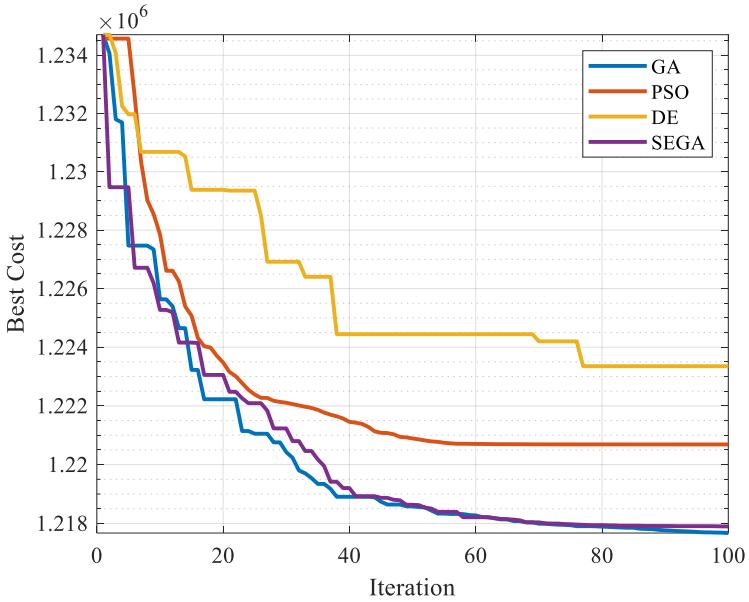

Figure 5.3. Objective functions of GA, PSO, DE and GA with selective evaluation (SEGA).

5.5 System Data

To generalize the findings, the IEEE 24-bus reliability test system (RTS) system [78] as in Figure 5.4 is considered during a winter and summer weeks. For the 24-bus RTS system, the hydro power plant at the bus 22 was replaced by the PSH plant. For the replacement of the hydro plant, the 6 units were deleted from the generator matrix as well as the generator cost matrix. Also, the bus type was changed from generator bus to load bus for the replacement.

Table 5.3. Additional system data

Parameter	Value
Total base load	3135 MW
Total wind capacity	960 MW (3x320MW) @ Bus 3, 11, and 21
Pumped hydro capacity	300 MW
Total conventional generation	3405 MW
Maximum hourly penetration	Summer: 31% Winter: 29%

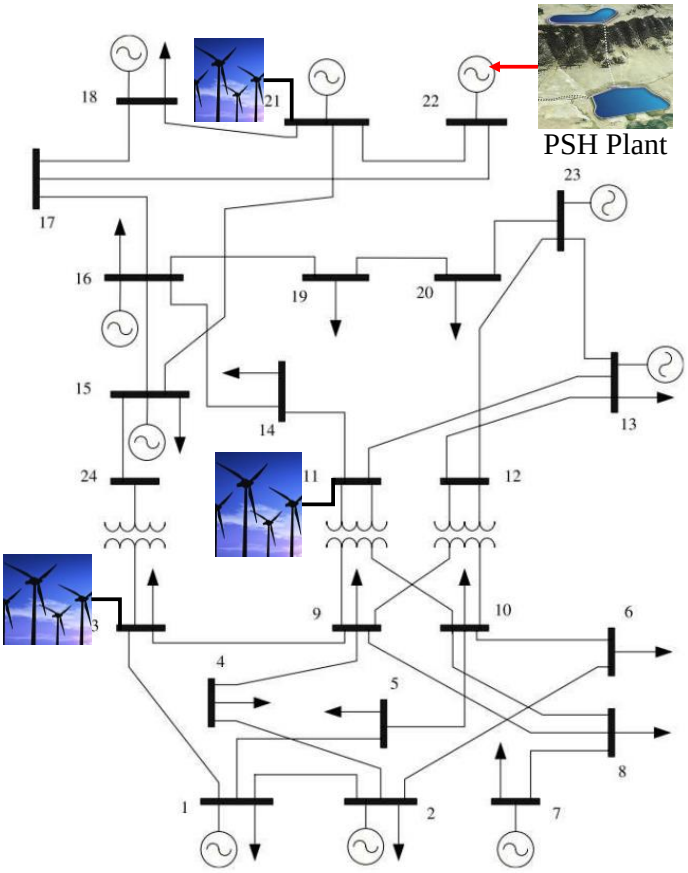

Figure 5.4. The modified 24-bus RTS system.

The reserve cost matrices were added to the test cases to obey security constraints. The PSH added was considered as a negative load. Reactive power of the PSH is maintained at 0. Further details about the sytem load, generation and wind can be found in Table 5.3.

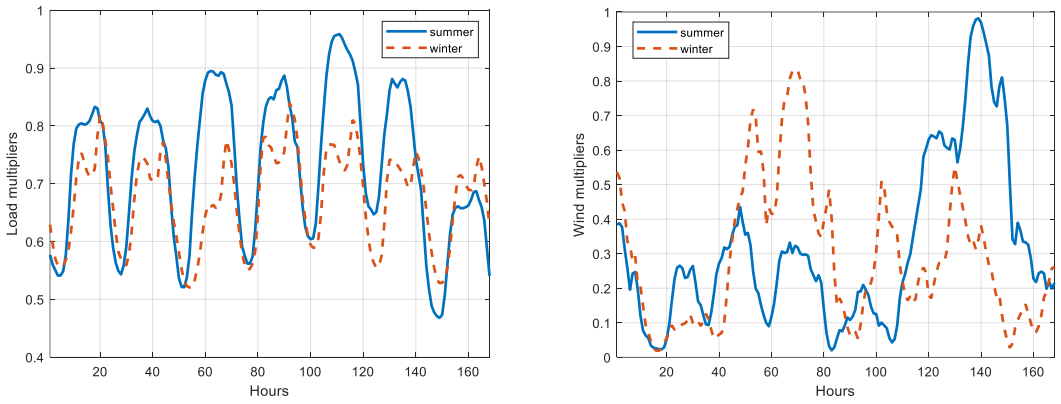

(a) (b)

Figure 5.5. Weekly (a) Load and (b) Wind Profile for summer and winter.

The wind and load profiles of one week that have been used for the summer and winter analysis are displayed in Figure 5.5 [79]. Much difference can be seen between the summer and winter load profiles. The variation in load between weekends and weekdays is low in winter as compared to the summer profile, which hints towards the low variation of nodal prices between the weekend and weekdays during winter. Also, the winter load profiles provide a dual peak load curve for most days which is mainly caused by residential use of electricity. The wind profile also displays a daily pattern; however, extended durations of high-power output can be observed which provide opportunities for charging for the PSH systems. Also, the wind profile displays significant ramping activity.

5.6 Results and Observations

5.5.1. Without Wind

Optimized results in Figure 5.6 display that CPSH *earns the least amount of revenue*. Although the 24-bus RTS system does provide ample opportunity for the PSH

plants to participate, CPSH is limited by inefficiency at the partial-load generation mode and inability to perform pump mode regulation, and hence earns lower revenue compared to the ASPSH and TPSH. Also, with reduced nodal price differences in the winter, the arbitrage revenue is reduced for all PSH types.

The operating mode analysis, as displayed in Table 5.4, reveals the participation of the plants in its different modes. *The CPSH and ASPSH remain idle for more than half the week.* However, as seen in Figure 5.6 the ASPSH plant beats the CPSH plant in revenue in both summer and winter which can be mainly attributed to its enhanced partial-load generation efficiency and enhanced performance factor. The TPSH, however, has the lowest number of idle hours which does indicate a higher O&M cost.

The ASPSH leads the partial-load generation hours among all PSH types. The ASPSH plant has the ability to efficiently participate in the partial-load generation, which

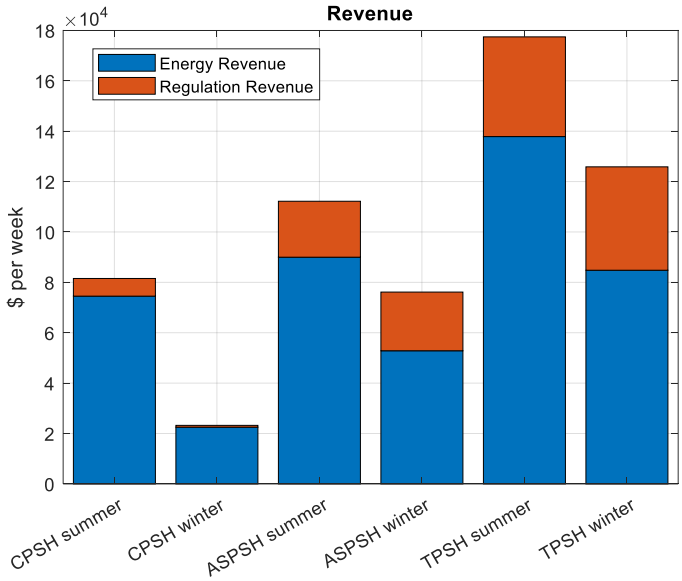

Figure 5.6. Weekly revenue collected from the energy and regulation markets combined with the storage technologies from the 24-bus system for summer and winter weeks.

is why it displays 11% and 13% of the week generating at partial-load in summer and winter, respectively. Also, the partial-load generation during peak hours provides the opportunity for the ASPSH system to participate in the reserve market and given its high-performance factor, it earns a significant portion of its regulation revenue by operating in partial-load generation. The comparatively higher (compared to CPSH) partial-load generation of the ASPSH plant is also strongly motivated by the opportunities provided by the network.

In the pump mode operation also, we find certain differences between each PSH types. First, the amount of time spent in pumping is different for each technology. As the hydraulic short circuit enables the TPSH to provide pump mode regulation, *the TPSH spends most of its time in the pump mode with the hydraulic short circuit engaged*. This results in smaller amount of time spent at pumping at rated capacity. *Although the ASPSH can participate in regulation in its pumping mode, that does not encourage its pump mode operation.*

As a result, the duration spent in pump mode operation for ASPSH is slightly lesser than the CPSH. *Thus, the ASPSH mostly relies on efficient partial-load generation for its regulation revenue.* Also, this higher participation of ASPSH in partial-load

Table 5.4. Time spent [%] in each mode of operation over the week; positive being generation and negative being pumping; S = summer and W = winter

Mode	CPSH		ASPSH		TPSH	
	S	W	S	W	S	W
0.8 to 1	11	13	6	5	11	12
0.4 to 0.8	4	0	11	13	11	10
Idle	66	70	68	69	22	12
0 to -0.75	0	0	0	0	43	53
-0.75 to -1	17	16	15	14	11	11

generation leads to reduced water usage, which leads to the reduced pumping requirements.

Another key observation is the comparatively higher participation of TPSH in the generating mode. This is mainly attributed to the higher reservoir levels as a result of the plant operating in pump mode for extended periods with hydraulic short circuit.

5.5.2. With Wind

Figure 5.7 shows the optimization results with wind generation included. Comparing Figures 5.7 and 5.6, it shows that the trend that the TPSH leads all other types of PSH from a revenue standpoint still holds. One major difference in revenue is the reduction of revenue collected by TPSH which can be attributed to the increased operational hours in pump mode that was required to prevent the curtailment of wind energy. Also, the reduction in nodal price due to the availability of wind resulted in

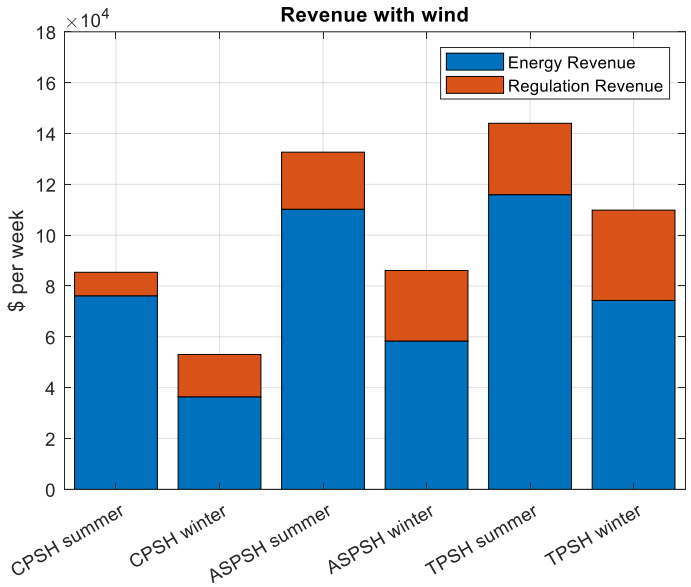

Figure 5.7. Weekly revenue collected from the energy and regulation markets earned by the PSH technologies from the 24-bus system with and without 30% wind.

reduced revenues. Another key observation is the increase of CPSH arbitrage and regulation revenue during winter. This can be justified by the availability of low-priced energy during increased operational hours with the inclusion of wind which provides the CPSH additional pumping opportunities at lower costs. Another important observation is the higher participation of CPSH in the regulation market especially in winter.

The regulation requirement increases as wind is included which is why the revenue from the regulation market is comparatively higher for all PSH variants. Winter months observe a greater participation in partial-load generation for all candidates, which could be attributed to the low load conditions and hence the lower revenue.

With the inclusion of wind resources, the PSH types display *an overall increase in activity which could be attributed to the ramping of wind resources* when comparing Table 5.4 and Table 5.5. As conventional PSH units have restricted ramp rates due to their physical characteristics, PSH systems provide the required flexibility. Especially in winter we observe repeated and high ramping of wind output which is accommodated by the pumping mode operation of PSH facilities. Greater participation in the generating mode for all PSH types leads to increased pumping hours. This indirectly has resulted in the decrease of idle hours for each PSH type.

Table 5.5. Time spent [%] in each mode of operation over the week with positive being generation and negative being pumping; S = summer and W = winter

Mode	CPSH		ASPSH		TPSH	
	S	W	S	W	S	W
0.8 to 1	14	5	13	8	19	14
0.4 to 0.8	10	20	8	15	5	12
Idle	50	48	54	54	7	7
0 to -0.75	0	0	0	0	50	52
-0.75 to -1	25	25	23	22	17	14

Table 5.6. Curtailment in MWhrs

	Summer	Winter
CPSH	360.21	20.21
ASPSH	0	15.62
TPSH	0	0

The network optimization algorithm supported greater partial-load operation with the inclusion of wind, especially during the winters, we see that ASPSH and CPSH spend much time in generating mode. This consecutively increases their pumping requirement. Apparently, it seems as if the ASPSH outruns the CPSH in terms of revenue even with reduced hours of generation. This that can be justified by the fact that during *the hours that ASPSH spends in partial-load generation, it does so more efficiently and hence conserves water which minimizes pumping and provides opportunities to work on full load.* To reveal the change in operation of these candidates with the inclusion of wind, Tables 5.4 and 5.5 have been compared. *The key strategy for the TPSH is to operate mostly in pump mode with hydraulic short-circuit that boosts reservoir level and revenue as it participates in the regulation market.* Table 5.6 reveals the benefits of advanced PSHs from a curtailment standpoint.

5.7 Discussion

The work done in this chapter is only concerned with the penetration of wind energy. However, if only solar PV penetration would be considered instead, the results would be different. All PSH systems have been observed to charge during the night and in the weekends as these periods provide low locational marginal prices (LMPs) and network congestion is minimal. These opportunities would not be available with solar PV as the nighttime charging would not be possible or would have to be done at a higher cost

than with wind and could lead to added congestion if day-time charging was attempted. This would lead to low state-of-charge for the PSH system for most of the week. Thus, revenue would be lower than compared to the only wind scenario.

Also, the inclusion of both solar and wind (which is a more practical scenario) could present different results. The availability of wind energy would provide the opportunities for nighttime charging. This would result in higher state-of-charge for the PSH system for most of the week. However, discharging would be performed during a very few peak load hours during the day, as the daytime LMPs would be lowered due to solar PV. As diurnal price differentials would decrease, the chances of arbitrage would also reduce and hence the net revenue would reduce.

As mentioned in Section 5.1 that with the inclusion of renewables, the price of ancillary services would rise and so would their requirement. Thus, the wind and solar scenario would yield higher revenue from the regulation market than from the PV only or the wind only scenario.

5.8 Conclusion

With the increasing penetration of renewable energy, the need for controllable resources is ever increasing. This chapter presents advanced pumped-storage hydro systems as such controllable resources and compares the revenue earning potential of CPSH, ASPSH and TPSH.

An optimal operational planning framework has been created using the co-simulation of MATLAB and MATPOWER. A comparison of modern heuristic optimization techniques, DE, PSO and the conventional GA, is presented where GA beats the others in solution optimality. To reduce the time consumed in the optimization

process, a variant of GA is proposed called SEGA (or GA with selective evaluation). The comparison shows that if the objective function takes considerably long time to evaluate, SEGA produces similar results to that of GA with a shorter time per iteration.

Key generalized conclusions from the optimization are: *a*) With and without wind ASPSH and TPSH show higher revenue earning potential compared to CPSH, *b*) The hydraulic short-circuit of the TPSH offers greater advantages than the converter based regulation of ASPSH, *c*) the generation mode efficiency enhancement in ASPSH system is of significant benefit and should be considered during governor design, and *d*) not only do the advanced PSH plants show greater participation in the regulation market, but their potential to participate in arbitrage is also greater than CPSH.

CHAPTER SIX

Impacts of Quaternary Pumped Storage Hydropower

6.1 Introduction

As renewable penetration increases in the United States, the primary challenge of grid operation is to ensure the stability and reliability of low-inertia power grid by providing sufficient frequency control capability. The advanced pumped storage hydro technologies (PSH) will be expected to play an important role for future grid as not only an energy supplier, but also an ancillary services provider.

Power system inertia is a critical parameter that indicates the resiliency of the system in the face of any disbalance in real power. Variation in system inertia significantly effects the deviation of system state variables [80, 81]. Conventionally, the increase in the number of generators on the system at any given time will increase system inertia. However, with the increase of renewable energy generation, the number of synchronous generators on the network are decreasing which is gradually reducing system inertia. The removal of synchronous generators from the schedule also removes the availability of controllable resources for primary and secondary frequency regulation.

Conventional PSH (CPSH), is the currently widely used PSH technology in the United States, however, this system can only provide frequency regulation in the generating mode but not in pumping mode. This limitation makes CPSH unfit for future needs to balance variable generation for an extremely high renewable penetration. The

advanced PSH technology evolves from CPSH and have gained popularity due to their superior capability in providing frequency regulation in all modes of operation.

This chapter presents the modeling and control of a new type of PSH technology called the quaternary pumped storage hydropower (QPSH) and studies the comparative benefits of using QPSH to provide primary frequency response service instead of using CPSH. Table 6.1 presents a few benefits of QPSH over CPSH. Currently, there is no publicly available dynamic model for QPSH in the existing commercial software such as Siemens PTI Power System Simulator (PSS/E) and GE Positive Sequence Load Flow (PSLF).

To quantify the impact of QPSH on frequency response of the U.S. Western Interconnection, a model of QPSH is developed using Engineering Process Control Language (EPCL) on the GE's PSLF platform and the newly-develop model is implemented in a set of detailed U.S. Western Electricity Coordinating Council (WECC) planning cases which renewable penetration levels are 20%, 40%, 60% and 80%. Results

Table 6.1 Comparison of CPSH and QPSH

Category	CPSH	QPSH
Ancillary services	In the pump mode, it is incapable of load following, primary and secondary frequency response.	In both the pumping and generating modes, it can provide required ancillary services.
Mode change	>2 mins	<60 secs
System efficiency and range of operation	Poor part-load generating mode efficiency. Limited range of operation.	Comparatively higher partial-load efficiencies as turbine and pump are separately optimized. Extended range of operation.

show that QPSH can provide primary frequency support by controlling both pump and turbine simultaneously in a unique operation mode called hydraulic short-circuit mode.

6.2 GE's PSLF and EPCL for User-Defined Component Modeling

The PSLF has 3 main types of file format extensions, a) The *.sav file* which consists of the load flow data tables (bus data table, line data table, etc.) and can only be created with the PSLF, PSS\E, POWERWORLD interface, b) The *.dyd file* which consists of the dynamic models for the generators, governor, excitation systems and stabilizers is created with notepad, and c) The *.p file* which is constructed with the EPCL code and may consist of any user-defined models that are associated with the dynamic data (*.dyd file*) or the code for automation procedure in PSLF.

The *.dyd file* is composed mainly of name value pairs where the parameter name and its value are stated for any component. As an example, consider the IEEE Type-1 speed governor model for steam turbines in Figure 6.1.

In the *.dyd file* the above model can be represented as, *ieeest 201 "2_BPSGEN " 20.00 "1 " : #9 1 0 0.01333 0.000044 0 0 0.128 0.0064 0 0 0 0 7.5 7.5 5.556 0.1 -0.1 0*

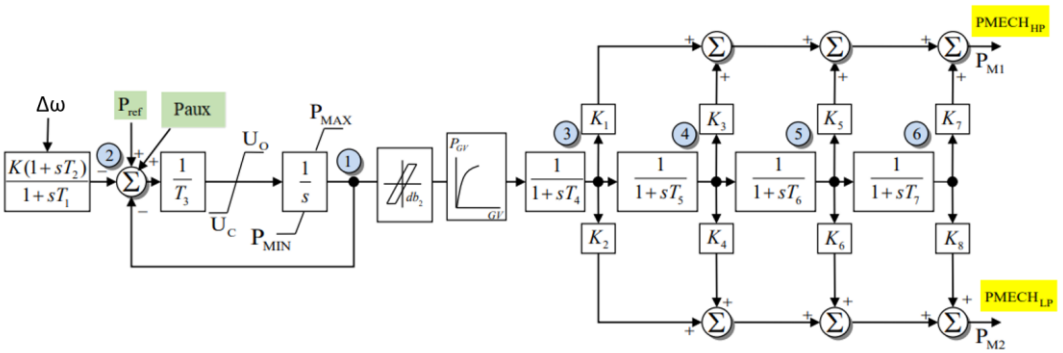

Figure 6.1. IEEE Type-1 speed governor model.

0 0, where the type of model is followed by the bus id number, the bus name, the voltage level and the generator id number at the bus since there can be multiple generators at a single bus. This is then followed by a table number "#9", which records the internal table number where the compiled model is located, and the 20 parameters in the model.

Automation of simulation provides a time saving method when repeated runs of the simulation are required. The EPCL code can be used as a Macro which can be used to access and edit any table in the *.sav file*, execute or pause any simulation, change dynamic model parameters, among others. For this project EPCL was used to perform both creating user-defined models and automation and data extraction.

To create a user-defined model in the EPCL, the entire code was organized into six different sections with the switch case command. Based on the stage of dynamic simulation, the particular case of the EPCL code will be simulated. The sections (these are generalized names of the sections and not abbreviations) are: a) INIT, where state variable were initialized from the results in the load flow result table, b) SORC which is used to define any network-interfaced equipment like generator or converter and where network current injections are calculated, c) ALGE, where algebraic equations are solved, e) RATE, where differential equations were solved and limits on state variables are applied, and f) OUTP, where the output channels are computed and exchanged with the dynamic simulation program. The PSLF allows 100 state variables for a single model. The preparation of a transfer function for the user-defined model is necessary and requires that each transfer function can be transformed into a set of the first-order transfer functions.

For the operation of the dynamic simulation, an EPCL file was created that first read the load flow case (*.sav file*) and solved it, next the dynamic data (*.dyd file*) is read and initialized with the results from the load flow solution and simulation parameters that were set. The EPCL file could also pause the simulation, apply a disturbance and resume the simulation. Later, another EPCL code is used to extract output channel data to *.csv* format and MATLAB was used to obtain the resulting figures.

6.3 Structure of QPSH

The structure of QPSH combines the benefits of both ASPSH and TPSH. As shown in Figure 6.2, QPSH consists of a separate pump-motor combination and a separate turbine-generator combination. Unlike TPSH, in the QPSH the pump-motor combination and the turbine-generator combination are situated on separate shafts. Both electrical machines are synchronous machines. Here, a full-sized converter is included to interface the pump-motor combination with the grid while the turbine-generator combination is directly connected to the grid. The choice of electrical machine can be varied based on the plant owners.

The structure of QPSH presents unique opportunities. The separation of the shaft leads to reduced space requirement which in turn facilitates ease of construction. Also, the availability of the converter helps enhance the response of the unit and pump mode flexibility. The rate of response of the QPSH unit is significantly higher than the CPSH as the pump and the turbine can respond to a disturbance simultaneously. However, the probability of failure increases as the number components increase with the pump converter. Nevertheless, a failure in converters will not affect the turbine as both are mechanically and electrically decoupled.

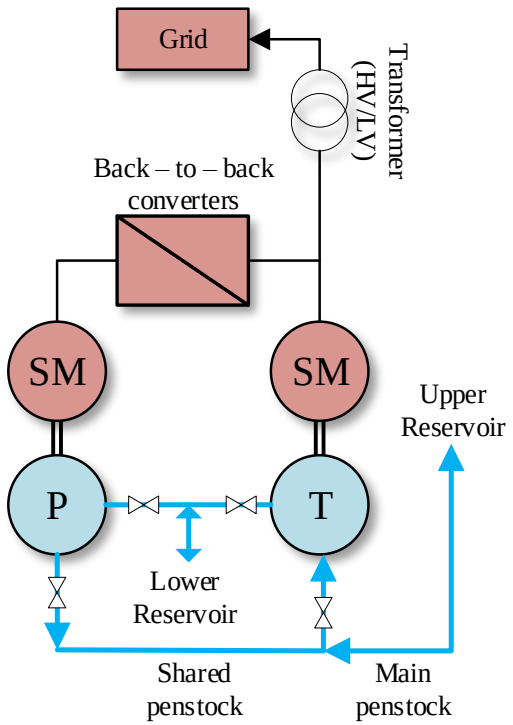

Figure 6.2. Functional diagram of QPSH.

6.4 Modelling and Control of QPSH

The modeling of the pump is performed as mentioned in Section (3.3.1) where the head generated by the pump is given as a quadratic function of speed and discharge by (3.9). The turbine is represented by (3.1) through (3.4) in Section 3.3.2. To model the hydraulic short-circuit, (4.2) of Section 4.3 is implemented.

The turbine control implements a HYGOV governor structure [82] with water starting time constant-based non-linear water column hydraulic turbine model. Similar to that mentioned in Sections 3.4 and 3.5, the back-to-back converter for the adjustable speed pump has two parts, the machine side converter (MSC) and the grid side converter (GSC). The MSC implements a rotor flux-oriented control to control the speed of the machine, which directly affects the power consumed from the grid. The GSC implements

a grid voltage-oriented control which enables it to control the terminal voltage and the maintain DC bus voltage by exchanging the required amount of real power with the grid. In addition to the droop control, additional methods of control can be used to provide better frequency support. These strategies can be implemented through the converter of the adjustable speed pump. Here, the converter controller implements a low frequency oscillation damping controller and a virtual inertia-based controller as can be seen in Figure 6.3.

The complete control system for the QPSH can be schematically presented as Figure 6.4 with the main inputs as system frequency and AGC signals. The power command distribution function, using distribution coefficients K_{d_p} and K_{d_t}, as in equation (1) is used to generate references for the turbine and pump controllers. When a power order is received, the order is distributed among the pump and the turbine using the distribution function:

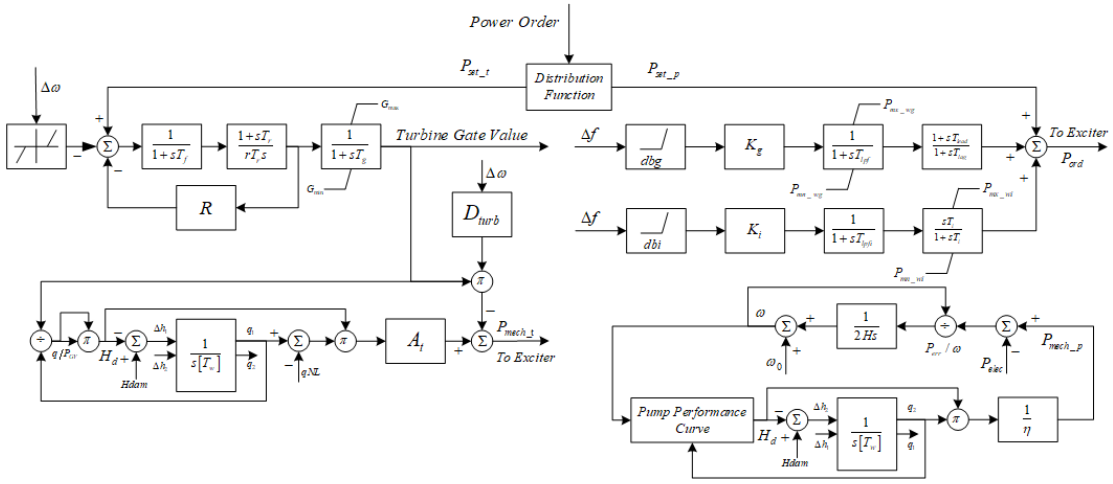

Figure 6.3. Governor turbine model for the QPSH with HYGOV based turbine control and inertia and low frequency oscillation damping controller through the converter.

$$\begin{cases} P_{ord\_p} = -K_{d\_p} \times \left| P_{demd} \right| \\ P_{ord\_t} = K_{d\_t} \times \left| P_{demd} \right| \end{cases} \tag{6.1}$$

These commands are used as primary references for the turbine governor and pump converter, and serve the purpose of secondary control of the system. These distribution coefficients can be determined based on the operator's choice or from a system optimizer based on the water level of the upper reservoir and market conditions.

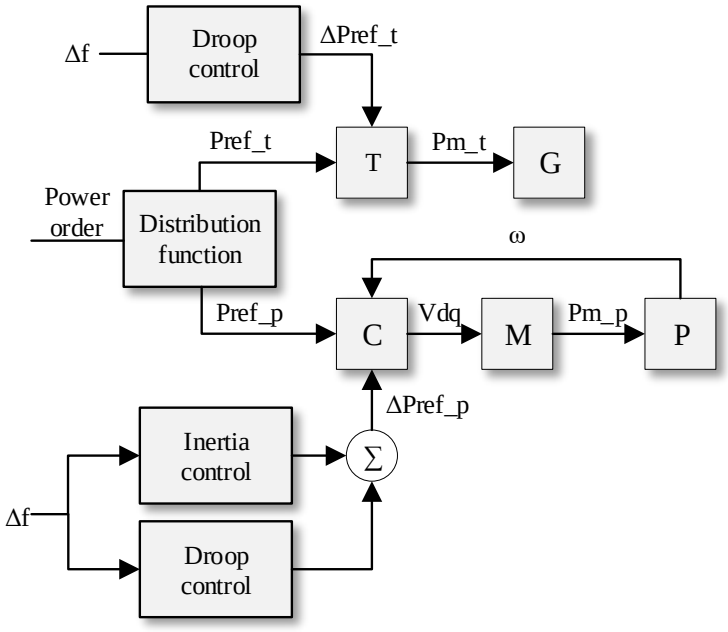

Figure 6.4. Control system for QPSH where, C=converter, M=motor, P=pump, G=generator and T=turbine and governor.

6.4 Simulation Results and Discussion

6.4.1 Test System - Detailed WECC System

This work considers the WECC 2022 light spring case (2022LSP) where the system conditions represent a low load and a planned amount of high renewable

penetration. Also, in the spring of 2015 four generation trip events were recorded which eased the process of model verification. Results from the model verification displayed that the model was successfully able to capture the time domain dynamics of system frequency. Detailed results can be found in [83].

The test system consists of 19000+ busses, 4000+ generators, and is divided among 21 areas, 424 zones and 492 owners. Table 6.2 describes the governors and generator models. Here, not all systems are equipped with governor systems, e.g., nuclear and a few coal-based plants [84]. Most of the governor response is derived from hydro, combined-cycle and gas-turbine units.

Table 6.2. Governor and generator models for the WECC system

Prime mover models	**Number of units**	**Generator models**	**Number of units**
Ggov1	1157	Genrou	1526
Hygov	285	Gentpj	1316
Ieeeg1	266	Gentpf	682
Ieeeg3	233	Motor1	59
Hyg3	131	Gencc	52
Hygov4	111	Gensal	13
Gpwscc	110		
Icfb1	88		
Pidgov	67		
Gast	39		
Tgov1	24		
G2wscc	34		
Hygovr	14		
Ggov3	11		
W2301	9		
Ccbt1	3		

6.4.2 Development of High Renewable Penetration Scenarios

The 20, 40, 60 and 80% scenarios in Table 6.3 have been developed by keeping the wind power constant at 15% and varying the rooftop PV penetration. Rooftop PV and utility scale PV have different behaviors. To consider these behaviors the scale of both have been moderated to suit the projected growth [85].

Regional technical potential-based method and National Solar Radiation Database (NSRDB) were respectively used to calculate the suitable space and insolation available at a zip code. In brief, rooftop PV technical potential-based method processes Light Detection and Ranging (LIDAR) data and building footprint data which are analyzed for shading, tilt and Azimuth in order to determine the suitability of rooftop area for PV [86]. The NSRDB is an open source NREL-built database that provides the solar irradiation data that can be further modified by using the geographical and weather information of the area of interest [87].

Table 6.3. Wind and PV penetration for different developed cases

Case	**System inertia**	**Wind penetration**	**PV penetration**	**Total penetration**
20%	3.02	14.36%	1.73%	21.03%
40%	2.21	14.36%	22.73%	42.02%
60%	1.93	14.53%	42.28%	60.16%
80%	0.93	14.53%	61.16%	80.61%

6.5 Results and Discussion

To realize the benefit of QPSH over CPSH, several existing CPSH units in the system were replaced by the QPSH. The hydraulic system of Figure 6.3 was developed

using user-defined model in GE's PSLF [88] platform. The generator, exciter and associated stabilizer models were left unaltered to retain a level of certainty.

6.5.1 Baseline Analysis

For the baseline analysis, the WECC system was considered with CPSH installed. The baseline analysis provides a sense of the problem at hand and in fact verifies the assumption that higher penetrations of renewable energy will reduce system inertia and cause larger deviations in system state-variables. At t=10s a plant (2.7 GW) trip is simulated, and the system experiences a frequency transient due to the sudden imbalance of real power. The frequency profile, as in Figure 6.5, displays a lower frequency nadir and settling frequency as the penetration level changes from 20% to 80%.

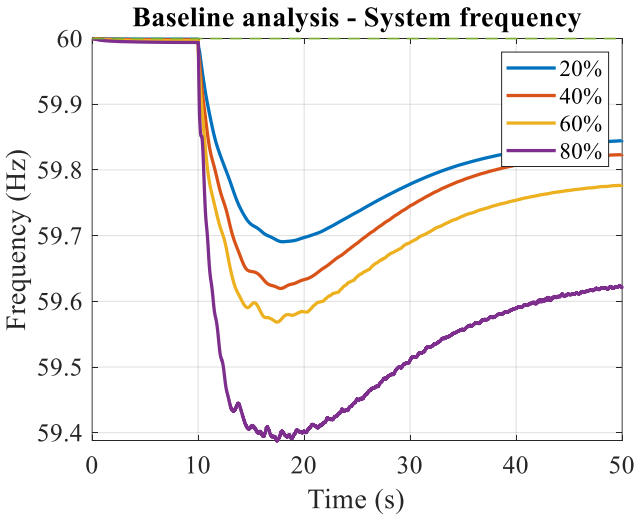

Figure 6.5. WECC System response to a plant trip event under 20%, 40%, 60% and 80% renewable penetration.

6.5.2. Effect of Penetration Levels

Figure 6.6(a) and 6.7(a) display the 20% and 80% penetration cases and the respective improvement in frequency nadir and settling frequency in both cases. Figure 6.6(b) and 6.7(b) display the response of the QPSH and CPSH from the entire system. Figure 6.6(b) and 6.7(b) verify the capability of QPSH to provide frequency support in the pumping mode. Significant reduction in real power consumption can be seen which results from the dual action of both the pump and turbine.

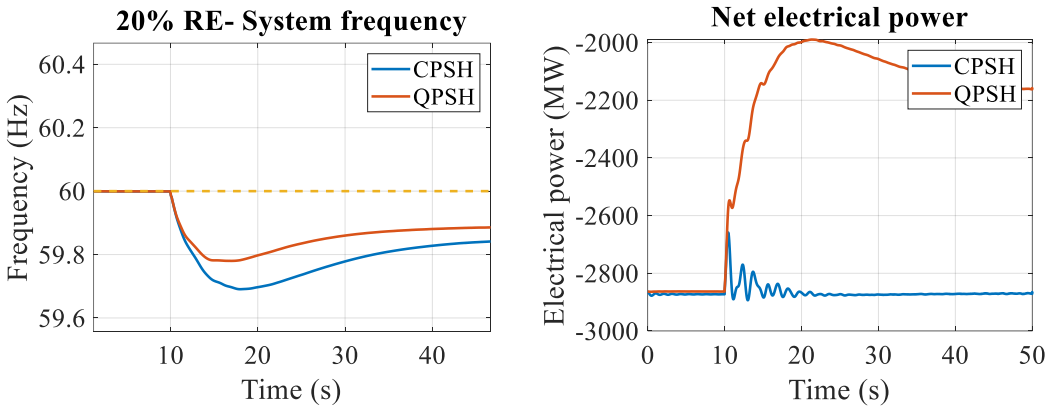

Figure 6.6. Analysis of WECC system: (a) frequency and (b) net response with QPSH vs. with CPSH under 20% RE penetration.

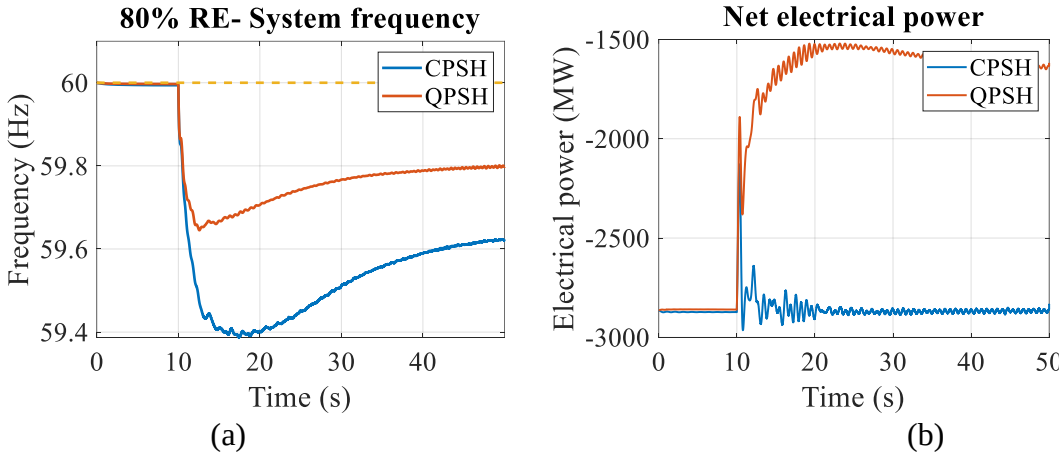

Figure 6.7. Analysis of WECC system: (a) frequency and (b) net response with QPSH vs. with CPSH under 80% RE penetration.

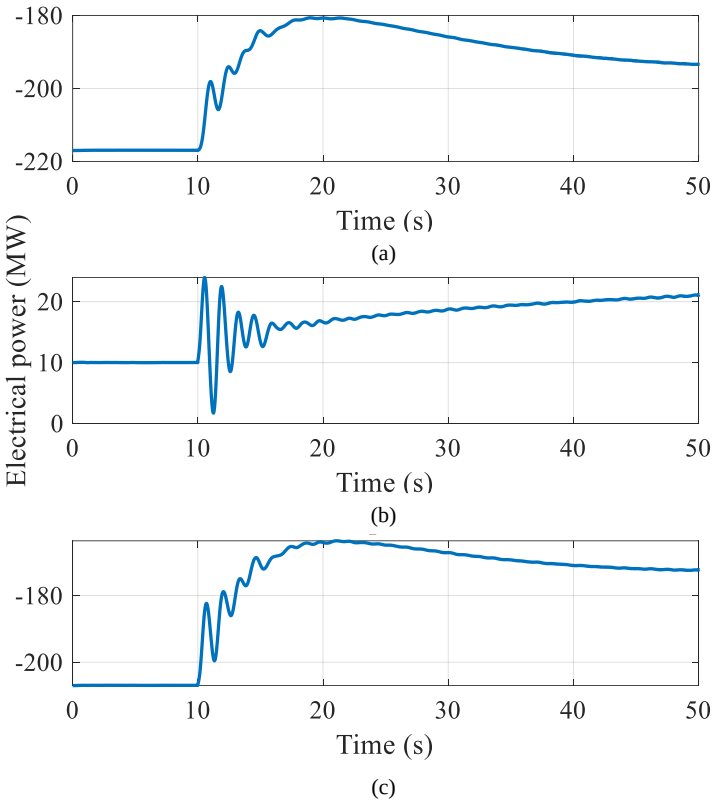

Figure 6.8. Electrical power from the (a) pump, (b) turbine and (c) combination.

Comparing Figure 6.6(b) and 6.7(b) shows that with the decrease in system inertia the response from the QPSH system increases by 500MW which provides the system with the much-required relief. Also, with the decrease in system, significant increase in fluctuations is also evident. To verify the simultaneous action of the pump and generator, Figure 6.8 breaks up the net action of one QPSH plant located at bus. The converter action regulates the pump output and governor action feeds water to the turbine through the hydraulic short circuit.

Figure 6.9 shows that with QPSH more than 80% renewables can be hosted in the same network from a dynamic stability standpoint as the frequency nadir is above the 59.5Hz mark. The settling frequency also shows better values which is mainly due to the

added relief from the primary frequency response of both pump and generator which is only possible with the QPSH.

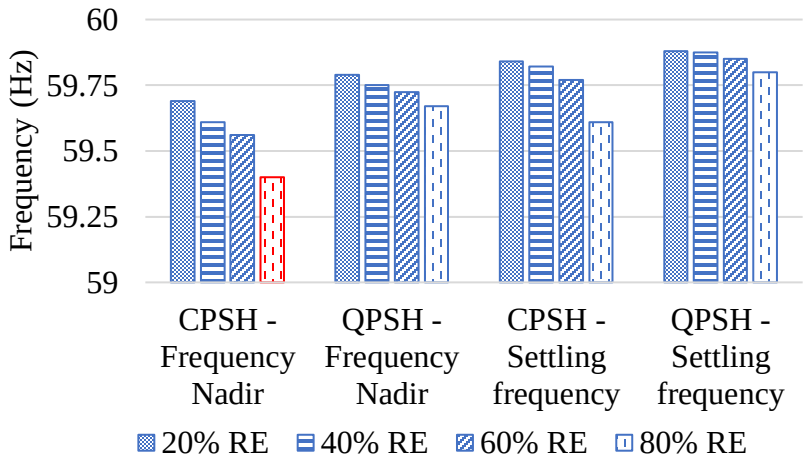

Figure 6.9. Summary chart for system frequency nadir and setling frequency indicating CPSH frequncy nadir with 80% RE penetration to be below 59.5Hz during pump mode operation.

6.6 Conclusion

The QPSH has been developed as a user-defined model in PSLF by using EPCL. The authors have considered futuristic cases where renewable penetration will be significantly higher (20%, 40%, 60% and 80% RE) than present conditions in the WECC system. A pump mode comparison of QPSH and CPSH has been performed that show that with QPSH the WECC system can be more stable even with significantly high levels of RE penetration. Also, results indicate that more RE can be hosted in the same WECC system when QPSH is used instead of CPSH. These benefits are attributed to the simultaneous action of the turbine governor and pump converter that is possible through the QPSH configuration.

CHAPTER SEVEN

Conclusions

With the advent of more efficient and economic renewable energy and energy storage systems, power system operation and control are undergoing significant changes. Although renewable energy is required, it presents significant challenges for existing power systems. Among these challenges, the primary one is the reduction of system inertia and secondly the reduction of available resources to deal with the intermittent nature of these renewable resources. Hence a more resilient power system is sought for with urgency. This dissertation considers different configurations of advanced pumped storage hydropower (PSH) energy storage as one of the grid-scale storage options that can provide significant flexibility required by the system.

7.1 Research Summary

First, the DFIM-based ASPSH is considered and a governor model is constructed. Through integration tests in the SMIB system it has been demonstrated that, the governor structure presented here, is successfully able to regulate the speed of the system and hence maintain the high efficiency, while tracking real power references in both generation and pump modes. Also, through the integration tests in the 9-bus test system it has been demonstrated that, the governor structure can provide primary frequency regulation in both pump and generation modes. Further, the converter interface allowed for the development of an adaptive droop (AD) scheme for primary control designed for

the ASPSH system which showed that the AD algorithm in-hand with the converter control could provide enhanced primary regulation for the system.

Second, the ternary PSH (TPSH) is considered and a governor model is constructed. The governor model is designed with the capability to display the use of the hydraulic short circuit and the use of the mode changing capability of the TPSH. The SMIB integration results were performed to demonstrate that the governor model can track power references in the pump mode and that, the mode change logic can facilitate the mode change from pump to generator, and vice-versa, without the loss of synchronism. Simultaneously, through the 9-bus test system integration it was shown that, in the face of disturbance, the pump mode reference tracking could be of great benefit, but the mode change capability could be an important emergency response tool for system operators.

Finally, during a summer internship at the National Renewable Energy Laboratory (NREL) in Golden, CO, Quaternary PSH (QPSH) was investigated. The governor model for the system was developed in GE's PSLF platform using a combination of the HYGOV and converter controls for turbine and pump, respectively. An integration test was performed into the US western interconnection for 20%, 40%, 60% and 80% renewable penetration. The benefits of combined action of the pump and the turbine were observed to give significant relief to the system even during high penetrations of renewable energy.

Although, the above governor models displayed significant flexibility, a revenue earning analysis of the PSH configurations (excluding QPSH) were performed considering arbitrage and regulation. First a generalized framework for revenue earning

potential analysis was performed that can be applied to converter and machine interfaced resources. For the system study, the IEEE 24-bus system was considered, along with a week-long period of wind and load profiles and with seasonal variation of these profiles. The TPSH showed that it could earn higher revenue results irrespective of the weather conditions and wind penetration.

7.2 Future Work

On the TPSH front, extension of this work could be the hybridization of the TPSH and with other generation and storage sources to provide enhanced response to system disturbance and load following. Since PSH reservoirs have large open areas that can be utilized for floating PV, the combination of both would provide symbiotic benefits. Also, the synchronous condenser mode of TPSH has not been explored here and the fact that TPSH can transition into either generation or pump mode from synchronous condenser mode needs to be simulated, as this can prove to be additional emergency control measures for the system operator. On the same note, although the governor shown in this work is capable of changing modes, an automated mode change algorithm would greatly benefit the system.

On the ASPSH front, the inverter interface of ASPSH provides the scope for solving numerous problems in power systems. Low frequency oscillation damping (LFOD) is one such problem in large-scale power systems and a stabilizer-based control of the converter interface could enhance the networks' LFOD capabilities. Also, virtual synchronous generator (VSG)-based synthetic inertia control can be made possible through the interfaces. This would enhance the system frequency profile.

APPENDIX

APPENDIX A

ASPSH and TPSH Mask Parameters and Internal Construction

This appendix presents the block diagrams and parameter entry masks created in Simulink shown in Figure 3.15 and for the TPSH system.

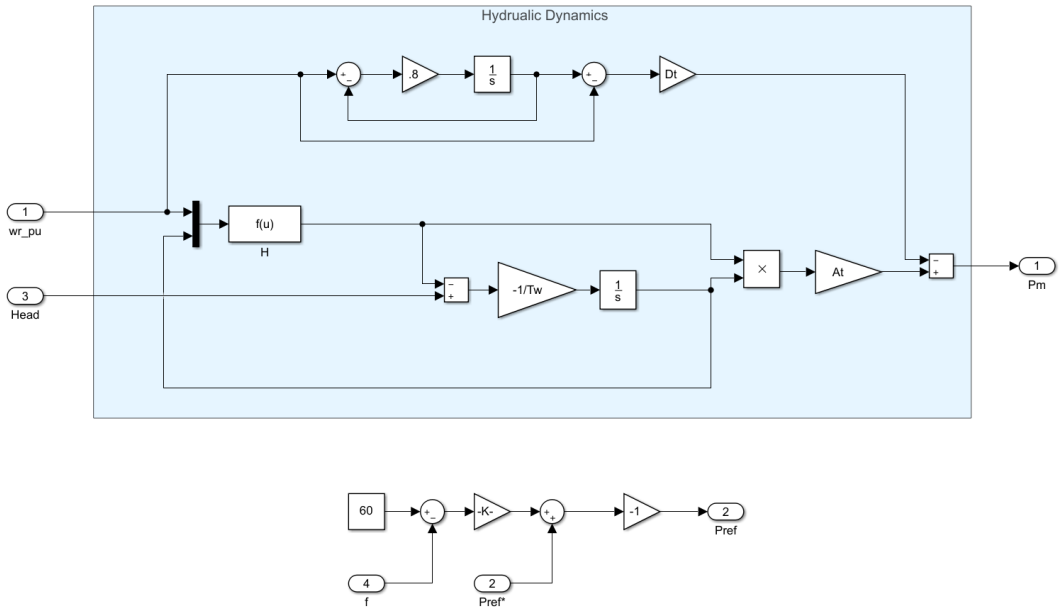

Figure A.1. Pump mode hydraulic dynamics and primary regulation with gate completely open. The function block deploys equation (3.9).

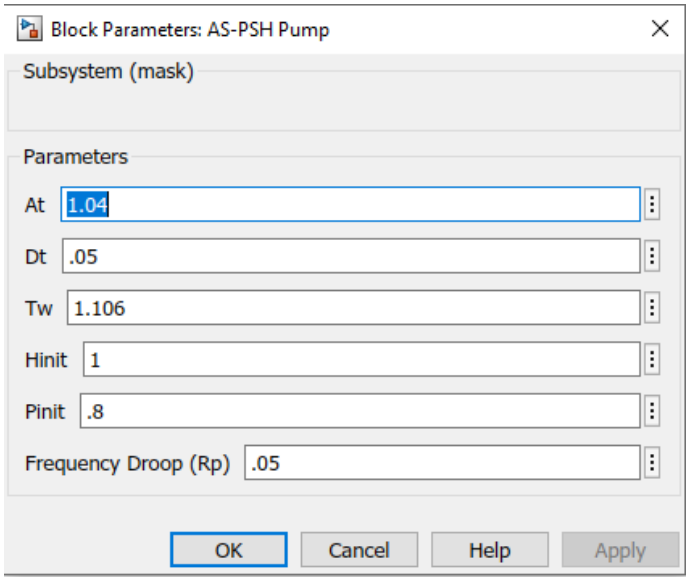

Figure A.2. ASPSH pump mode mask for parameter value entry.

Table A.1. Parameters and definitions of the ASPSH pump mode mask

Parameter	Description
Tw	Water Time constant
At	Power conversion coefficient
Dt	Damping factor
Po	Initial mechanical power
Ho	Initial head
Frequency Droop	Frequency and power droop coefficient

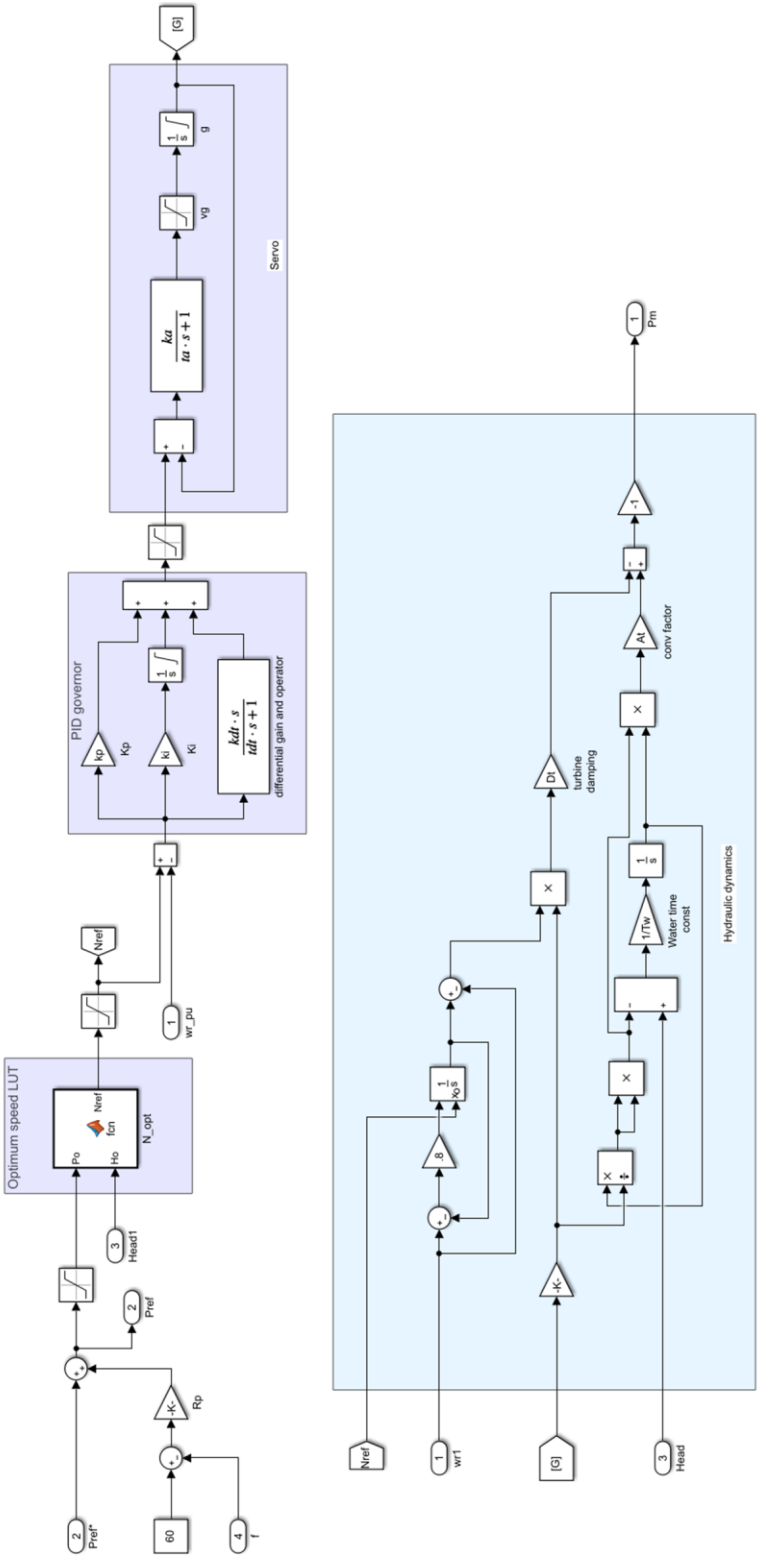

Figure A.3. Turbine mode governor and hydraulic dynamics for ASPSH.

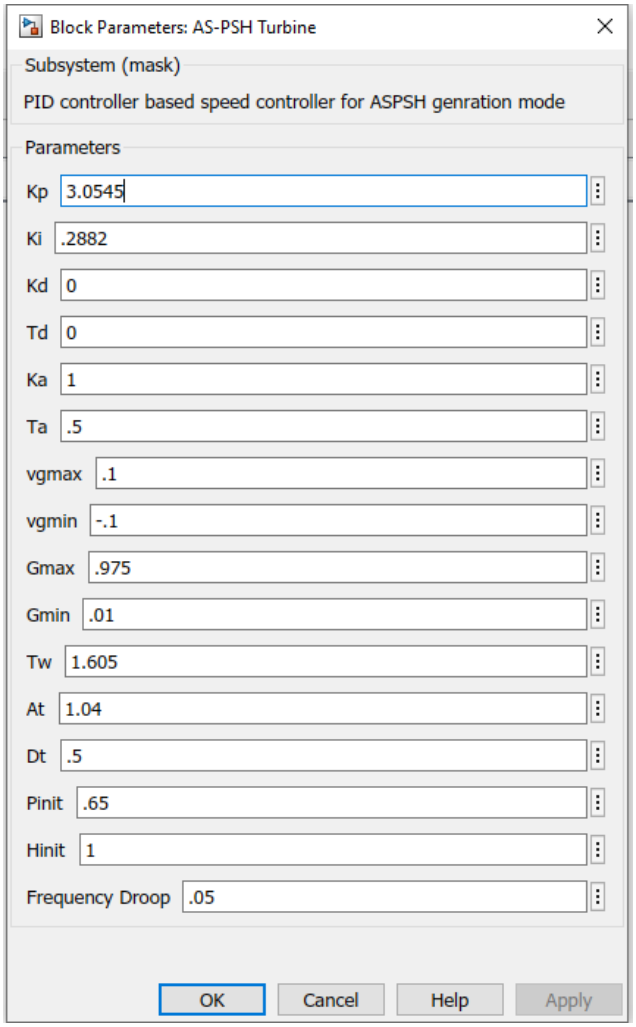

Figure A.4. ASPSH turbine mode mask for parameter value entry.

Table A.2. Parameters and definitions of the ASPSH mask

Parameter	Description
Kp, Ki, Kd, Td	Proportional, integral, and derivative gains and derivative filter time constant
Ka, Ta	Servo motor, gain and time constant
Vgmax, vgmin	Maximum and minimum gate velocity
Gmax, Gmin	Maximum and minimum gate position
Tw	Water Time constant
At	Power conversion coefficient
Dt	Damping factor
Pinit	Initial mechanical power
Hinit	Initial head
Frequency Droop	Frequency and power droop coefficient

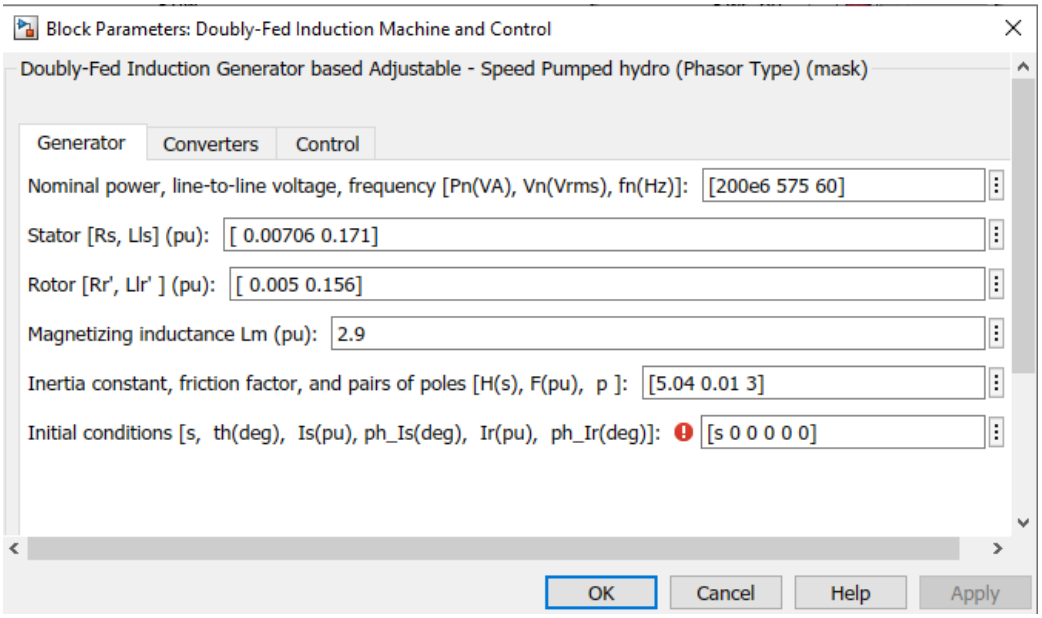

Figure A.5. DFIM machine and control mask, generator parameter entry.

Table A.3. Parameters and definitions of the DFIM machine and control mask for generator parameter entry

Parameter symbols	Symbol details
Rs, Lls	Stator resistance and leakage reactance
Rr', Llr'	Stator resistance and leakage reactance referred to the rotor
S, th(deg), Is(pu), ph_Is(deg), Ir(pu), ph_Ir(deg)	Slip, rotor angle, stator current, phase angle of stator current, rotor current, Phase angle of rotor current

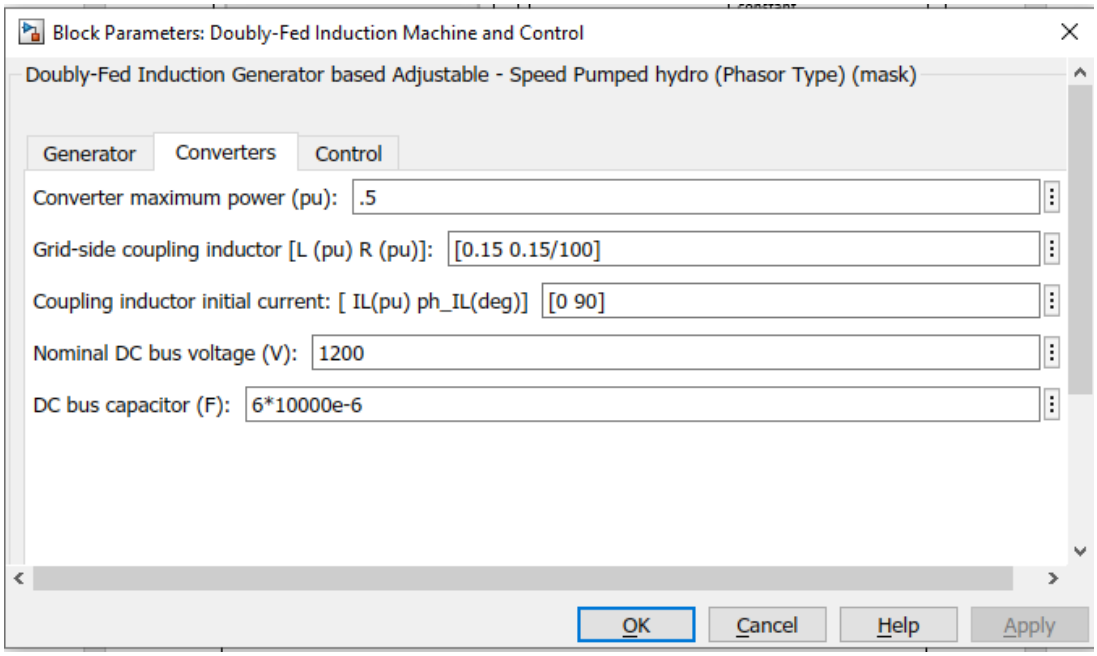

Figure A.6. DFIM machine and control mask, Converter parameter entry.

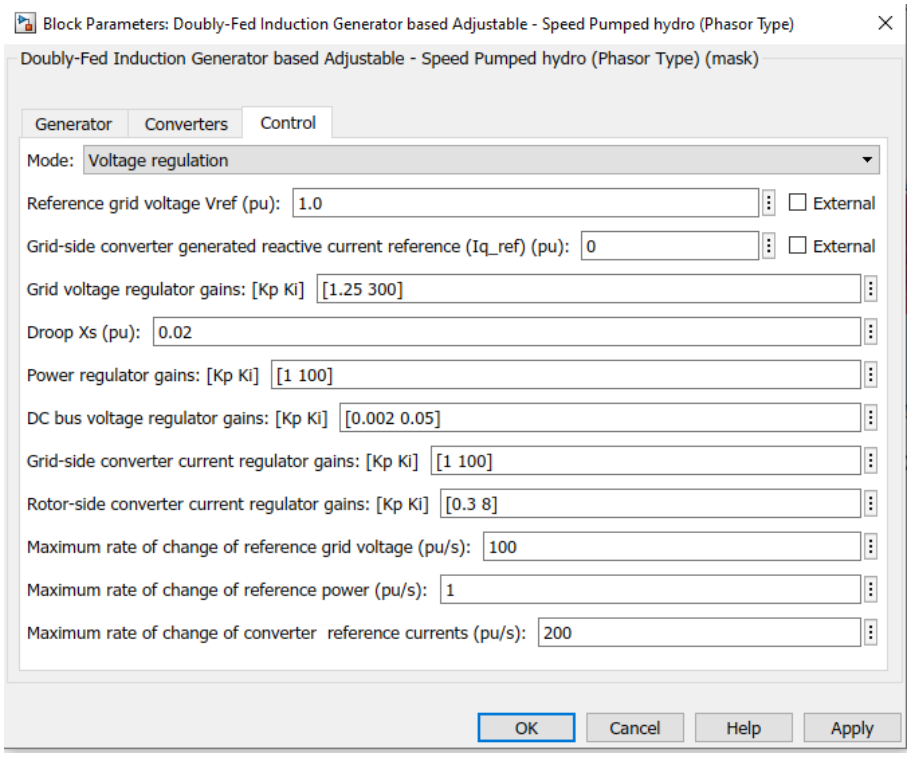

Figure A.7. DFIM machine and control mask, controller parameter entry.

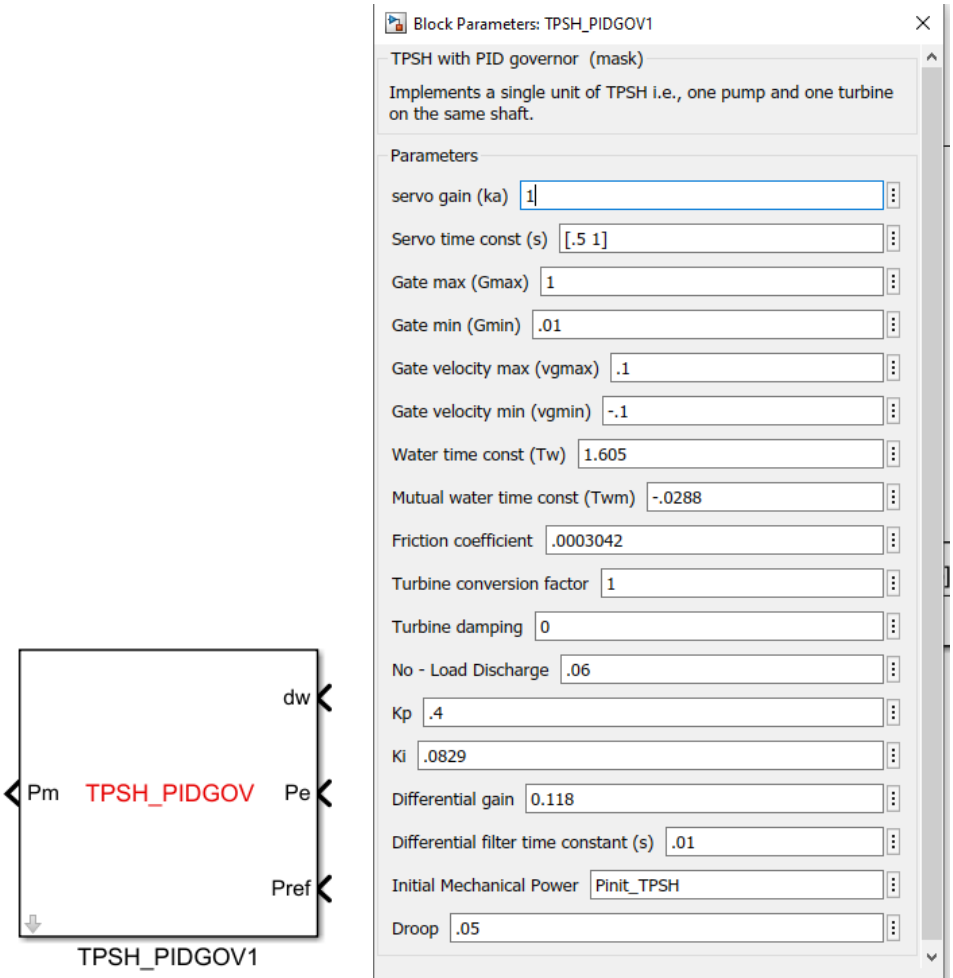

(a) (b)

Figure A.8. TPSH (a) governor mask and (b) parameter entry interface.

BIBLIOGRAPHY

[1] G. Kavlak, J. McNerney and J. Trancik, "Evaluating the causes of cost reduction in photovoltaic modules", *Energy Policy*, vol. 123, pp. 700-710, 2018. Available: 10.1016/j.enpol.2018.08.015.

[2] Center for Climate and Energy Solutions. (2019). Hurricanes and Climate Change | Center for Climate and Energy Solutions. [online] Available at: https://www.c2es.org/content/hurricanes-and-climate-change/.

[3] Clark, A. (2016). What's the Difference between Reliability and Resilience?. [online] Aaron Clark-Ginsberg. Available at: http://www.aaroncg.me /2016/04/21/whats-the-difference-between-reliability-and-resilience/ [Accessed 18 Nov. 2019].

[4] Z. Bie, Y. Lin, G. Li and F. Li, "Battling the Extreme: A Study on the Power System Resilience", *Proceedings of the IEEE*, vol. 105, no. 7, pp. 1253-1266, 2017. Available: 10.1109/jproc.2017.2679040.

[5] Ana Fernández-Guillamón, Emilio Gómez-Lázaro, Eduard Muljadi, Ángel Molina-García, Power systems with high renewable energy sources: A review of inertia and frequency control strategies over time, Renewable and Sustainable Energy Reviews, Volume 115, 2019, 109369, ISSN 1364-0321, https ://doi.org/10.1016/j.rser.2019.109369.

[6] Seel, J.; Mills, A.;Wiser, R.; Deb, S.; Asokkumar, A.; Hassanzadeh, M.; Aarabali, A. Impacts of High Variable Renewable Energy Futures on Wholesale Electricity Prices, And on Electric-Sector Decision Making; Lawrence Berkeley National Laboratory: Berkeley, CA, USA, 2020. Available online: https://emp.lbl.gov/publications/impacts-high-variable-renewable (accessed on 25 July 2020).

[7] L. Chang, "Review on Distributed Energy Storage Systems for Utility Applications," *CPSS Transactions on Power Electronics and Applications*, vol. 2, no. 4, pp. 267-276, 2017.

[8] M. Geuss, "German institute successfully tests underwater energy storage sphere," Ars Technica, 2017. [Online]. Available: https://arstechnica.com/science/2017/03/ german-institute-successfullytests-underwater-energy-storage-sphere/.

[9] M. Coren, "Germany is building the world's first wind turbines with built-in hydroelectric batteries," *Quartz*, 2017. [Online]. Available: https://qz.com/823054/germany-wind-turbine-hydroelectric-batteries/.

[10] "Gravity Power Module | Energy Storage | Grid-Scale Energy Storage," Gravitypower.net, 2017. [Online]. Available: http://www.gravitypower.net/.

[11] X. Qiu, T. Nguyen, J. Guggenberger, M. Crow and A. Elmore, "A Field Validated Model of a Vanadium Redox Flow Battery for Microgrids", *IEEE Transactions on Smart Grid*, vol. 5, no. 4, pp. 1592-1601, 2014. Available: 10.1109/tsg.2014.2310212.

[12] H. Shen, X. Zhu, M. Shao and H. Cao, "Neural Network Predictive Control for Vanadium Redox Flow Battery", *Journal of Applied Mathematics*, vol. 2013, pp. 1-7, 2013. Available: 10.1155/2013/538237.

[13] M. Akter, Y. Li, J. Bao, M. Skyllas-Kazacos and M. Rahman, "Optimal Charging of Vanadium Redox Flow Battery with Time-Varying Input Power", *Batteries*, vol. 5, no. 1, p. 20, 2019. Available: 10.3390/batteries5010020.

[14] Y. Mazloum, H. Sayah and M. Nemer, "Dynamic modeling and simulation of an Isobaric Adiabatic Compressed Air Energy Storage (IA-CAES) system", *Journal of Energy Storage*, vol. 11, pp. 178-190, 2017. Available: 10.1016/j.est.2017.03.006.

[15] C. Prieto and L. Cabeza, "Thermal energy storage (TES) with phase change materials (PCM) in solar power plants (CSP). Concept and plant performance", *Applied Energy*, vol. 254, p. 113646, 2019. Available: 10.1016/j.apenergy.2019.113646.

[16] "Thermal energy storage with ETES I Siemens Gamesa", *Siemensgamesa.com*, 2020. [Online]. Available: https://www.siemensgamesa.com/en-int/products-and-services/hybrid-and-storage/thermal-energy-storage-with-etes. [Accessed: 11- Feb- 2020].

[17] E. Muljadi and V. Gevorgian, "Flywheel Energy Storage - Dynamic Modeling," *2017 Ninth Annual IEEE Green Technologies Conference (GreenTech)*, Denver, CO, 2017, pp. 312-319, doi: 10.1109/GreenTech.2017.52.

[18] N. Zhang, C. Kang, D. Kirschen, W. Xi, J. Huang and Q. Zhang, "Planning Pumped Storage Generation for Wind Power Integration", *IEEE Transactions on Sustainable Energy*, 2011. Available: 10.1109/tste.2011.2165345.

[19] D. Giosio, A. Henderson, J. Walker and P. Brandner, "Rapid Reserve Generation from a Francis Turbine for System Frequency Control", *Energies*, vol. 10, no. 4, p. 496, 2017. Available: 10.3390/en10040496.

[20] G. Munoz-Hernandez and D. Jones, "MIMO Generalized Predictive Control for a Hydroelectric Power Station", *IEEE Transactions on Energy Conversion*, vol. 21, no. 4, pp. 921-929, 2006. Available: 10.1109/tec.2005.860405.

[21] M. Beus and H. Pandžić, "Application of Model Predictive Control Algorithm on a Hydro Turbine Governor Control," *2018 Power Systems Computation Conference (PSCC)*, Dublin, 2018, pp. 1-7, doi: 10.23919/PSCC.2018.8442594.

[22] M. Beus and H. Pandžić, "Application of an adaptive model predictive control algorithm on the Pelton turbine governor control," in *IET Renewable Power Generation*, vol. 14, no. 10, pp. 1720-1727, 27 7 2020, doi: 10.1049/iet-rpg.2019.1291.

[23] P. Sankaramurthy, B. Chokkalingam, S. Padmanaban, Z. Leonowicz and Y. Adedayo, "Rescheduling of Generators with Pumped Hydro Storage Units to Relieve Congestion Incorporating Flower Pollination Optimization", *Energies*, vol. 12, no. 8, p. 1477, 2019. Available: 10.3390/en12081477.

[24] D. Harpman, J. Platt and S. Coberly, "Advanced Algorithms for Hydropower Optimization", U.S. Department of the Interior, Bureau of Reclamation, Technical Service Center, Denver, Colorado, 2012.

[25] D. Harpman, T. Gaston and T. Steves, "Phase 2 -Advanced Algorithms for Hydropower Optimization", U.S. Department of the Interior Bureau of Reclamation Technical Service Center, Denver, CO, 2020.

[26] A. L. Diniz, "Test cases for unit commitment and hydrothermal scheduling problems," IEEE PES General Meeting, Providence, RI, 2010, pp. 1-8, doi: 10.1109/PES.2010.5589757.

[27] J. Arroyo and A. Conejo, "Modeling of Start-Up and Shut-Down Power Trajectories of Thermal Units", *IEEE Transactions on Power Systems*, vol. 19, no. 3, pp. 1562-1568, 2004. Available: 10.1109/tpwrs.2004.831654.

[28] M. Chazarra, J. Perez-Diaz and J. Garcia-Gonzalez, "Optimal Joint Energy and Secondary Regulation Reserve Hourly Scheduling of Variable Speed Pumped Storage Hydropower Plants", *IEEE Transactions on Power Systems*, vol. 33, no. 1, pp. 103-115, 2018. Available: 10.1109/tpwrs.2017.2699920.

[29] E. Muljadi, M. Singh, V. Gevorgian, M. Mohanpurkar, R. Hovsapian, and V. Koritarov, "Dynamic modeling of adjustable-speed pumped storage hydropower plant," *2015 IEEE Power & Energy Society General Meeting*, Denver, CO, 2015, pp. 1-5.

[30] J. Filipe, R. Bessa, C. Moreira, and B. Silva, "On the Profitability of Variable Speed Pump-Storage-Power in Frequency Restoration Reserve," *Journal of Physics: Conference Series*, vol. 813, p. 012010, 2017.

[31] A. Joseph, K. Desingu, R. Semwal, T. Chelliah, and D. Khare, "Dynamic Performance of Pumping Mode of 250 MW Variable Speed Hydro-Generating Unit Subjected to Power and Control Circuit Faults," *IEEE Transactions on Energy Conversion*, vol. 33, no. 1, pp. 430-441, 2018.

[32] Xibo Yuan, Jianyun Chai, and Yongdong Li, "A Converter-Based Starting Method and Speed Control of Doubly Fed Induction Machine With Centrifugal Loads," *IEEE Transactions on Industry Applications*, vol. 47, no. 3, pp. 1409-1418, 2011.

[33] A. Joseph, R. Selvaraj, T. Chelliah, and S. Sarma, "Starting and Braking of a Large Variable Speed Hydrogenerating Unit Subjected to Converter and Sensor Faults," *IEEE Transactions on Industry Applications*, vol. 54, no. 4, pp. 3372-3382, 2018.

[34] A. Dida and D. Benattous, "A complete modeling and simulation of DFIG based wind turbine system using fuzzy logic control," *Frontiers in Energy*, vol. 10, no. 2, pp. 143-154, 2016.

[35] H. Schlunegger and A. Thoni, "100 MW full-size converter in the Grimsel 2 pumped-storage plant", Oberhalsi Hydroelectric Power Company, 2014.

[36] Koritarov, V., T. Veselka, J. Gasper, B. Bethke, A. Botterud, J. Wang, M. Mahalik, Z. Zhou, C. Milostan, J. Feltes, Y. Kazachkov, T. Guo, G. Liu, B. Trouille, P. Donalek, K. King, E. Ela, B. Kirby, I. Krad, and V. Gevorgian, "Modeling and Analysis of Value of Advanced Pumped Storage Hydropower in the United States," Argonne National Laboratory Report ANL/DIS-14/7, Argonne, Illinois, June 2014.

[37] Y. Mishra, S. Mishra, Fangxing Li, Zhao Yang Dong and R. Bansal, "Small-Signal Stability Analysis of a DFIG-Based Wind Power System Under Different Modes of Operation", *IEEE Transactions on Energy Conversion*, vol. 24, no. 4, pp. 972-982, 2009. Available: 10.1109/tec.2009.2031498.

[38] F. Wu, X. Zhang, K. Godfrey and P. Ju, "Small signal stability analysis and optimal control of a wind turbine with doubly fed induction generator", *IET Generation, Transmission & Distribution*, vol. 1, no. 5, p. 751, 2007. Available: 10.1049/iet-gtd:20060395.

[39] T. Harbort, G. Lein and E. Goede, "Power Frequency Control of a Pump Turbine as an Example for the Operation with Adjustable Speed of Hydraulic Machines", *IFAC Proceedings Volumes*, vol. 30, no. 17, pp. 335-341, 1997. Available: 10.1016/s1474-6670(17)46430-5.

[40] V. Koritarov, L. Guzowski, J. Feltes, Y. Kazachkov, B. Trouille and V. Gevorgian, "Modeling Ternary Pumped Storage Units", Argone National Laboratory, 2013.

[41] C. Nicolet, Y. Vaillant, B. Kawkabani, P. Allenbach, J. Simond and F. Avellan, "Pumped storage units to stabilize mixed islanded power network: a transient analysis", École Polytechnique Fédérale de Lausanne, Lausanne Switzerland, 2008.

[42] Federal Energy Regulatory Commission. Final Rule Order No. 890: Preventing Undue Discrimination and Preference in Transmission Service; Office of the General Counsel: Washington, DC, USA, 16 February 2007.

[43] Federal Energy Regulatory Commission. Final Rule Order No. 755: Frequency Regulation Compensation in the Organized Wholesale Power Markets; Office of the General Counsel: Washington, DC, USA, October 2011.

[44] Federal Energy Regulatory Commission. Third-Party Provision of Ancillary Services; Accounting and Financial Reporting for New Electric Storage Technologies; 144 FERC 61,056; Office of the General Counsel: Washington, DC, USA, July 2013.

[45] Federal Energy Regulatory Commission. Final Rule Order No. 841: Electric Storage Participation in Markets Operated by Regional Transmission Organizations and Independent System Operators; Office of the General Counsel: Washington, DC, USA, 2018.

[46] Bolun Xu, Y. Dvorkin, D. S. Kirschen, C. A. Silva-Monroy, and J. Watson, "A comparison of policies on the participation of storage in U.S. frequency regulation markets," 2016 IEEE Power and Energy Society General Meeting (PESGM), Boston, MA, 2016, pp. 1-5.

[47] T. A. Nguyen, R. H. Byrne, R. J. Concepcion and I. Gyuk, "Maximizing revenue from electrical energy storage in MISO energy & frequency regulation markets," 2017 IEEE Power & Energy Society General Meeting, Chicago, IL, 2017, pp. 1-5, doi: 10.1109/PESGM.2017.8274348.

[48] R. H. Byrne, R. J. Concepcion, and C. A. Silva-Monroy, "Estimating potential revenue from electrical energy storage in PJM," *2016 IEEE Power and Energy Society General Meeting (PESGM)*, Boston, MA, 2016, pp. 1-5.

[49] R. H. Byrne and C. A. Silva-Monroy, "Potential revenue from electrical energy storage in the Electricity Reliability Council of Texas (ERCOT)," 2014 IEEE PES General Meeting | Conference & Exposition, National Harbor, MD, 2014, pp. 1-5, doi: 10.1109/PESGM.2014.6939886.

[50] G. Fong, R. Moreira and G. Strbac, "Economic analysis of energy storage business models," 2017 IEEE Manchester PowerTech, Manchester, 2017, pp. 1-6, doi: 10.1109/PTC.2017.7980829.

[51] B. Zakeri and S. Syri, "Value of energy storage in the Nordic Power market - benefits from price arbitrage and ancillary services," *2016 13th International Conference on the European Energy Market (EEM)*, Porto, 2016, pp. 1-5.

[52] M. H. Ahmed, M. Arif, T. K. Abdel-Galil, L. M. Alhems, and W. Kotiuga, "Quantifying the value of pumped storage hydro (PSH) in the Saudi electric grid," *2016 Saudi Arabia Smart Grid (SASG)*, Jeddah, 2016, pp. 1-6.

[53] J. Filipe, R. Bessa, C. Moreira, and B. Silva, "On the Profitability of Variable Speed Pump-Storage-Power in Frequency Restoration Reserve," *Journal of Physics: Conference Series*, vol. 813, p. 012010, 2017.

[54] J. M. Filipe, C. L. Moreira, R. J. Bessa and B. A. Silva, "Optimization of the variable speed pump storage participation in frequency restoration reserve market," 2016 13th International Conference on the European Energy Market (EEM), Porto, 2016, pp. 1-6, doi: 10.1109/EEM.2016.7521336.

[55] H. Aburub, S. M. Basnet and W. Jewell, "A study of EPA GHG emissions standards for existing power plants in WECC region," 2016 Clemson University Power Systems Conference (PSC), Clemson, SC, 2016, pp. 1-6, doi: 10.1109/PSC.2016.7462858.

[56] M. A. Hozouri, A. Abbaspour, M. Fotuhi-Firuzabad and M. Moeini-Aghtaie, "On the Use of Pumped Storage for Wind Energy Maximization in Transmission-Constrained Power Systems," in IEEE Transactions on Power Systems, vol. 30, no. 2, pp. 1017-1025, March 2015, doi: 10.1109/TPWRS.2014.2364313.

[57] K. Salevid, "Market Requirements for Pumped Storage Profitability Expected Costs and Modelled Price Arbitrage Revenues, Including a Case Study of Juktan", Uppsala Universitet, 2013.

[58] B. Hayes, A. Wilson, R. Webster and S. Djokic, "Comparison of two energy storage options for optimum balancing of wind farm power outputs," *IET Generation, Transmission & Distribution*, vol. 10, no. 3, pp. 832-839, 2016.

[59] X. Yan and S. Y. A. Mohamed, "Comparison of virtual synchronous generators dynamic responses," 2018 IEEE 12th International Conference on Compatibility,

Power Electronics and Power Engineering (CPE-POWERENG 2018), Doha, 2018, pp. 1-6, doi: 10.1109/CPE.2018.8372573.

[60] S. You et al., "Energy Storage for Frequency Control in High Photovoltaic Power Grids," IEEE EUROCON 2019 -18th International Conference on Smart Technologies, Novi Sad, Serbia, 2019, pp. 1-6, doi: 10.1109/EUROCON.2019.8861993.

[61] M. Hwang, E. Muljadi, J. Park, P. Sørensen and Y. C. Kang, "Dynamic Droop–Based Inertial Control of a Doubly-Fed Induction Generator," in IEEE Transactions on Sustainable Energy, vol. 7, no. 3, pp. 924-933, July 2016, doi: 10.1109/TSTE.2015.2508792.

[62] J. Zhu et al., "Synthetic Inertia Control Strategy for Doubly Fed Induction Generator Wind Turbine Generators Using Lithium-Ion Supercapacitors," in IEEE Transactions on Energy Conversion, vol. 33, no. 2, pp. 773-783, June 2018, doi: 10.1109/TEC.2017.2764089.

[63] "5 largest solar farms in the world - Origin Energy", *Originenergy.com.au*, 2018. [Online]. Available: https://www.originenergy.com.au/blog/lifestyle/5-largest-solar-farms-in-the-world.html. [Accessed: 05- Nov- 2018].

[64] A. Joseph, K. Desingu, R. Semwal, T. Chelliah, and D. Khare, "Dynamic Performance of Pumping Mode of 250 MW Variable Speed Hydro-Generating Unit Subjected to Power and Control Circuit Faults," *IEEE Transactions on Energy Conversion*, vol. 33, no. 1, pp. 430-441, 2018.

[65] S. Sharma, S. Huang, and N. Sarma, "System Inertial Frequency Response estimation and impact of renewable resources in ERCOT interconnection," *Proc. of IEEE Power and Energy Society General Meeting*, Detroit, 2011.

[66] Demello, F., Koessler, R., Agee, J., Anderson, P., Doudna, J., Fish, J., Hamm, P., Kundur, P., Lee, D. and Rogers, G. (1992). Hydraulic turbine and turbine control models for system dynamic studies. IEEE Transactions on Power Systems, 7(1), pp.167-179

[67] Y. Yu, C. Wu, J. Chen and H. Chen, "Algorithm for the selection of multiple VSPs", *World Pumps*, vol. 2016, no. 1, pp. 37-41, 2016. Available: 10.1016/s0262-1762(16)30034-7.

[68] A. Delavari, I. Kamwa and P. Brunelle, "Simscape Power Systems Benchmarks for Education and Research in Power Grid Dynamics and Control," *2018 IEEE Canadian Conference on Electrical & Computer Engineering (CCECE)*, Quebec City, QC, 2018, pp. 1-5, doi: 10.1109/CCECE.2018.8447645.

[69] "Hydraulic turbine and turbine control models for system dynamic studies," in IEEE Transactions on Power Systems, vol. 7, no. 1, pp. 167-179, Feb. 1992, doi: 10.1109/59.141700.

[70] Zimmerman, R.D.; Murillo-Sanchez, C.E.; Thomas, R.J. MATPOWER: Steady-State Operations, Planning and Analysis Tools for Power Systems Research and Education. *IEEE Trans. Power Syst.* 2011, 26, 12–19.

[71] Restrepo, J.F.; Galiana, F.D. Effects of wind power on day-ahead reserve schedule. In Proceedings of the 2009 IEEE PES/IAS Conerence on Sustainable Alternative Energy (SAE), Valencia, Spain, 28–30 September 2009; IEEE: Valencia, FL, USA, 2009; pp. 1–4.

[72] Hodge, B.; Florita, A.; Orwig, K.; Lew, D. Milligan, M. *A Comparison of Wind Power and Load Forecasting Error Distributions*; NREL: Denver, CO, USA, 2012; pp. 1–10.

[73] Murillo-Sanchez, C.E.; Zimmerman, R.D.; Anderson, C.L.; Thomas, R.J. Secure Planning and Operations of Systems with Stochastic Sources, Energy Storage and Active Demand. *IEEE Trans. on Smart Grid* 2013; 4, 2220–2229.

[74] Lee, K.Y.; El-Sharkawi, M.A. (Eds.) *Modern Heuristic Optimization Techniques with Applications to Power Systems*; Wiley-IEEE Press: New York, NY, USA, 2008; ISBN 978-0-471-45711-4.

[75] Storn, R.; Price, K. Differential Evolution—A Simple and Efficient Heuristic for global Optimization over Continuous Spaces. *J. Glob. Optim.* **1997**, *11*, 341–359, doi:10.1023/A:1008202821328.

[76] Goldberg, D.E. (1989). *Genetic Algorithms in Search Optimization and Machine Learning*; Addison Wesley: Boston, MA, USA, 2011; p. 41; ISBN 0-201-15767-5.

[77] Kennedy, J.; Eberhart, R. Particle swarm optimization. In Proceedings of the ICNN'95-International Conference on Neural Networks, Perth, WA, Australia, 27 November–1 December 1995; IEEE: Perth, WA, Australia, 1995; Volume 4, pp. 1942–1948.

[78] Grigg, C.; Wong, P.; Albrecht, P.; Allan, R.; Bhavaraju, M.; Billinton, R.; Chen, Q.; Fong, C.; Haddad, S.; Kuruganty, S. A report prepared by the Reliability Test System Task Force of the Application of Probability Methods Subcommittee. IEEE Transactions on Power Systems. *IEEE Reliab. Test Syst.* 1999, 14, pp. 1010–1020.

[79] Eia.gov. U.S. Energy Information Administration (EIA)-Embed. 2020. Available online: https://www.eia.gov/opendata/widgets.php

[80] D. Gautam, V. Vittal, and T. Harbour, “Impact of increased penetration of DFIG–based wind turbine generators on transient and small signal stability of power systems,” IEEE Trans. Power Syst., vol. 24, no. 3, pp. 1426–1434, Aug. 2009.

[81] W. Bignell, H. Saffron, T. T. Nguyen and W. D. Humpage, “Effects of machine inertia constants on system transient stability,” Electric Power System Research, vol. 51, no. 3, pp. 153–165, Sep. 1999,

[82] “Governor Model: HYGOV and HYGOVD", *Powerworld.com*, 2020. [Online]. Available: https://www.powerworld.com/WebHelp/Content/ Transient Models_HTML /Governor%20HYGOV%20and%20HYGOVD.htm ?TocPath=Transient%20Stability%20Add-On %20(TS)% 7CTransient %20Models%7 CGenerator%7CGovernor %7C_____27.

[83] N. W. Miller, M. Shao, R. D'aquila, S. Pajic, and K. Clark, "Frequency Response of the US Eastern Interconnection Under Conditions of High Wind and Solar Generation," in 2015 Seventh Annual IEEE Green Technologies Conference, 2015, pp. 21-28.

[84] J. Tan, Y. Zhang, S. Veda, T. Elgindy and Y. Liu, "Developing High PV Penetration Cases for Frequency Response Study of U.S. Western Interconnection," *2017 Ninth Annual IEEE Green Technologies Conference (GreenTech)*, Denver, CO, 2017, pp. 304-311. doi: 10.1109/GreenTech.2017.51

[85] "Solar Industry Research Data | SEIA", SEIA, 2019. [Online]. Available: https://www.seia.org/solar-industry-research-data.

[86] P. Gagnon, R. Margolis, J. Melius, C. Phillips, and R. Elmore, "Rooftop Solar Photovoltaic Technical Potential in the United States: A Detailed Assessment," Rep. No. NREL/TP-6A20-65298). Retrieved March, vol. 30, p. 2016, 2016.

[87] "NSRDB Data Viewer", Maps.nrel.gov, 2019. [Online]. Available: https ://maps.nrel. gov/nsrdb-viewer/.

[88] “Energy Management System | PSLF | GE Energy Consulting", Geenergy consulting.com, 2019. [Online]. Available: https://www.geenergyconsulting. com/practice-area/software-products/pslf.